

Chapter IV: Results and Discussion

4.1. Screening and Selection of nitro-PAHs Accumulating Plant Species

In this study, the selection of potential plant species was conducted using standardized field ecological methods to ensure a robust and scientifically valid approach. Quadrat sampling (1 m × 1 m) was employed to determine key vegetation parameters, including frequency, relative frequency, relative density, and the Importance Value Index (IVI) (Sarma et al., 2017). The IVI was calculated as the summation of the relative values of frequency, density, and abundance, following the methodology established by Sarma et al. (2017). Based on the IVI values, four plant species exhibiting the highest indices were selected for further investigation: *Cyperus rotundus* L. (25.55), *Axonopus compressus* (Sw.) P. Beauv. (25.50), *Cyperus esculentus* L. (25.00), *Imperata cylindrica* (L.) Raeusch. (19.77).

A detailed floristic analysis was performed, and the results systematically presented in Table 4.1, alongside key ecological parameters. The selected plant species *C. rotundus* and *C. esculentus* (Cyperaceae family), and *I. cylindrica* and *A. compressus* (Poaceae family), were chosen due to their dominance in crude oil-contaminated habitats, particularly in areas surrounding the ONGC GGS site in eastern Assam (Borholla), which falls within the Indo-Burma biodiversity hotspot. Their widespread occurrence, adaptability, and resilience in highly polluted environments underscore their potential for phytoremediation applications.

Previous studies have extensively reported their capacity to uptake and tolerate toxic metals, further reinforcing their suitability for phytoremediation research (Li et al., 2018; Sarma et al., 2017). Given their well-established role in metal accumulation, these species were selected to specifically assess their efficacy in eliminating nitro-PAHs from crude oil-contaminated ecosystems. Their inclusion provides a strong foundation for evaluating plant-based remediation strategies aimed at mitigating nitro-PAH contamination. The chosen species are shown in Fig. 4.1 as photographs taken in the field.

The 1-nitropyrene and 2-nitrofluorene accumulation was evaluated by using standard calibration curves, which were constructed by plotting standard concentration against retention area derived from HPLC spectra (Table 4.2 and Table 4.3). These calibration curves served as the foundation for quantifying nitro-PAH concentrations in the experimental samples. For both compounds, the calibration curve showed linear regression. The calibration curve for 1-

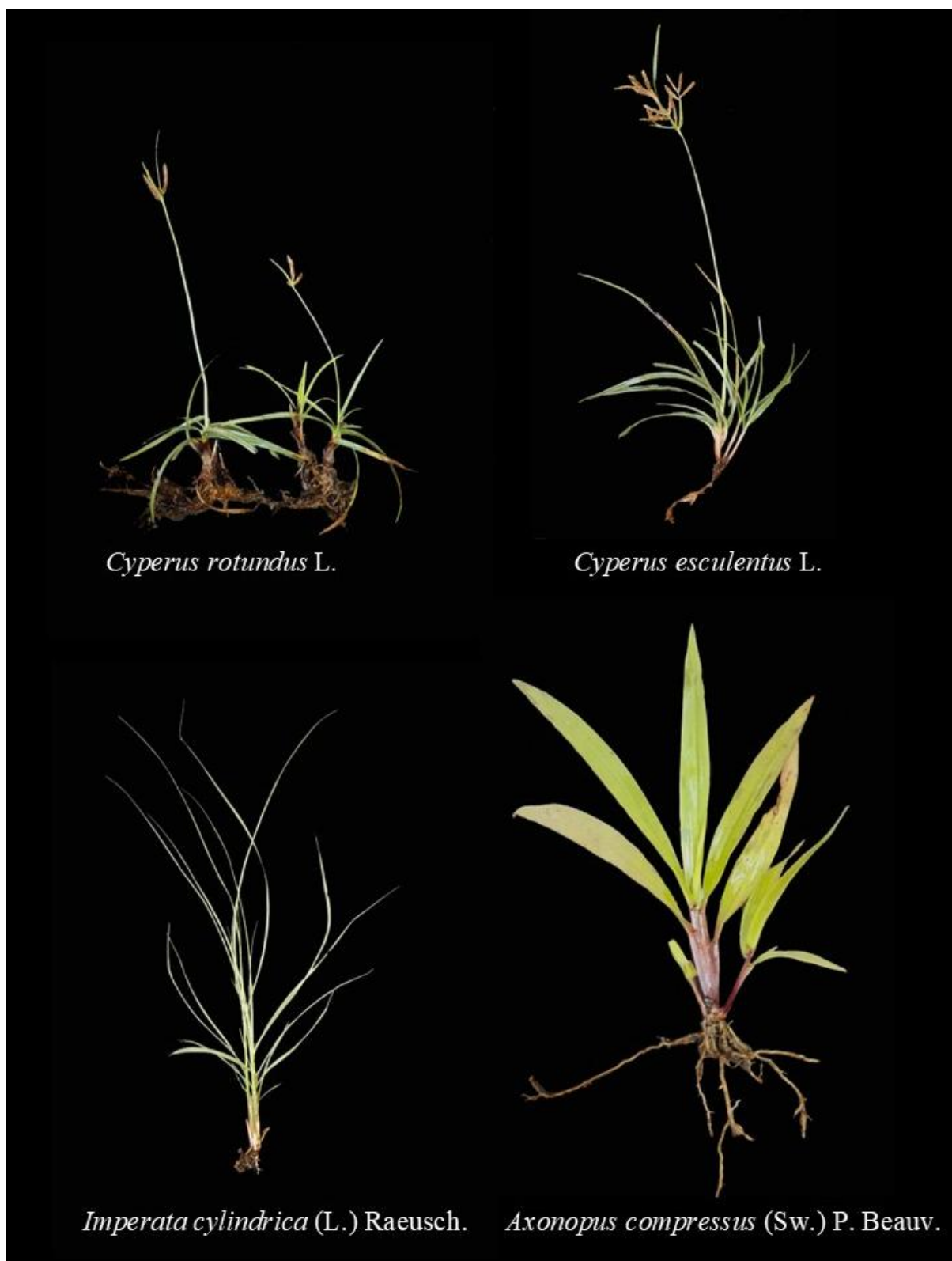


Fig. 4.1. The screened-out plant species from the sampling site.

Table 4.1. Detailed floristic diversity of the sampling site showing relative density, relative frequency, and importance value index.

Sl no.	Species	Collection No.	Total no. of Quadrats in which species occurred	Total Number of individuals	Frequency	Relative Frequency	Relative density	Importance value index
1	<i>Cyperus rotundus</i> L.	B.Gogoi 101	29	462	96.67	10.90	14.66	25.56
2	<i>Cyperus esculentus</i> L.	B.Gogoi 118	26	480	86.67	9.77	15.23	25.00
3	<i>Imperata cylindrica</i> (L) Raeusch.	B.Gogoi 103	20	386	66.67	7.52	12.25	19.77
4	<i>Axonopus compressus</i> P. (Sw.) Beauv	B.Gogoi 106	28	472	93.33	10.53	14.97	25.50
5	<i>Cynodon dactylon</i> (L) Pers.	B.Gogoi 104	21	132	70	7.89	4.19	12.08
6	<i>Poa annua</i> L.	B.Gogoi 121	23	119	76.67	8.65	3.78	12.42
7	<i>Echinochloa colona</i> (L.) Link	B.Gogoi 113	20	106	66.67	7.52	3.36	10.88
8	<i>Leersia hexandra</i> Sw.	B.Gogoi 108	16	221	53.33	6.02	7.01	13.03
9	<i>Oryza sativa</i> L.	B.Gogoi 107	7	31	23.33	2.63	0.98	3.62
10	<i>Digitaria sanguinalis</i> (L.) Scop.	B.Gogoi 115	10	83	33.33	3.76	2.63	6.39
11	<i>Fimbristylis dichotoma</i> (L.) Vahl	B.Gogoi 124	11	158	36.67	4.14	5.01	9.15
12	<i>Saccharum spontaneum</i> L.	B.Gogoi 117	18	219	60	6.77	6.95	13.71
13	<i>Kyllinga brevifolia</i> Rottb.	B.Gogoi 116	12	125	40	4.51	3.97	8.48
14	<i>Paspalum conjugatum</i> P.J. Bergius.	B.Gogoi 102	19	131	63.33	7.14	4.16	11.30
15	<i>Dactyloctenium aegyptium</i> (L.) Willd.	B.Gogoi 109	6	27	20	2.25	0.86	3.11

nitropyrene followed the equation $Y=635038x-19189$, with a coefficient of determination ($R^2=0.999$), as shown in Fig. 4.2 (a). Fig. 4.2 (b) shows that the calibration curve for 2-nitrofluorene follows the equation $Y=457716x-27506$ and has a coefficient of determination of $R^2=0.999$. These linear relationships validated the accuracy and dependability of the calibration technique. Tables 4.2 and 4.3 summarize the complete HPLC data detailing the standard nitro-PAH values. Fig. 4.3 and Fig. 4.4 show chromatograms of the standard samples, 1-nitropyrene and 2-nitrofluorene respectively, highlighting retention times and peak regions. Moreover, Fig. 4.5 and Fig. 4.6 illustrate the HPLC chromatograms of 1-nitropyrene in root samples collected on day 30 and day 60, respectively, from pots treated with different plant species. Similarly, Fig. 4.7 and Fig. 4.8 display the chromatograms of 2-nitrofluorene in root samples at the same time points. These figures provide insights into the uptake and accumulation of nitro-PAHs by various plant species, aiding in the assessment of accumulation efficiency. At 30 days, all examined plant species exhibited a remarkable capability to accumulate 1-nitropyrene and 2-nitrofluorene within their root tissues, highlighted their potential for pollutant uptake and sequestration. Among these species, *I. cylindrica* displayed the highest accumulation of 1-nitropyrene, achieving a concentration of 60.8 mg/g, followed by *A. compressus* (43.6 mg/g), *C. esculentus* (39.8 mg/g), and *C. rotundus* (39.6 mg/g).

Similarly, 2-nitrofluorene-accumulation was noted to be significantly high in *I. cylindrica* (80.6 mg/g), followed closely by *A. compressus* (80.2 mg/g), with *C. rotundus* (73.6 mg/g) and *C. esculentus* (60 mg/g). After 60 days, the accumulation of 1-nitropyrene and 2-nitrofluorene within the root tissues of the examined plant species significantly reflected a prolonged absorption over the duration. Among them, *I. cylindrica* showed a higher accumulation, attaining concentrations of 250 mg/g for 1-nitropyrene, and 279.6 mg/g for 2-nitrofluorene. This finding indicates that *I. cylindrica* possesses a robust capacity to absorb both nitro-PAHs, likely attributable to its extensive root architecture and substantial biomass production, which enhance its ability to uptake contaminants effectively. *A. compressus* showed a significant accumulation of nitro-PAHs, with concentrations of 220 mg/g for 1-nitropyrene and 270.8 mg/g for 2-nitrofluorene after 60 days, although these values were slightly lower than those found in *I. cylindrica*. At the same time, *C. rotundus* and *C. esculentus* accumulated the respective nitro-PAHs, with concentrations ranging from 210-200 mg/g for 1-nitropyrene and from 240-233.8 mg/g for 2-nitrofluorene. The comprehensive findings of the quantitative accumulation ability of 1-nitropyrene and 2-nitrofluorene of the selected plant species within their root systems are

Table 4.2. Standard calibration for 1-nitropyrene.

S.No.	Type	Code	Conc.(µg/ml)	RT (min)	Area
1		Blank	0	0	0
2		Std-5µg/ml	5	5.623	3292353
3	Standard	Std-10µg/ml	10	5.607	6088279
4		Std-20µg/ml	20	5.623	12768928

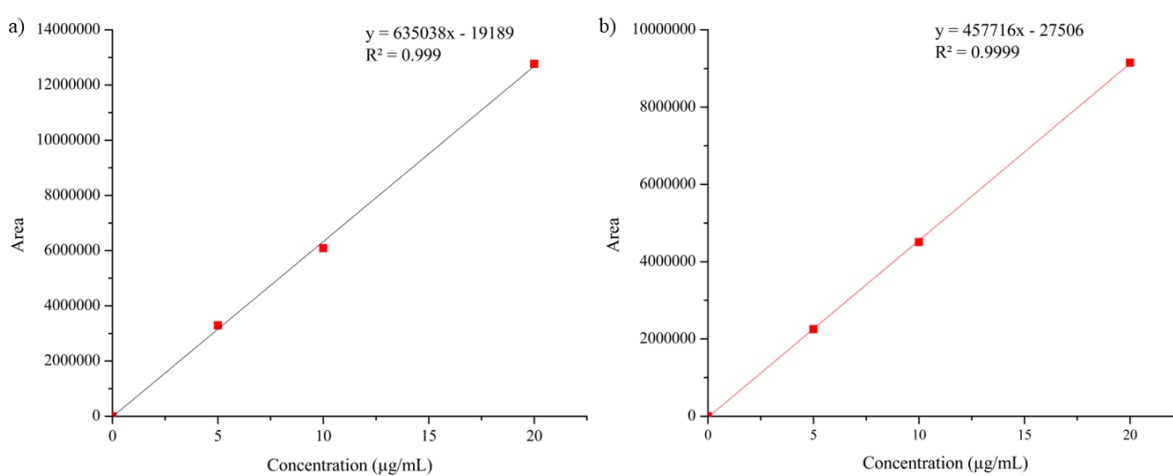


Fig. 4.2. Standard calibration curve for 1-nitropyrene (a) and 2-nitrofluorene (b).

Table 4.3. Standard calibration for 2-nitrofluorene.

Sl.No.	Type	Code	Conc.(µg/ml)	RT (min)	Area
1		Blank	0	0	0
2		Std-5µg/ml	5	4.497	2252740
3	Standard	Std-10µg/ml	10	4.520	4507148
4		Std-20µg/ml	20	4.520	9150156

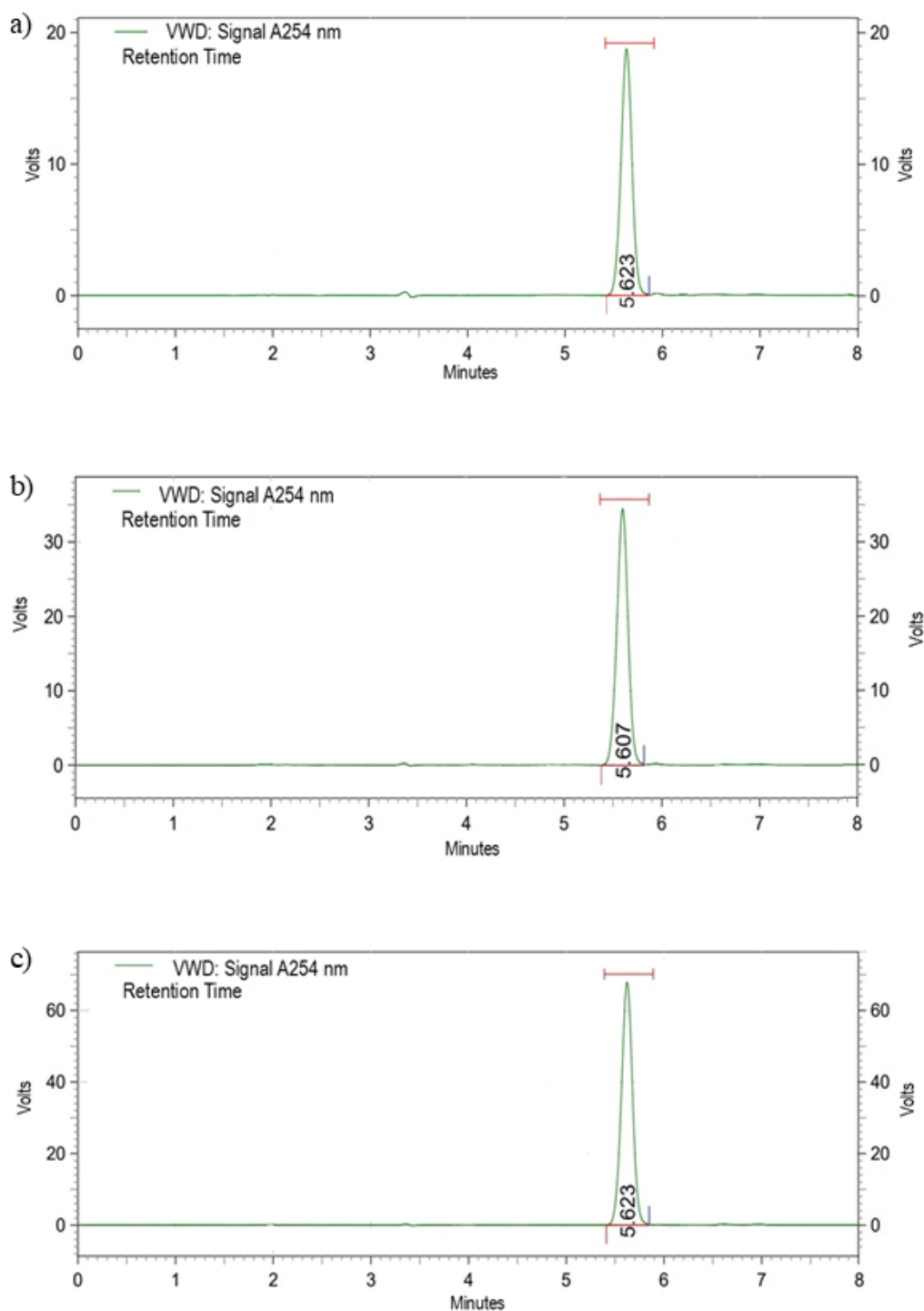


Fig. 4.3. Standard HPLC chromatogram of 1-nitropyrene at varying concentrations: (a) 5 $\mu\text{g/mL}$, (b) 10 $\mu\text{g/mL}$, and (c) 20 $\mu\text{g/mL}$. The chromatograms highlight the retention for each concentration. These results serve as a reference for identifying and quantifying 1-nitropyrene in experimental samples.

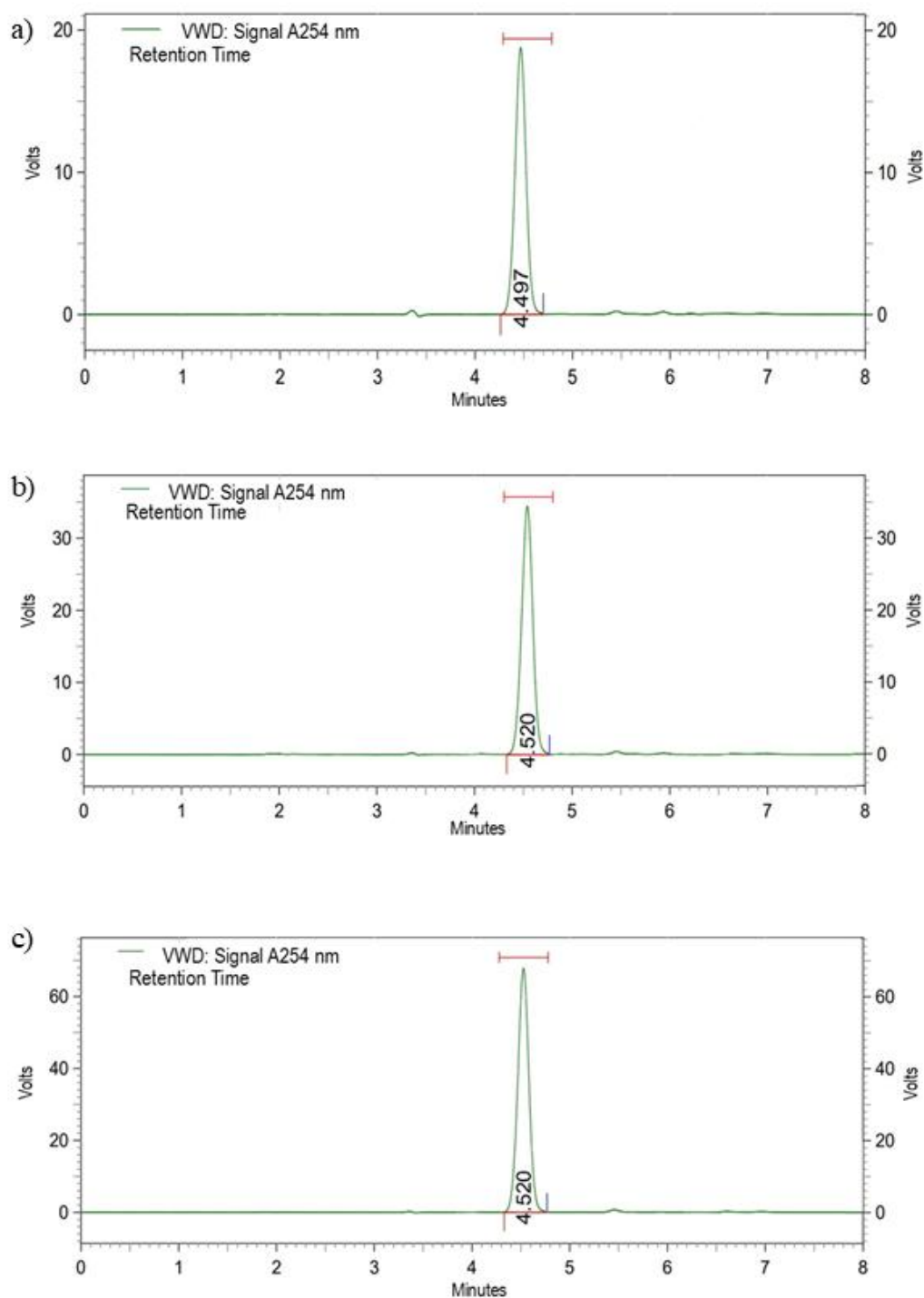


Fig. 4.4. Standard HPLC chromatogram of 2-nitrofluorene at varying concentrations: (a) 5 $\mu\text{g/mL}$, (b) 10 $\mu\text{g/mL}$, and (c) 20 $\mu\text{g/mL}$. The chromatograms highlight the retention for each concentration. These results serve as a reference for identifying and quantifying 2-nitrofluorene in experimental samples.

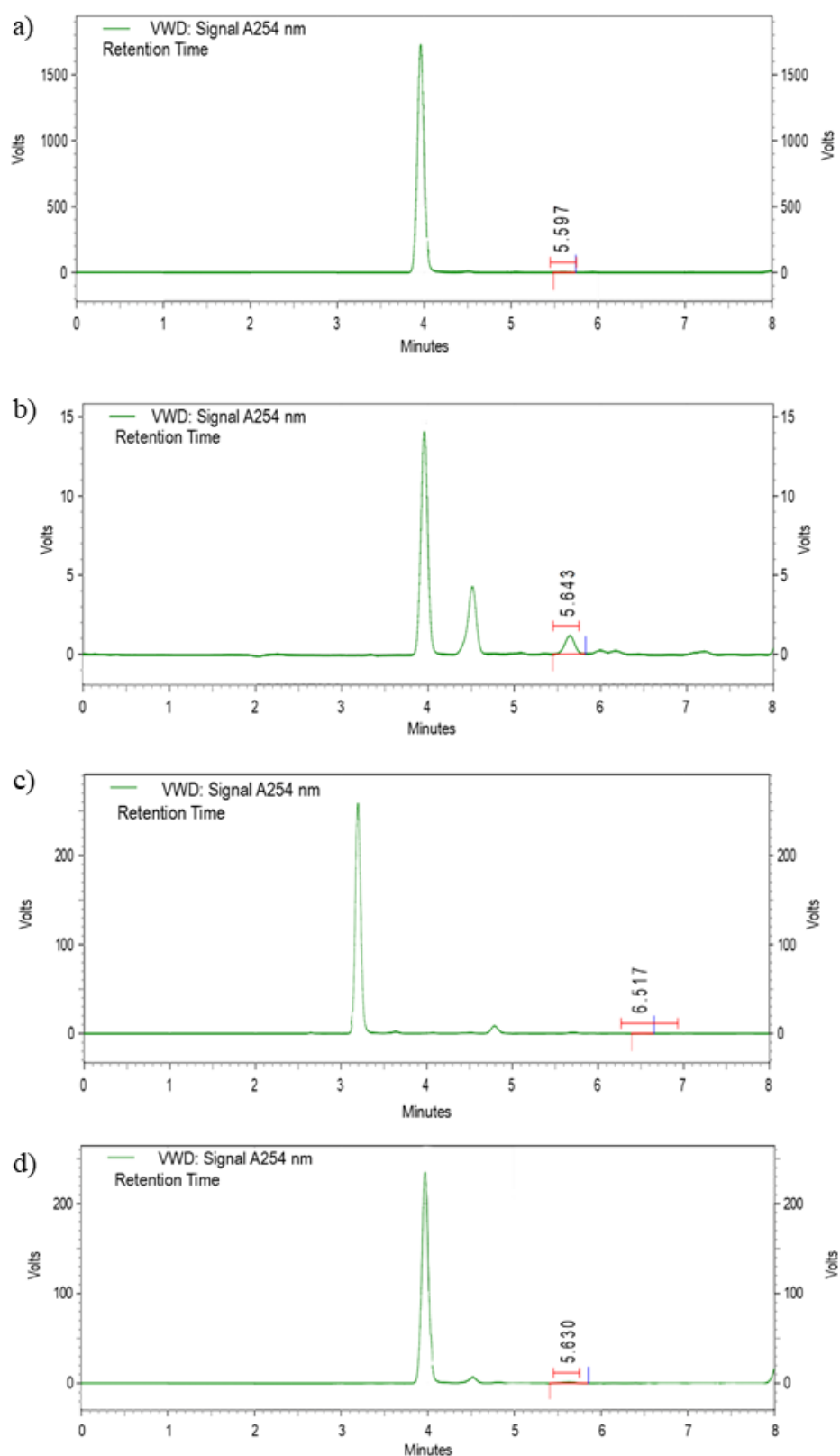


Fig. 4.5. Representative HPLC chromatogram of 1-nitropyrene in root samples collected on day 30 from pots treated with different plant species: (a) *Cyperus rotundus*, (b) *Cyperus esculentus*, (c) *Axonopus compressus*, and (d) *Imperata cylindrica*.

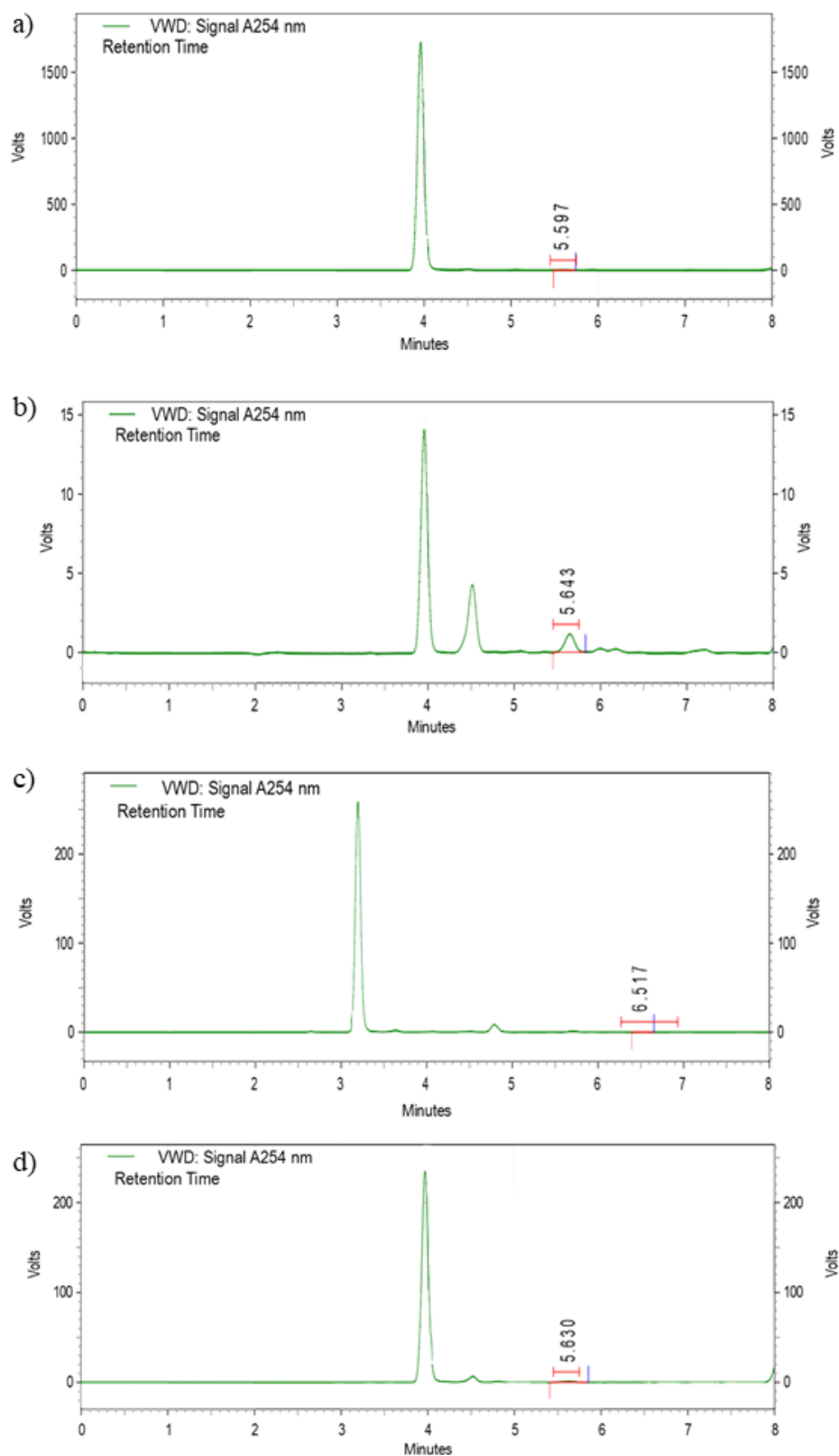


Fig. 4.6. Representative HPLC chromatogram of 1-nitropyrene in root samples collected on day 60 from pots treated with different plant species: (a) *Cyperus rotundus*, (b) *Cyperus esculentus*, (c) *Axonopus compressus*, and (d) *Imperata cylindrica*.

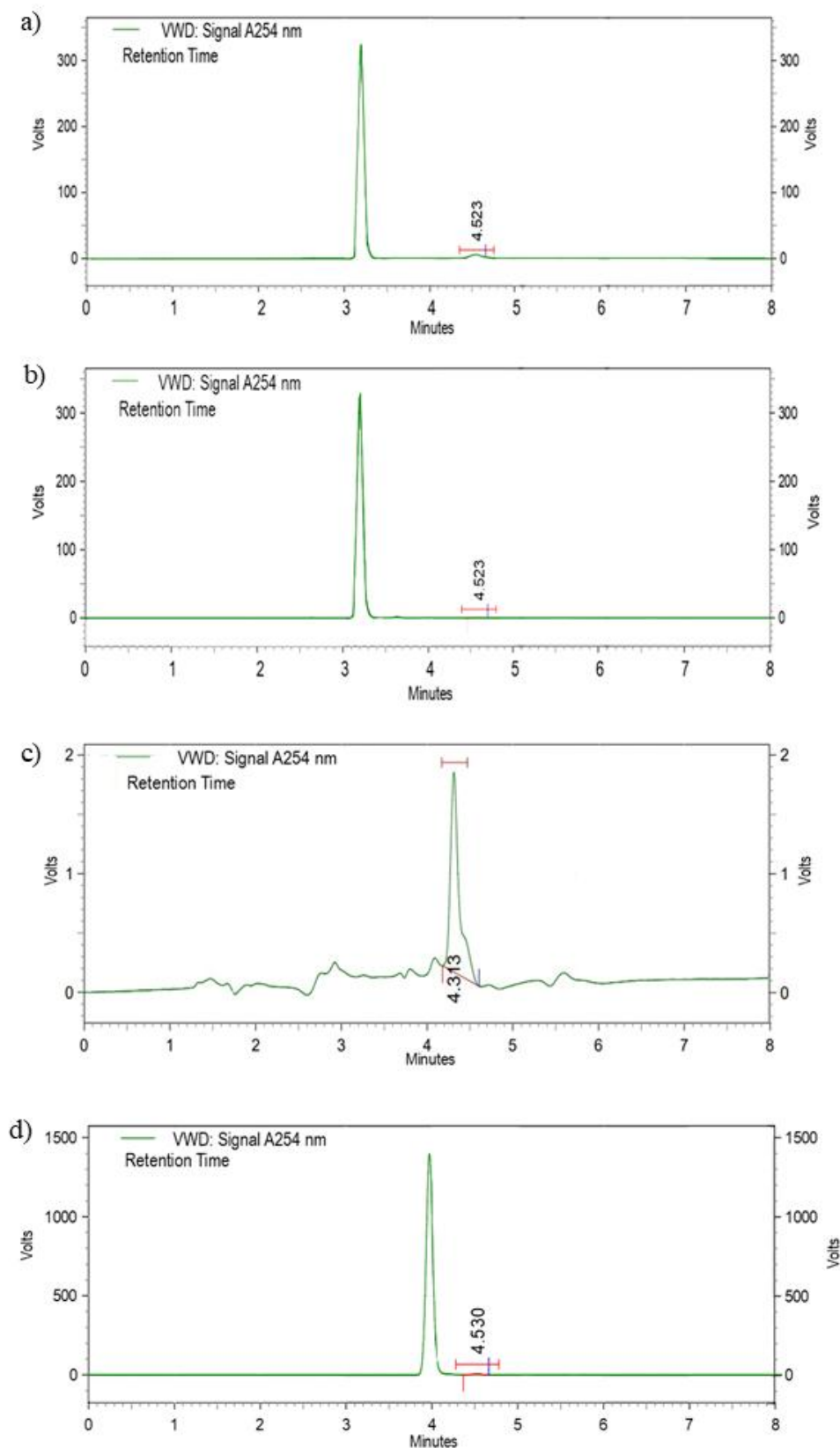


Fig. 4.7. Representative HPLC chromatogram of 2-nitrofluorene in root samples collected on day 30 from pots treated with different plant species: (a) *Cyperus rotundus*, (b) *Cyperus esculentus*, (c) *Axonopus compressus*, and (d) *Imperata cylindrica*.

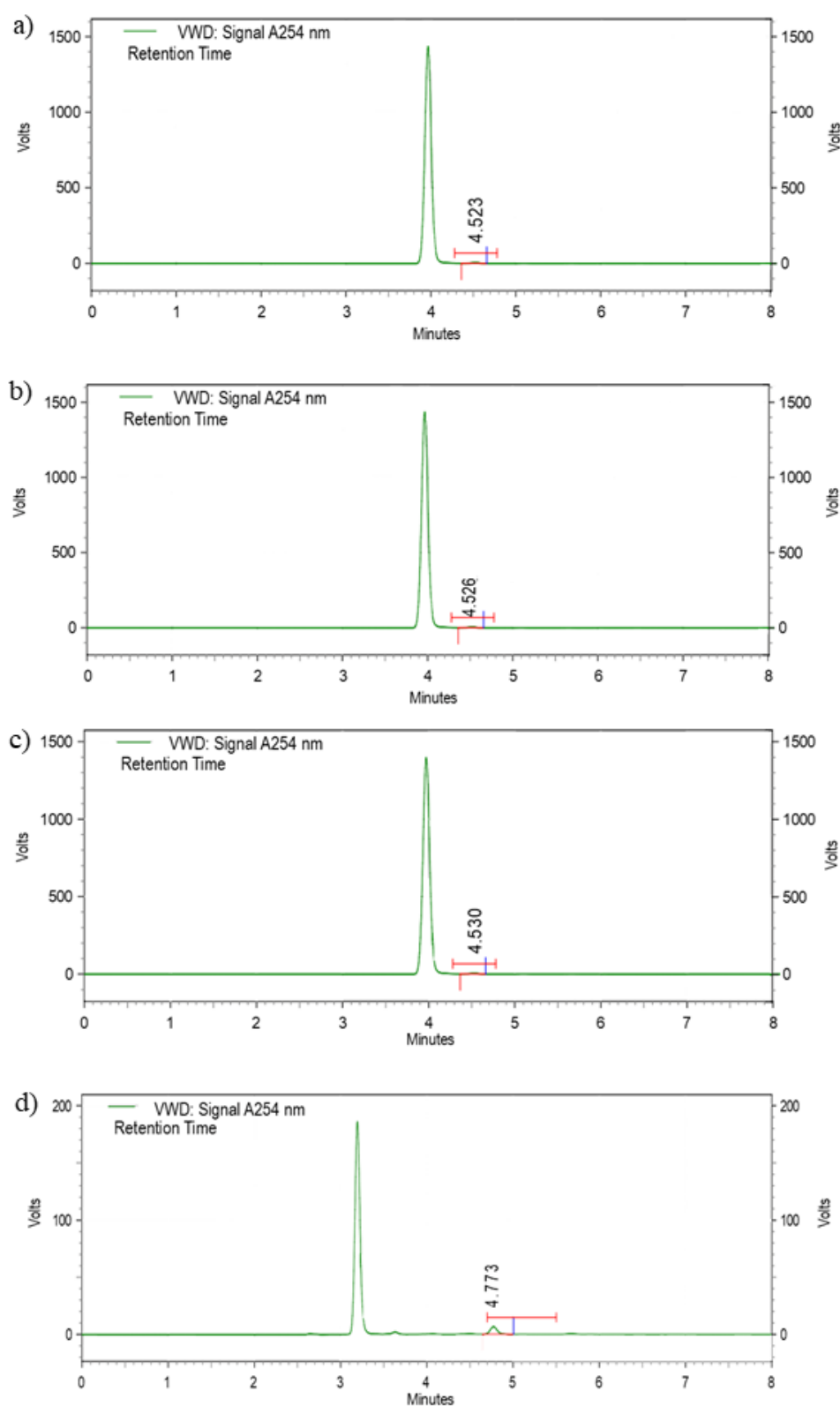


Fig. 4.8. Representative HPLC chromatogram of 2-nitrofluorene in root samples collected on day 60 from pots treated with different plant species: (a) *Cyperus rotundus*, (b) *Cyperus esculentus*, (c) *Axonopus compressus*, and (d) *Imperata cylindrica*.

depicted in Fig. 4.9. The accumulation of 1-nitropyrene and 2-nitrofluorene in plant species increased significantly with prolonged exposure. This suggests that extended exposure enhances the plants' ability to absorb and sequester pollutants within their tissues. This trend is likely attributed to the plants' metabolic adaptations, interactions between their roots and the soil, and the gradual uptake of pollutants into plant cells through specialized root transporters. Yang et al. (2024) reported that 1-nitropyrene and 9-nitroanthracene were absorbed in soybean and mung bean roots via active transport mediated by amino acid transporters (Yang et al., 2024). Even though we did not perform amino acids transporter in this study, it is believed that the previous result was consistent with the current findings, as it is hypothesized that they use similar transport pathways to absorb nitro-PAHs from contaminated soil. Further corroborating this, Alp-Turgut et al. (2024) reported that *Salvinia natans*, a freshwater macrophyte efficiently absorbed 1000 μM 3-nitronitrofluoranthene. The presence of nitro-PAHs in plant biomass indicated that certain species possessed natural mechanisms to tolerate and accumulate these emerging contaminants without immediately breaking them down. Similarly, the findings of this study strongly support the argument that *I. cylindrica*, *A. compressus*, *C. rotundus*, and *C. esculentus* possess a significant capacity to accumulate 1-nitropyrene and 2-nitrofluorene. Their demonstrated ability to absorb and retain nitro-PAHs reinforces the critical role of plant species selection in phytoremediation efforts. The presence of PAHs in plant biomass further validates their natural mechanisms for tolerating and sequestering these emerging contaminants, emphasizing their potential for remediating crude oil-contaminated environments. However, the accumulation of hydrocarbons in plant roots does not occur at a uniform rate due to the influence of photodegradation, which significantly alters the fate of pollutants within the rhizosphere. Agamuthu et al. (2010) provided compelling evidence that hydrocarbon-degrading rhizosphere bacteria actively break down hydrocarbons rather than allowing their accumulation, thereby reducing pollutant concentrations within plant tissues. This underscores the complex interplay between plant uptake and microbial degradation, highlighting that phytoremediation is not solely dependent on plant absorption but is also shaped by microbial activity in the root zone. Therefore, species with strong rhizosphere interactions may exhibit lower hydrocarbon accumulation despite their phytoremediation potential, reinforcing the need for a comprehensive evaluation of plant-microbe dynamics in remediation strategies (Agamuthu et al., 2010).

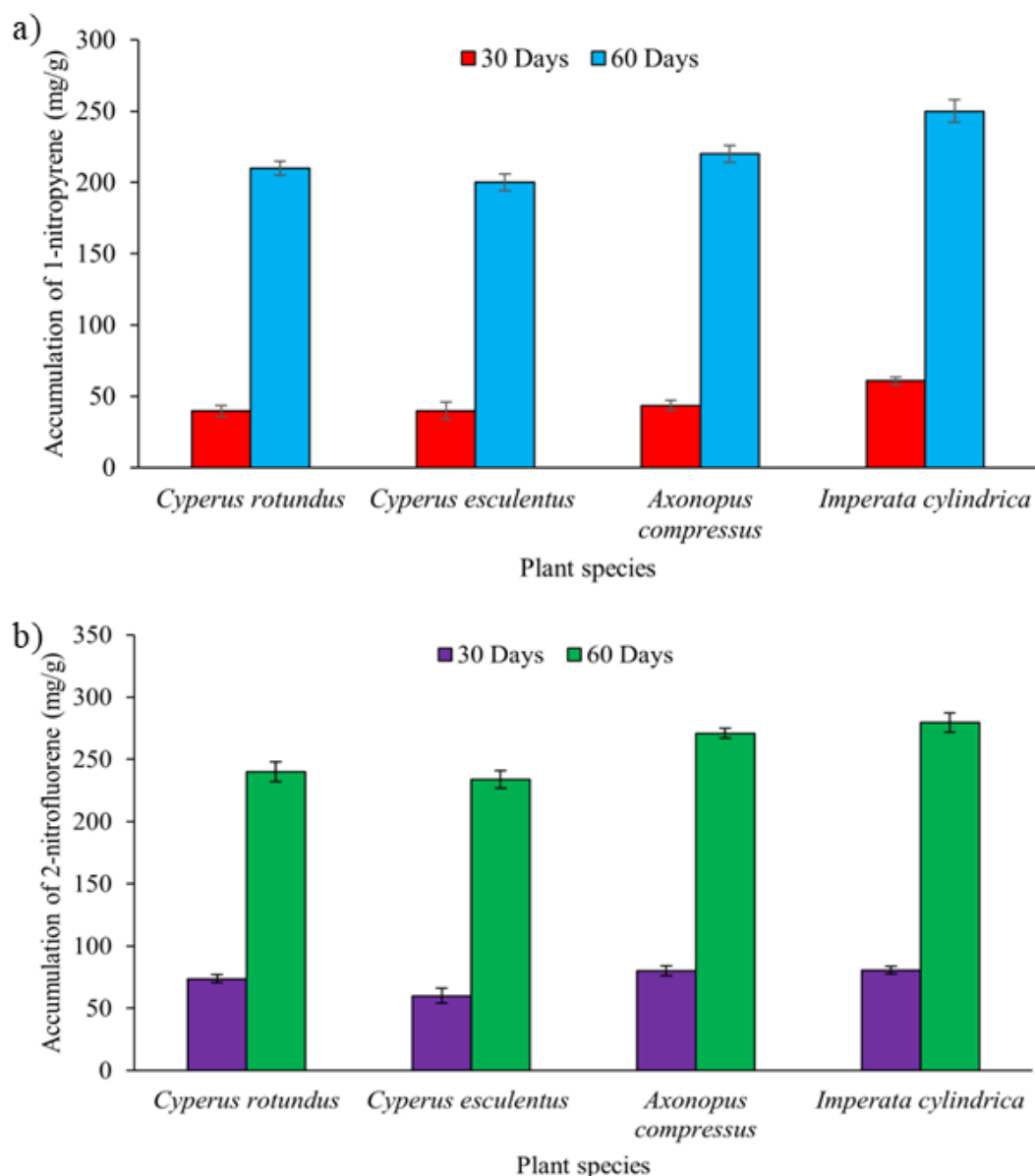


Fig. 4.9. Accumulation of 1-nitropyrene (a) and 2-nitrofluorene (b) in the root tissues of *Cyperus esculentus*, *Cyperus rotundus*, *Imperata cylindrica*, and *Axonopus compressus* over 30-day and 60-day interval. The data illustrate a significant increase in pollutant accumulation by the plants, with *Imperata cylindrica* having the highest accumulation levels at 60 days. Data expressed mean \pm S.D. (n = 3).

4.2. Isolation of Potential nitro-PAHs Degrading Rhizobacteria

The survival and growth of *C. esculentus*, *C. rotundus*, *I. cylindrica*, and *A. compressus* in contaminated soil demonstrated strong ecological resilience. These species exhibited a high IVI, which emphasized their dominance and adaptability in polluted environments. Their

resilience was likely supported by symbiotic associations with rhizosphere bacteria that tolerated nitro-PAHs, including 1-nitropyrene and 2-nitrofluorene. These bacteria enhanced the ability of these plant species to survive and grow under challenging conditions where other species struggled.

Notable differences in cfu/g of rhizobacteria were recorded when soil samples from the rhizosphere of each plant species were inoculated onto nutrient agar amended with 1-nitropyrene and 2-nitrofluorene. The findings, presented in Fig. 4.10, showed that *A. compressus* exhibited the highest bacterial colonization, with 117.33 cfu/g on 1-nitropyrene and 108 cfu/g on 2-nitrofluorene-amended nutrient agar. In contrast, *Imperata cylindrica*, *Cyperus esculentus*, and *Cyperus rotundus* showed comparatively lower bacterial counts: 57.33, 103.33, and 63.66 cfu/g on 1-nitropyrene, and 78, 102.66, and 45.66 cfu/g on 2-nitrofluorene, respectively. These findings suggest that rhizosphere bacteria in the studied plant species significantly enhance their potential for phytoremediation of soil contaminated with nitro-PAHs.

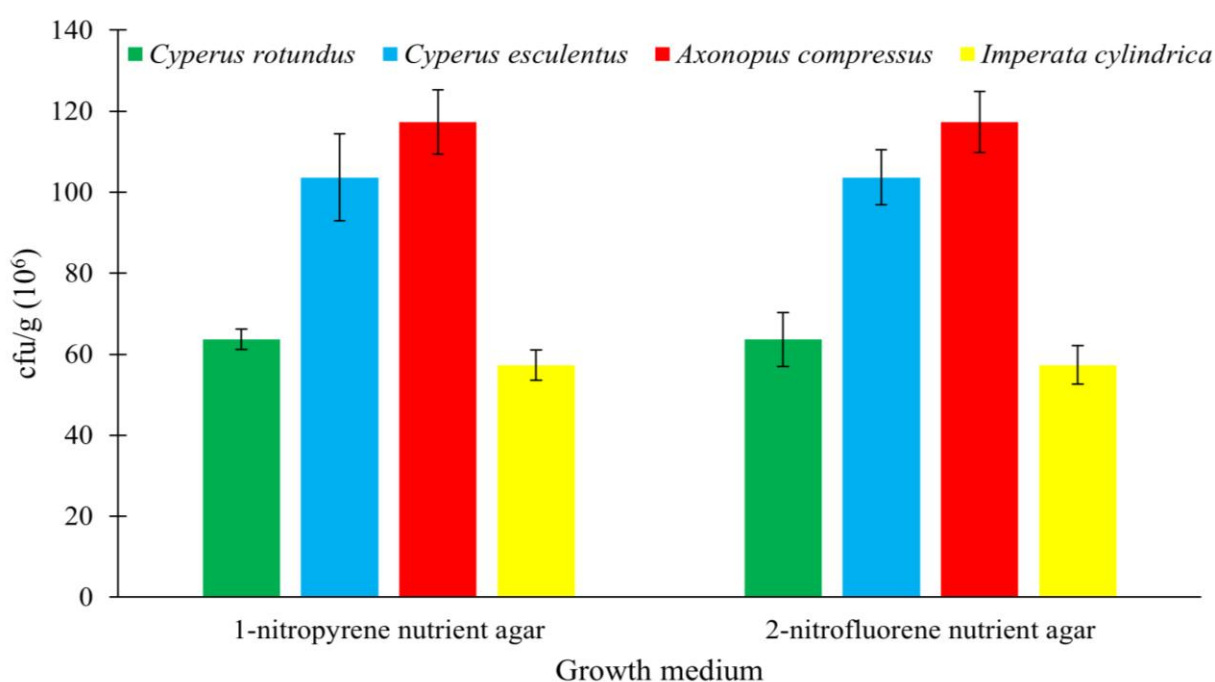


Fig. 4.10. Average count ($\times 10^6$ cfu/g soil) of total rhizosphere bacteria in the rhizosphere soil samples of screened plant species was recorded. The data represented bacterial population dynamics, highlighting variations in bacterial abundance among different plant species under experimental conditions. The data were expressed as mean \pm S.D. (n=3).

From the collected soil samples, two bacterial colonies were selected for further study based on their tolerance to nitro-PAHs and their ability to yield good biomass on nitro-PAHs-PBYS medium. This specialized medium was formulated to exclude commonly used carbon sources, relying solely on 1-nitropyrene and 2-nitrofluorene as carbon and energy substrates for bacterial survival. The growth of the isolates in these flasks indicated that the bacteria efficiently utilized nitro-PAHs, demonstrating their ability to survive in these contaminants.

After a 7-day incubation period in respective nitro-PAHs-PBYS medium, the growth dynamics of the two bacterial strains at different nitro-PAH concentrations were recorded and are depicted in Fig. 4.11. The study revealed that both bacterial strains grew optimally at a nitro-PAHs concentration of 25 mg/L, as evidenced by the maximal bacterial biomass observed at this concentration. Beyond this threshold, at 37.50 mg/L and 50 mg/L, bacterial growth declined significantly, showing that high concentrations of organic pollutants restricted microbial reproduction. Similarly, at a lower concentration of 12.5 mg/L, the growth of both strains was inhibited, demonstrating that insufficient carbon levels did not support optimal microbial activity. For bacterial growth and survival, an appropriate concentration of organic contaminants serving as carbon sources was crucial. Deviations from this threshold, whether above or below, affected bacterial growth and development. This finding aligned with previous research, which showed that both excessive and inadequate substrate concentrations impacted microbial metabolic activities (Bonkowski et al., 2000; Gonzalez & Aranda, 2023).

This finding emphasized that the concentration of pollutants played a critical role in modifying bacterial activity. The distinctly evident growth of rhizobacteria in nitro-PAH-contaminated soil underscored their remarkable metabolic versatility and suggested their inherent adaptability to the harsh environmental conditions. The differential bacterial colonization among the studied plant species indicated that specific root exudates and plant-microbe interactions influenced bacterial abundance and survival. Furthermore, the ability of these bacterial strains to thrive in the presence of 1-nitropyrene and 2-nitrofluorene without supplementary nutrients highlighted their potential for effective bioremediation applications. Their sustained activity in contaminated soil demonstrated their role in natural attenuation processes, thereby supporting their use in strategies aimed at mitigating the detrimental effects of emerging contaminants in polluted ecosystems.

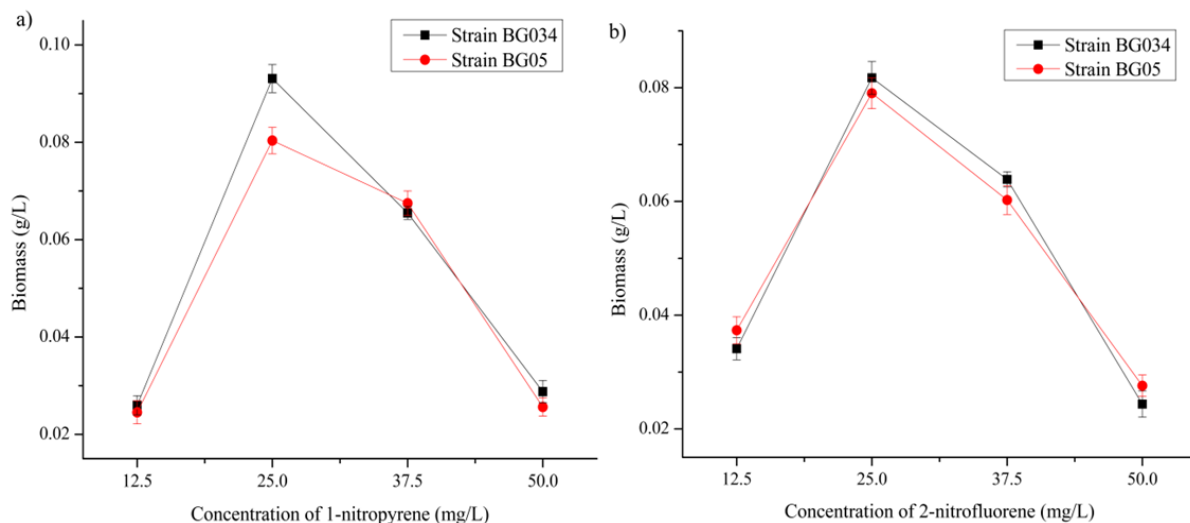


Fig. 4.11. Bacterial biomass (g/L) at different concentrations of 1-nitropyrene (a) and 2-nitrofluorene (b) after 7 days of incubation. The biomass of each bacterial strain increased with rising pollutant concentration, reaching the highest values at the threshold concentration of 25 mg/L in the respective nitro-PBYS medium. Data were expressed as means \pm S.D. (n = 3).

4.3. Biochemical Characterization

4.3.1. Gram Staining

Preliminary characterization of bacterial isolates was conducted by assessing their morphological traits after growth on nutrient agar. The colonies appeared circular with entire margins and exhibited a smooth surface texture, ranging from translucent to opaque. Gram staining was performed to further analyze the cell wall morphology. Microscopic examination at 100x magnification (Omax, Model No: M83EZ-C50U) confirmed that both isolates were Gram-positive, rod-shaped cocci (Fig. 4.12).

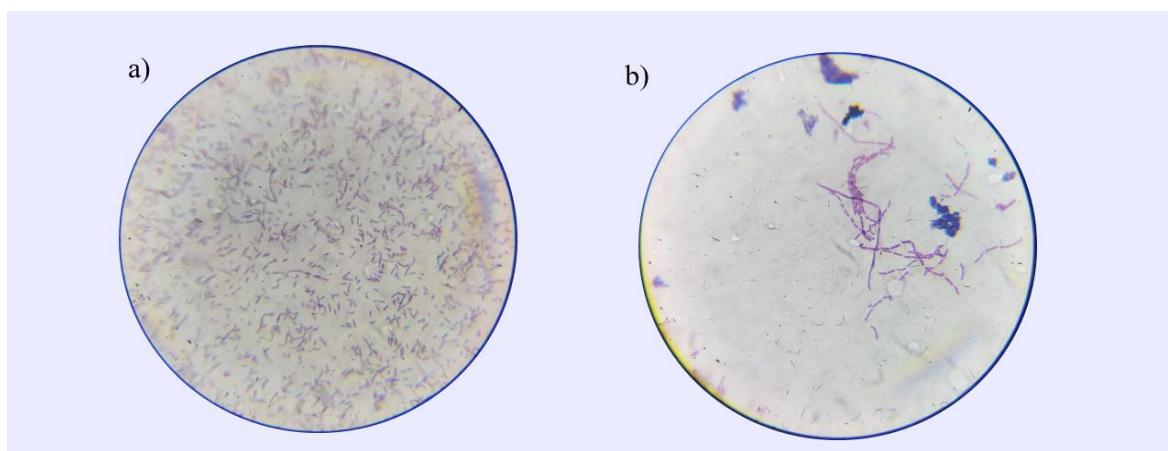


Fig. 4.12. Gram staining of isolated nitro-PAHs tolerant rhizobacterial strains BG034 (strain 1) (a), and strain BG05 (strain 2) (b).

4.3.2. Citrate Utilization

The citrate utilization assay was carried out to assess the ability of the isolated bacterial strains to use citrate as a sole carbon source. A positive outcome was noted by a change in the medium's color from green to blue, demonstrating the bacterial isolates' capacity to metabolize citrate. This color change is caused by an alkaline shift in the medium due to the formation of sodium carbonate, a metabolic product of citrate breakdown. The capacity to use citrate is a significant trait in bacterial classification, assisting in the distinguishing of species that flourish in citrate-abundant environments (Fig. 4.13 (a)). The positive citrate utilization results confirmed that the isolated bacterial strains possessed the enzyme citrate permease, enabling them to metabolize citrate as a sole carbon source (MacWilliams, 2009; Uzair, 2025). This metabolic capability not only supports their survival in citrate-rich environments but also provides valuable insights into their physiological and ecological adaptations. These findings contribute to bacterial classification and highlight the potential of these isolates in bioremediation processes.

4.3.3. Methyl Red Test

The methyl red test was used to assess the ability of bacterial isolates to produce stable acidic end products via glucose fermentation. A positive outcome was recorded in the isolates, evidenced by a prominent red coloration in the medium after the incorporation of the methyl red indicator (Mcdevitt, 2009). This color transition indicates a low pH (less than 4.4), which was caused by the formation of stable acidic metabolites including lactic, acetic, and formic acids during mixed acid fermentation pathways. The positive methyl red test result confirms that these isolates are capable of engaging in mixed acid fermentation, demonstrating their potential to metabolize nitro-PAHs efficiently and adapt to contaminated environments (Masi et al., 2021; Uzma et al., 2025). This metabolic trait is crucial to bacterial species that live in habitats with varied nutrition supplies, allowing them to effectively metabolize glucose and sustain growth across diverse conditions (Fig. 4.13 (b)).

4.3.4. Voges Proskauer Test

The Voges-Proskauer test was used to assess the bacterial isolates BG034 and BG05 to produce acetoin, which is a neutral byproduct of glucose fermentation via the butanediol pathway. Both isolates showed positive results in the Voges-Proskauer test, as demonstrated by a strong red color with the addition of Barritt's reagents (alpha-naphthol and potassium hydroxide) after a

few minutes incubation periods. The formation of this red coloration shows the presence of acetoin, which is oxidized to diacetyl in an alkaline environment, suggesting that BG034 and BG05 use the butanediol fermentation pathway (Mcdevitt, 2009; Mohany et al., 2025) (Fig. 4.13 (c)). The production of acetoin as a neutral byproduct of glucose metabolism, further supports their metabolic adaptability in nitro-PAH-contaminated environments.

4.3.5. Urease Test

The urease test was used to assess the bacterial isolates BGO34 and BG05 to hydrolyze urea, a process catalyzed by the enzyme urease. Both isolates were positive for the urease test by a color transformation in the urea agar slant to pink following incubation (Brink, 2010; Ahmeda & Patgiri, 2025). This color change indicates the conversion of urea into ammonia and carbon dioxide, which results in an alkaline atmosphere and a change in the pH indicator (Ali et al., 2020; Chang et al., 2022). The demonstrated urease activity in BG034 and BG05 (Fig. 4.13 (d)). The positive urease test confirmed that bacterial isolates BG034 and BG05 can hydrolyze urea, producing ammonia and carbon dioxide, which create an alkaline environment. This enzymatic activity suggests their ability to utilize urea as a nitrogen source, supporting survival in nitrogen-limited conditions

4.3.6. Catalase Test

The catalase assay evaluated the ability of bacterial isolates BG034 and BG05 to produce the enzyme catalase, which breaks down H_2O_2 into water and oxygen. Both isolates revealed good catalase activity, as seen by quick effervescence or bubbling when H_2O_2 was applied to the bacterial colonies (Iwase et al., 2013; Sharma et al., 2024). This reaction demonstrates that both of the isolates produce catalase, an enzyme that protects cells from oxidative damage by converting toxic byproducts of oxygen metabolism into less reactive entities (Yuan et al., 2021) (Fig 4.13 (e)). The strong catalase activity observed in BG034 and BG05 indicates their ability to detoxify hydrogen peroxide, highlighting their oxidative stress resistance and adaptability to aerobic environments.

4.3.7. Gelatine Test

The gelatinase assay was used to determine the isolated bacterial strains to produce gelatinase, an enzyme that hydrolyzes gelatine. Both isolates had positive gelatinase activity, as revealed by the liquefaction of the gelatine medium after incubation (dela Cruz & Torres, 2012). This result shows that BG034 and BG05 can degrade gelatine, indicating that they contain

gelatinase, an extracellular enzyme known for its role in nutrition acquisition and bacterial pathogenicity (Phuong et al., 2021) (Fig. 4.13 (f)). The positive gelatinase activity in BG034 and BG05 confirms their ability to hydrolyze gelatin, suggesting their potential role in nutrient acquisition in the environment.

4.3.8. Oxidase Test

The oxidase test was used to assess the bacterial isolates BG034 and BG05 for their production of the enzyme cytochrome c oxidase, which is an essential component of the electron transport chain in aerobic respiration (Chavan et al., 2022). Both isolates exhibited a positive oxidase response, evidenced by a color transition to dark purple following the introduction of the oxidase reagent (Kovács oxidase reagent), indicating the presence of cytochrome c oxidase (Khushboo et al., 2023). This positive result implies that BG034 and BG05 can use oxygen as the terminal electron acceptor in their respiratory pathways, underscoring their aerobic metabolic proficiency (Fig. 4.13 (g)).

The biochemical characterization of the isolated bacterial strains, including their enzymatic activities, is summarized in Table 4.4. The results of the citrate utilization, methyl red, Voges-Proskauer, oxidase, urease, catalase, and gelatinase tests provide insights into the metabolic capabilities of BG034 and BG05, highlighting their ability to utilize various substrates and produce key enzymes involved in bacterial survival and adaptation.

Table 4.4. The biochemical characterization of the isolated strains.

Strains	Citrate test	Methyl red test	Voges Proskauer test	Oxidase test	Urease test	Catalase test	Gelatine test
Strain BG034	+ ve	+ ve	+ ve	+ ve	+ ve	+ ve	+ ve
Strain BG05	+ ve	+ ve	+ ve	+ ve	+ ve	+ ve	+ ve

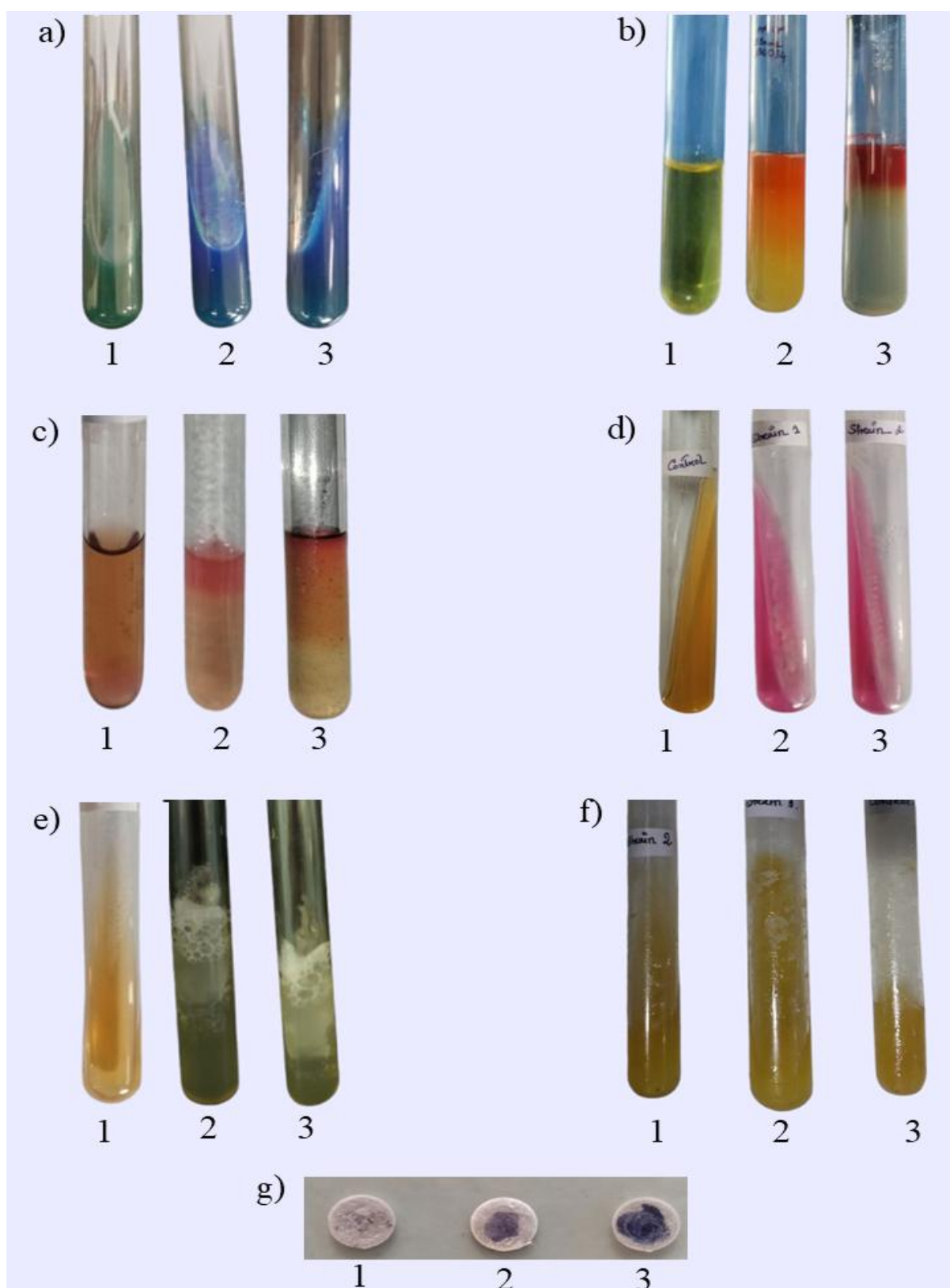


Fig. 4.13. Various biochemical tests of the isolated strains—Citrate test (a), Methyl red test (b), Voges-Proskauer test (c), Urease test (d), Catalase test (e), Gelatin test (f), and Oxidase Test (g). In each test, (1) represents the control, (2) represents strain BG034, and (3) represents strain BG05.

4.4. Molecular Characterization and Phylogenetic Analysis

DNA extraction and 16S rDNA sequencing were performed to identify the bacterial strains, isolated from the rhizosphere soils of selected plant species. The 16S rDNA region was effectively amplified using the universal primers 27F (5'-CAGAGTTTGATCCTGGCT-3') and 1492R (5'-AGGAGGTGATCCAGCCGCA-3'), resulting in a distinct band of about 1500 bp for both isolates, as shown in Fig. 4.14. The electropherograms of corresponding 16S rDNA sequences of the isolates are illustrated in Fig. 4.15 and 4.16, providing a detailed visual representation of the sequencing results. The resultant sequences were subsequently BLAST in the NCBI to identify correlations within the GenBank database, thereby validating the identity of the bacterial isolates. One isolate had a 99.66% similarity to *Bacillus cereus*, while the other had a 99.15% similarity to *Bacillus altitudinis*, indicating that they were closely related to known sequences from these species. These sequences were subsequently submitted to GenBank, with accession numbers PQ394621 for *Bacillus cereus* BG034 (strain 1) and PQ390296 for *Bacillus altitudinis* BG05 (strain 2), thereby augmenting the database for future reference and comparative investigations (Fig. 4.17 and 4. 18).

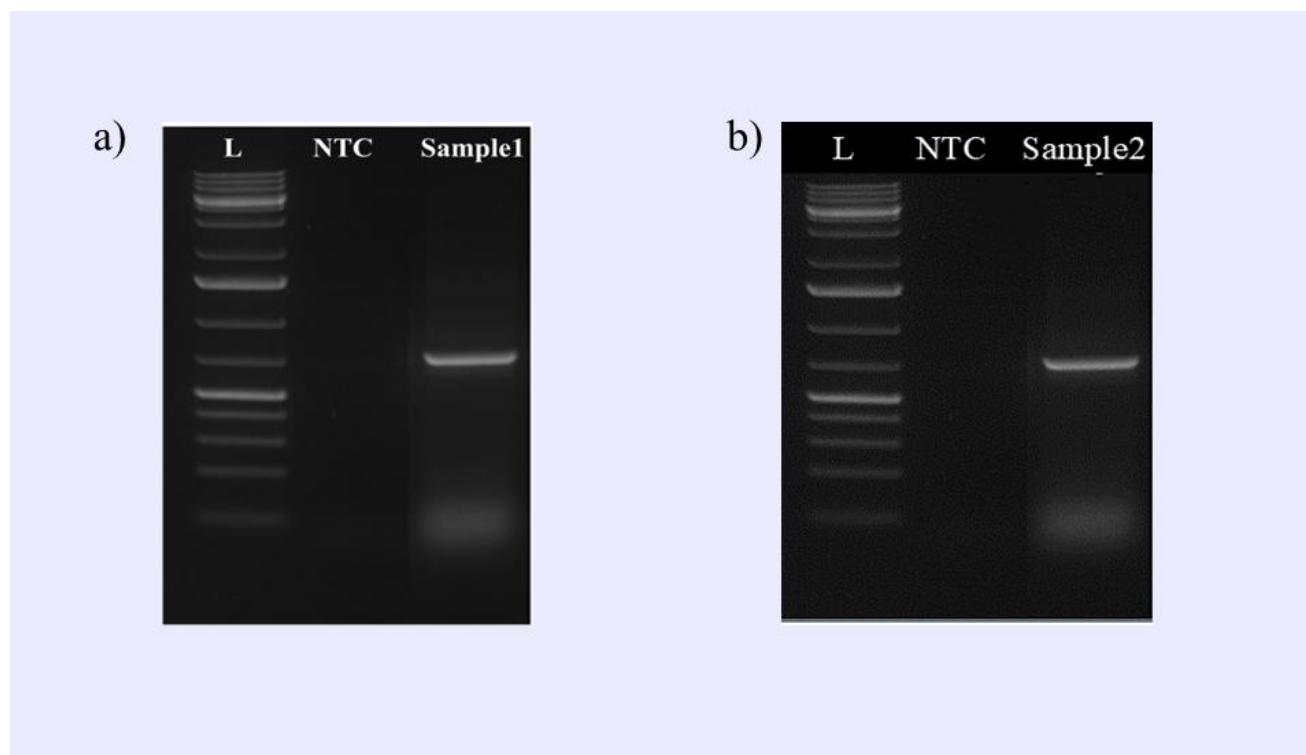


Fig. 4.14. Amplicon photographs of (a) *Bacillus cereus* BG034 and (b) *Bacillus altitudinis* BG05

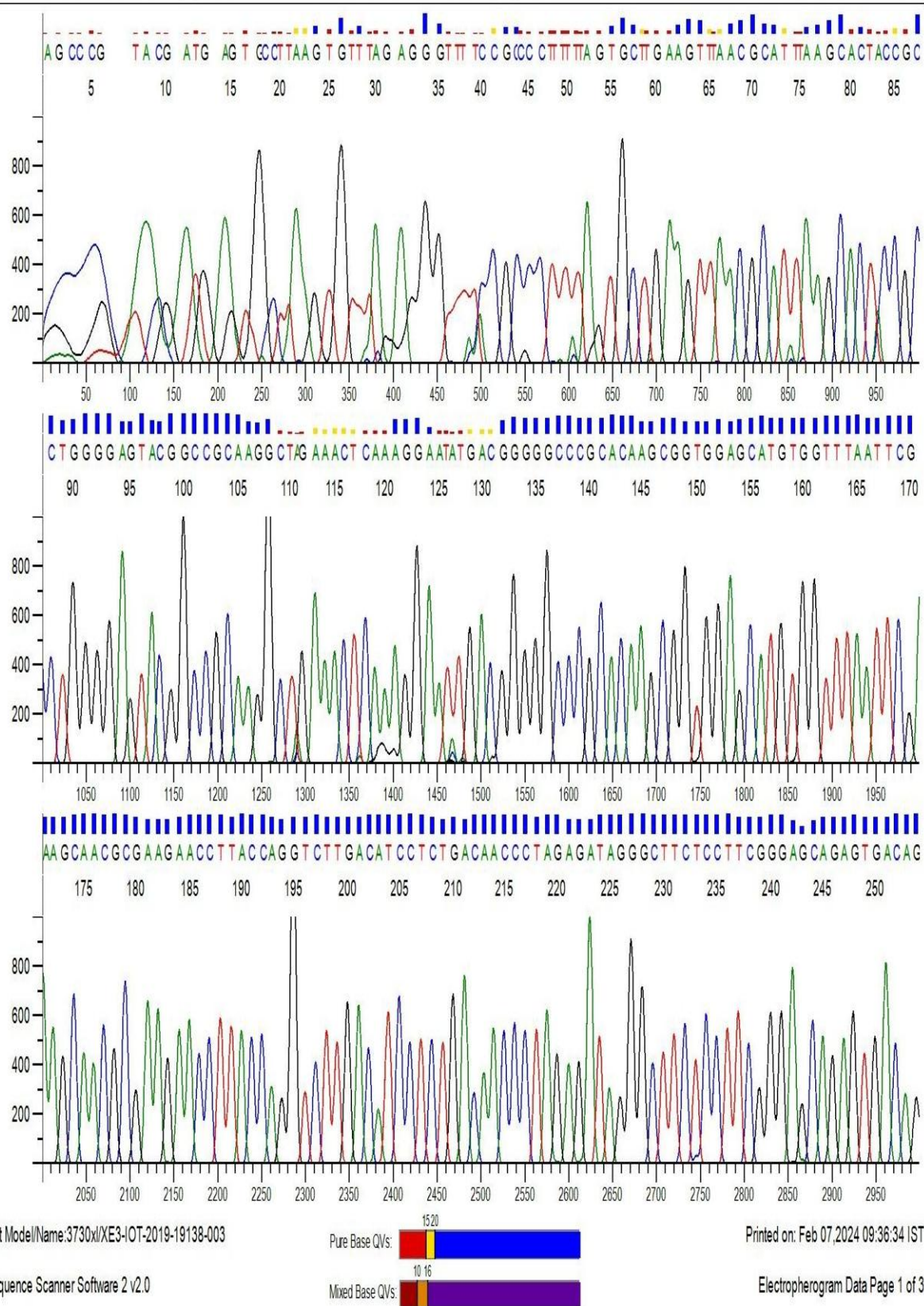


Fig. 4.15. Electropherogram of *Bacillus cereus* BG034 16S rDNA

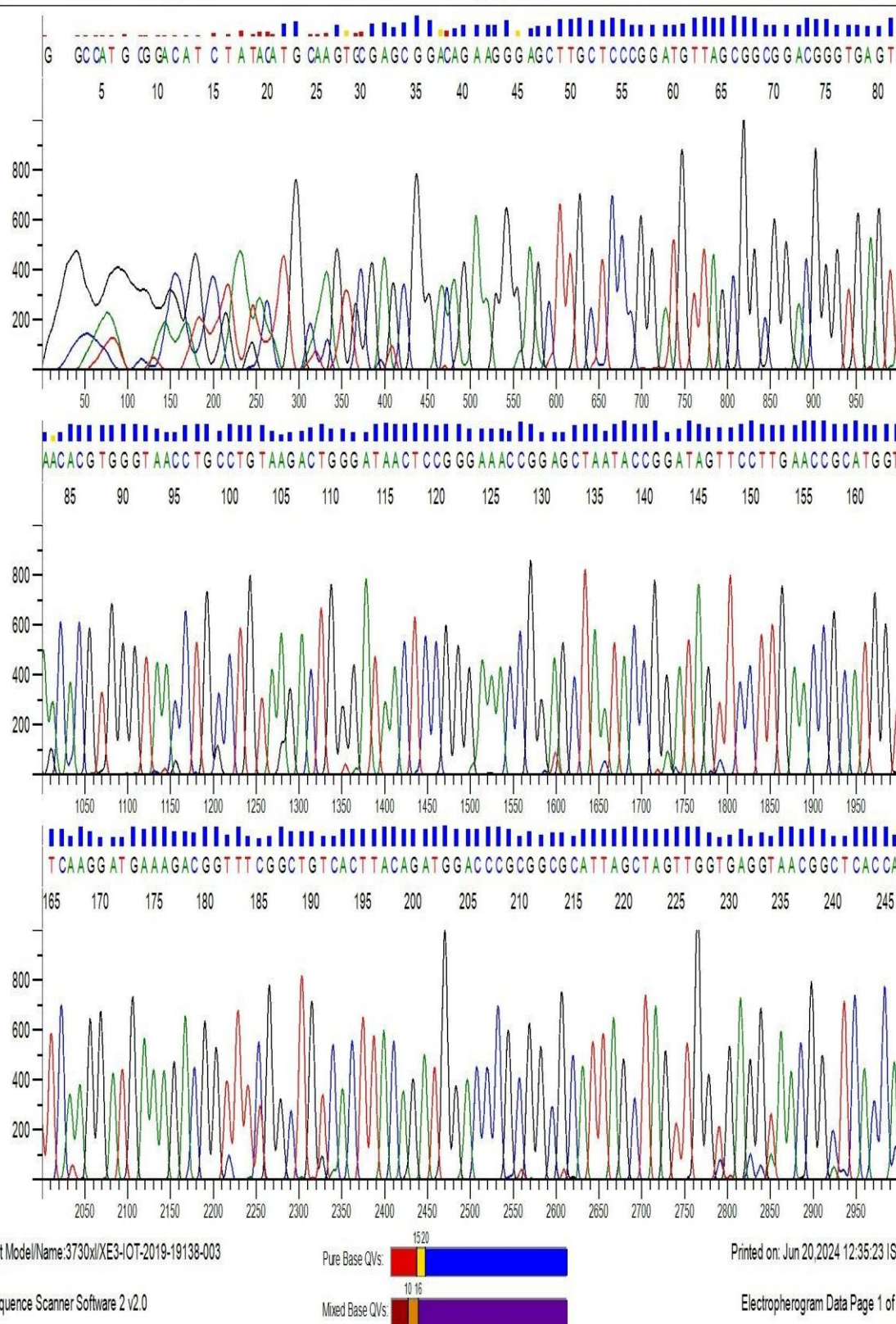


Fig. 4.16. Electropherogram of *Bacillus altitudinis* BG05 16S rDNA

Bacillus cereus strain BG034 16S ribosomal RNA gene, partial sequence

GenBank: PQ394621.1

[FASTA](#) [Graphics](#)

Go to: ☐

LOCUS PQ394621 906 bp DNA linear BCT 03-OCT-2024
DEFINITION Bacillus cereus strain BG034 16S ribosomal RNA gene, partial sequence.
ACCESSION PQ394621
VERSION PQ394621.1
KEYWORDS .
SOURCE Bacillus cereus
ORGANISM [Bacillus cereus](#)
Bacteria; Bacillati; Bacillota; Bacilli; Bacillales; Bacillaceae; Bacillus; Bacillus cereus group.
REFERENCE 1 (bases 1 to 906)
AUTHORS Gogoi,B. and Sarma,H.
TITLE Bacterial isolated from rhizosphere of nitro-PAHs tolerate plant species grown near Borhulla ONGC's GGS
JOURNAL Unpublished
REFERENCE 2 (bases 1 to 906)
AUTHORS Gogoi,B. and Sarma,H.
TITLE Direct Submission
JOURNAL Submitted (28-SEP-2024) Botany, Bodoland University, Deborgaon, Kokrajhar, Assam 783370, India
COMMENT ##Assembly-Data-START##
Sequencing Technology :: Sanger dideoxy sequencing
##Assembly-Data-END##
FEATURES
source Location/Qualifiers
1..906
/organism="Bacillus cereus"
/mol_type="genomic DNA"
/strain="BG034"
/db_xref="taxon:1396"
/geo_loc_name="India: Borhulla ONGC's GGS"
/collection_date="04-May-2023"
rRNA
<1..906
/product="16S ribosomal RNA"
ORIGIN
1 ttttagagtt taatcctggc tcaggatgaa cgctggcggc gtcctaata catgcaagtc
61 gagcgaatgg attaagagct tgctcttatg aagtttagcg cggacgggtg agtaacacgt
121 gggtaacctg ccataagac tgggataact cgggaaacc ggggctaata ccggataaca
181 ttctgaactg catggttcga aattgaaagg cggcttcggc tgtcacttat ggatggaccc
241 gcgtcgcatg agctagttgg tgaggtaacg gctcaccaag gcaacgatgc gtagccgacc
301 tgagaggggtg atcggccaca ctgggactga gacacggccc agactcctac gggaggcagc
361 agtaggggaat cttccgcaat ggacgaaagt ctgacggagc aacgccgcgt gagtgatgaa
421 ggctttcggg tcgtaaaact ctgttgtagt ggaagaacaa gtgctagttg aataagctgg
481 caccttgacg gtacctaacc agaaagccac ggctaactac gtgccagcag ccgggtaat
541 acgtagggtg caagcgttat ccggaattat tgggcgtaaa gcgcgcgcag gtgtttctt
601 aagtctgatg tgaagccca cggctcaacc gtggagggtc attggaact gggagacttg
661 agtcgagaag aggaagtgg aattccatgt gtagcgggtg aatgcgtaga gatatggagg
721 aacaccagtg gcgaaggcga ctttctggtc tgtaactgac actgaggcgc gaaagcgtgg
781 ggagcaaaca ggattagata ccctgtagt ccacgccgta aacgatgagt gctaagtgtt
841 agagggttc cgccctttag tgctgaagtt aacgcattaa gcactccgca tggggagacc
901 gtccca
//

Fig. 4.17. The submitted gene sequence of *Bacillus cereus* BG034 in GenBank

Bacillus altitudinis strain BG05 16S ribosomal RNA gene, partial sequence

GenBank: PQ390296.1

[FASTA](#) [Graphics](#)

LOCUS PQ390296 945 bp DNA linear BCT 02-OCT-2024

DEFINITION *Bacillus altitudinis* strain BG05 16S ribosomal RNA gene, partial sequence.

ACCESSION PQ390296

VERSION PQ390296.1

KEYWORDS .

SOURCE *Bacillus altitudinis* (*Bacillus invictae*)ORGANISM [Bacillus altitudinis](#)Bacteria; Bacillati; Bacillota; Bacilli; Bacillales; Bacillaceae; *Bacillus*.

REFERENCE 1 (bases 1 to 945)

AUTHORS Gogoi, B. and Sarma, H.

TITLE Bacterial isolated from rhizosphere of nitro-PAHs tolerate plant species grown near Borhulla ONGC's GGS

JOURNAL Unpublished

REFERENCE 2 (bases 1 to 945)

AUTHORS Gogoi, B. and Sarma, H.

TITLE Direct Submission

JOURNAL Submitted (27-SEP-2024) Botany, Bodoland University, Deborgaon, Kokrajhar, Assam 783370, India

COMMENT ##Assembly-Data-START##

Sequencing Technology :: Sanger dideoxy sequencing

##Assembly-Data-END##

FEATURES Location/Qualifiers

source 1..945

/organism="Bacillus altitudinis"

/mol_type="genomic DNA"

/strain="BG05"

/db_xref="taxon:293387"

/geo_loc_name="India: Borhulla ONGC's GGS"

/collection_date="04-May-2023"

rRNA <1..945

/product="16S ribosomal RNA"

ORIGIN

```

1  gaggcagcaa tagggatttt tccgcaatgg acgaaagttt gacggagcaa cgccgcgtga
61  gggatgaagg ttttcggatc gtaaagcttt gttgttaggg aagaacaagt gcaagagtaa
121  ttgcttgcac cttgacggta cctaaccaga aagccccggc taactacgtg ccagcagccg
181  cggtaatagc taggtggcaa gcgttggtcc gaattattgg gcgtaaaggg ctgcagggcg
241  gtttccttaa gtctgatgtg aaagcccccg gctcaaccgg ggagggtcat tggaaactgg
301  gaaacttgag tgcagaagag gagagtggaa ttccacgtgt agcggtgaaa tgcgtagaga
361  tgtggaggaa caccagtggc gaaggcgact ctctggtctg taactgacgc tgaggagcga
421  aagcgtgggg agcgaacagg attagatacc ctggtagtcc acgccgtaaa cgatgagtgc
481  taagtgttag ggggtttccg ccccttagtg ctgcagctaa cgattaagc actccgcctg
541  gggagtacgg tcgcaagact gaaactcaaa ggaattgacg ggggcccgca caagcgggtg
601  agcatgtggt ttaattcgaa gcaacgcgaa gaaccttacc aggtcttgac atcctctgac
661  aaccctagag atagggtttt cccttcgggg acagagtgcg aggtggtgca tgggtgtcgt
721  cagctcgtgt cgtgagatgt tgggttaagt cccgcaacga gcgcaaccct tgatcttagt
781  tgccagcatt cagttgggca ctctaagggt actgccggtg acaaaccgga ggaagggtggg
841  gatgacgtca aatcatcatg ccccttatga cctgggctac acacgtgcta caatggacag
901  aacaaagggc tgcgagaccg caaggttttag ccaatccac aaatc

```

//

Fig. 4.18. The submitted gene sequence of *Bacillus altitudinis* BG05 in GenBank

Phylogenetic analysis was performed to elucidate the evolutionary relationships and genetic distances between the isolates and other related species. Phylogenetic trees were generated in MEGA11 using neighbor-joining and maximum likelihood methods, revealing information on their taxonomic placements within the *Bacillus* genus. The neighbor-joining tree illustrated the relationships among these sequences, underscoring the clustering of strain 1 (BG034) with *Bacillus cereus* and strain 2 (BG05) with *Bacillus altitudinis*, corroborating the findings from the BLAST analysis. To improve visual clarity, the phylogenetic tree was exported to iTOL and subsequently annotated (Fig. 4.19). The use of iTOL simplified the graphical representation of evolutionary relationships, with each branch length and node offering a visual knowledge of genetic similarity and divergence between isolates and related species.

The positioning of *Bacillus cereus* and *Bacillus altitudinis* within the phylogenetic tree affirms their close genetic relationship with other *Bacillus* species, further reinforcing their resilience and potential functional roles in environmental remediation. For instance, Mandree et al. (2021) isolated *Bacillus cereus* from a hydrocarbon-contaminated location and demonstrated its ability to degrade PAHs, emphasizing its utility in managing recalcitrant pollutants (Mandree et al., 2021). In a similar vein, Zhang et al. (2024) reported that *Bacillus cereus* GX7, which was isolated from an oil-contaminated environment, has an extraordinary ability to degrade petroleum compounds. These studies highlight *Bacillus cereus*' strain-specific capacity to remove pollutants under a variety of environmental settings (Zhang et al., 2024). Likewise, Kalami and Pourbabaee (2021) isolated *Bacillus altitudinis* from oil-contaminated soils and identified it as a promising candidate for bioremediation (Kalami & Pourbabaee, 2021). Further research by Su et al. (2023) corroborated this, revealing that *Bacillus altitudinis* effectively degrades complex hydrocarbon compounds, establishing it as a viable tool for tackling environmental pollution (Su et al., 2023). In addition to hydrocarbon degradation, members of the *Bacillus* genus are reported to withstand a broad range of environmental stress, such as severe temperatures, salt, and pH variations. Their capacity to generate robust endospores is critical to their survival and functional effectiveness in polluted or nutrient-deficient settings. Furthermore, their broad enzymatic repertoire aids in the reduction of complex hazardous organic compounds and helps to be a viable candidate for the remediation of contaminants (Mandree et al., 2021). These studies corroborated our hypothesis that *Bacillus cereus* and *Bacillus altitudinis* have the potential to be key agents in bioremediation. The discovery of these two strains highlights their potential utility in upcoming phytoremediation

research, notably their capacity to tolerate and potentially degrade nitro-PAHs, as demonstrated by previous growth experiments on nitro-PAH.



Fig. 4.19. The neighbor-joining phylogenetic tree is based on 16S rDNA sequences, illustrating the taxonomic position of nitro-PAHs tolerance isolated bacteria (yellow highlighted) and NCBI bacteria references.

4.5. Compatibility Assessment and Biodegradation Efficiency of nitro-PAH-Degrading Rhizobacteria

The compatibility assessment of *Bacillus cereus* BG034 and *Bacillus altitudinis* BG05 showed that both strains coexisted without inhibitory interactions, as evidenced by their sustained

growth near a shared medium (Fig. 4.20). This result was significant as it indicated their potential to function as a co-inoculum in biotechnological applications. The successful co-cultivation of these strains suggested their suitability for multi-strain formulations, particularly in biofertilization and bioremediation. The use of a co-inoculum containing these bacterial species could have improved soil nutrient cycling and pollutant degradation, emphasizing the importance of microbial synergy in sustainable environmental management.

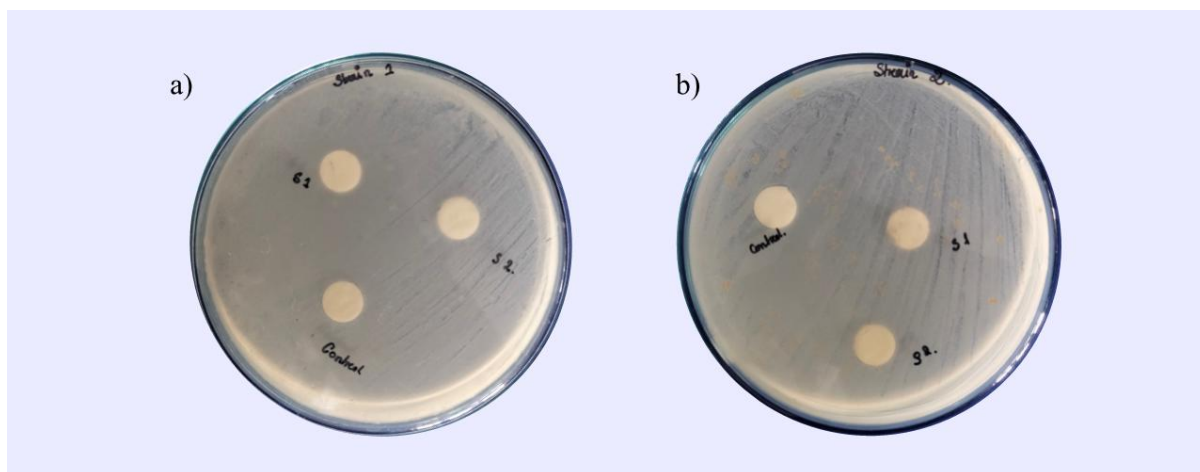


Fig. 4.20. Compatibility test of the bacterial strains *Bacillus cereus* BG034, and against *Bacillus altitudinis* BG05 (a) and *Bacillus altitudinis* BG05 against *Bacillus cereus* BG034 (b).

The degradation capabilities of isolated bacterial strains on nitro-PAHs, focusing on two model contaminants: 1-nitropyrene and 2-nitrofluorene, were conducted in a shaker flask. The nitro-PAHs chosen for this experiment are prevalent in polluted environments and pose significant challenges for removal. Their complex chemical structures make them resistant to natural degradation processes. The nitro-PAH-tolerant rhizosphere bacterial species were isolated and identified from rhizosphere soils collected from plant species known for their exceptional adaptability in the polluted sampling site, and they are reported to have the potential to accumulate nitro-PAHs in previous controlled experiments. In this study, nitro-PAHs-PBYS medium was used in a controlled environment (Fig. 4.21). In this medium, 1-nitropyrene and 2-nitrofluorene were used as the only carbon sources at a concentration of 25 mg/L, which the bacterial strains potentially utilized in the absence of additional carbon sources. By constraining the bacteria to rely only on nitro-PAHs for energy and growth, the experimental design directly examined each strain and co-inoculum's capacity to use these substances. The quantitative evaluation of 1-nitropyrene and 2-nitrofluorene was further facilitated by using

similar standard calibration curves depicted in Fig. 4.2. The HPLC chromatogram illustrating the abiotic degradation of 1-nitropyrene over different time intervals is presented in Fig. 4.22. The bacterial degradation of 1-nitropyrene by *Bacillus cereus* BG034 is shown in Fig. 4.23, while Fig. 4.24 and Fig. 4.25 depict the degradation by *Bacillus altitudinis* BG05 and the co-inoculum BGC01, respectively. Similarly, the HPLC chromatogram for the abiotic degradation of 2-nitrofluorene is presented in Fig. 4.26. The corresponding microbial degradation is illustrated in Fig. 4.27 for *Bacillus cereus* BG034, Fig. 4.28 for *Bacillus altitudinis* BG05, and Fig. 4.29 for the co-inoculum BGC01.

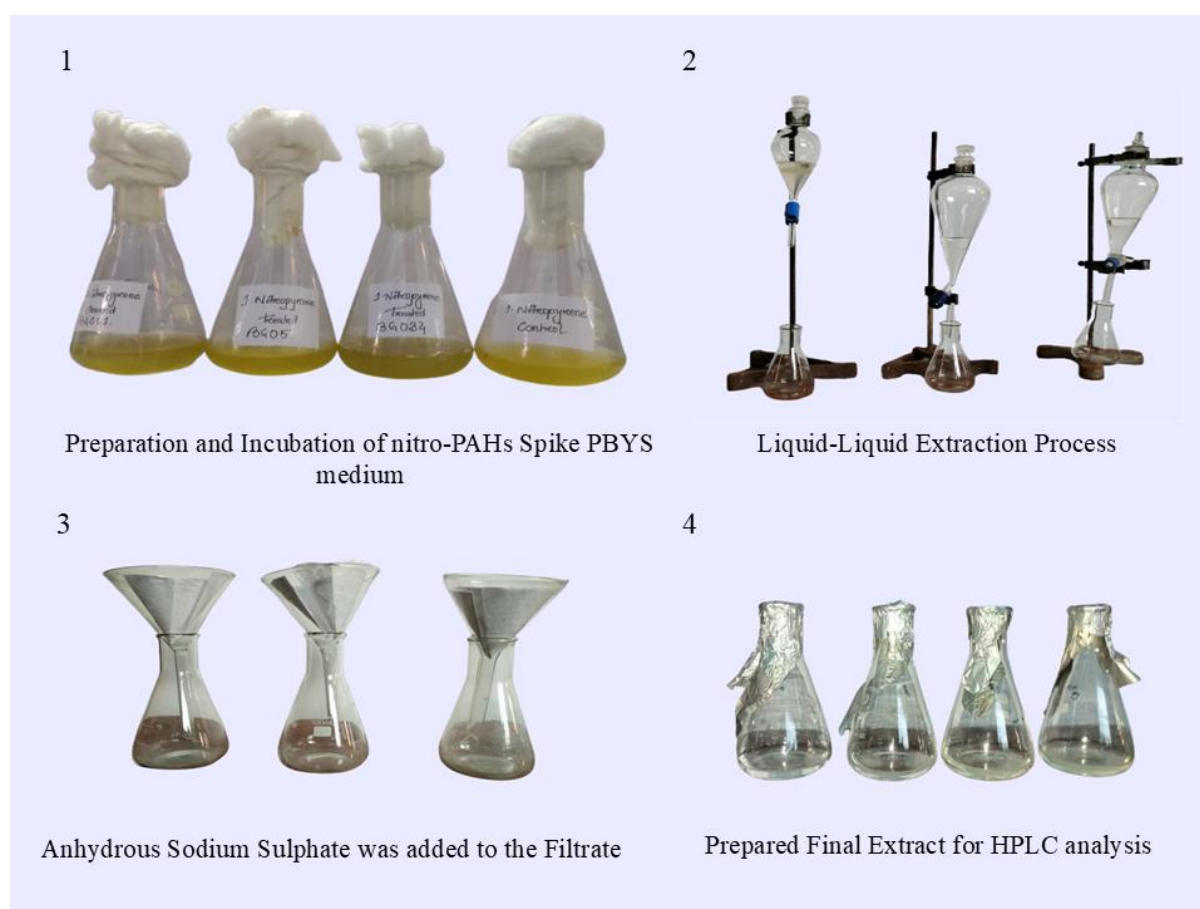


Fig. 4.21. Schematic representation of the degradation study conducted under shaker flask conditions.

To achieve consistent and reliable results, 1-nitropyrene and 2-nitrofluorene concentrations (mg/L) were normalized at the onset of each experiment, allowing for precise comparisons of breakdown rates between different bacterial treatments. This standardization provided a baseline against which the efficacy of each bacterial strain and its co-inoculum could be assessed. By specifying a specific beginning concentration, degradation trends (in terms of

percentage) were carefully tracked at regular intervals and documented in Table 4.5, with any drop in nitro-PAH concentration (mg/L) explicitly tied to bacterial activity rather than changes in the initial circumstances. The biodegradation of the respective pollutants was determined by using the following formula

$$\text{Degradation \%} = \frac{\text{Initial concentration} - \text{Final concentration}}{\text{Initial concentration}} \times 100\% \quad (\text{Sarma, et al., 2019})$$

The results of the degradation experiments show that using the co-inoculum BGC01, which contains two bacterial strains—*Bacillus cereus* BG034 and *Bacillus altitudinis* BG05—significantly improves the degradation of nitro-PAHs throughout the experiment. BGC01 consistently outperformed each individual strain in breaking down both 1-nitropyrene and 2-nitrofluorene, indicating a synergistic effect when both strains are used together. For the degradation of 1-nitropyrene, BGC01 demonstrated rapid breakdown, achieving 46% degradation within the first 24 hours. In comparison, strain BG034 and strain BG05 recorded 19% and 26.4%, respectively. By the end of 48 hours, the degradation efficiency had significantly increased, with BGC01 reaching 66%, BG034 at 40%, and BG05 at 36%. The highest degradation percentages were recorded at 72 hours, with BGC01 at 76%, BG034 at 47.84%, and BG05 at 49.04%.

Similarly, Strain BG034 degraded 2-nitrofluorene by 31.16% over a 24-hour period, while strain BG05 closely followed with a degradation rate of 26.16%. Notably, the co-inoculum exhibited enhanced efficiency, achieving a degradation percentage of 54.08% within the same timeframe. As incubation time increased, degradation levels also rose, with strain BGC01 reaching 87.20% degradation at 72 hours. This surpassed both BG034 and BG05, which recorded degradation rates of 59.96% and 59.88%, respectively. Fig. 4.30 (a, b) shows a decrease in nitro-PAH concentrations (mg/L) over time, illustrating the degradation patterns of the two bacterial strains, the co-inoculum, and the control, plotted against the treatment duration.

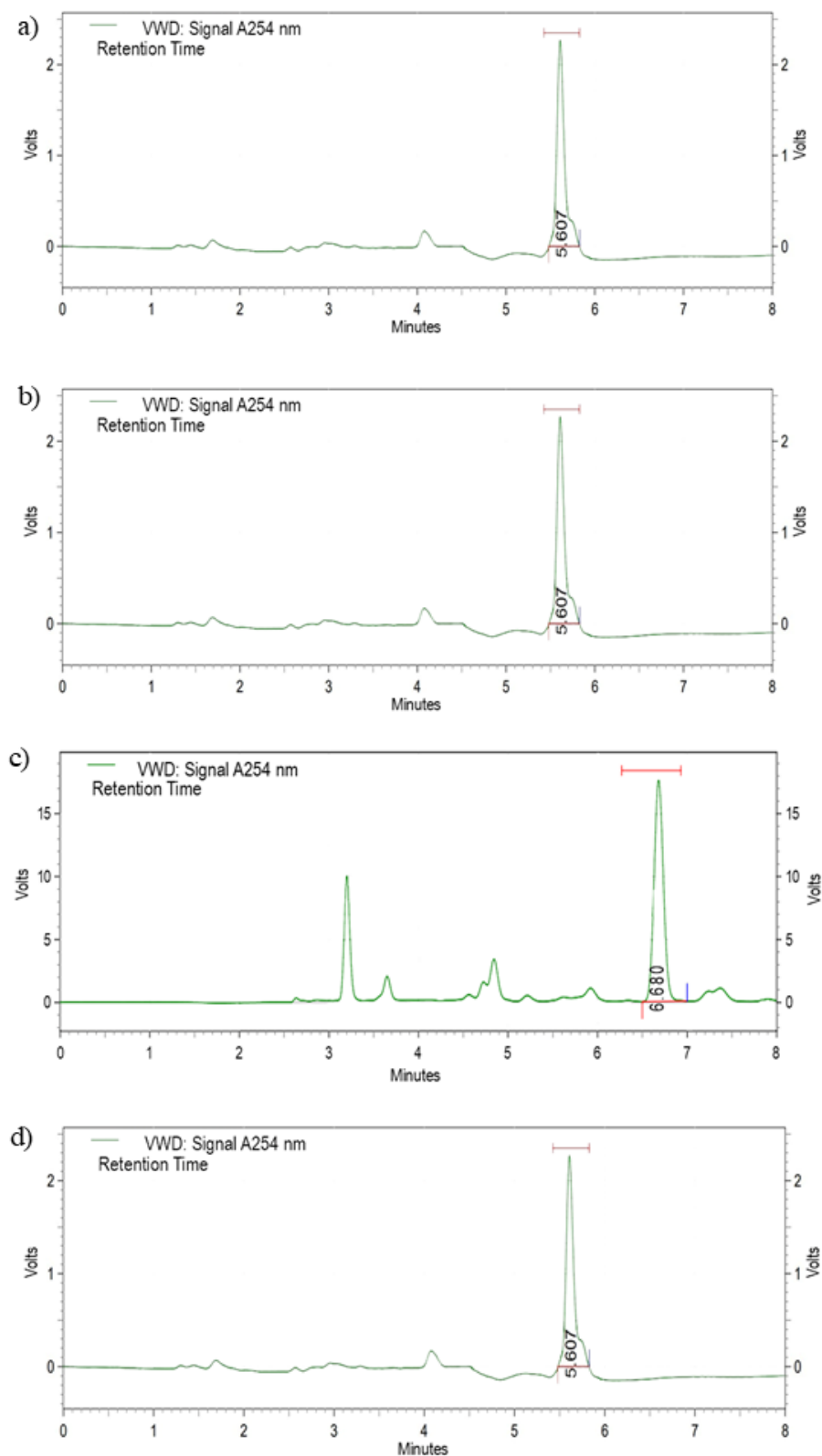


Fig. 4.22. Representative HPLC chromatogram illustrating the abiotic degradation of 1-nitropyrene in 1-nitropyrene-spiked PBYS medium at different time intervals: (a) 0 hours, (b) 24 hours, (c) 48 hours, and (d) 72 hours.

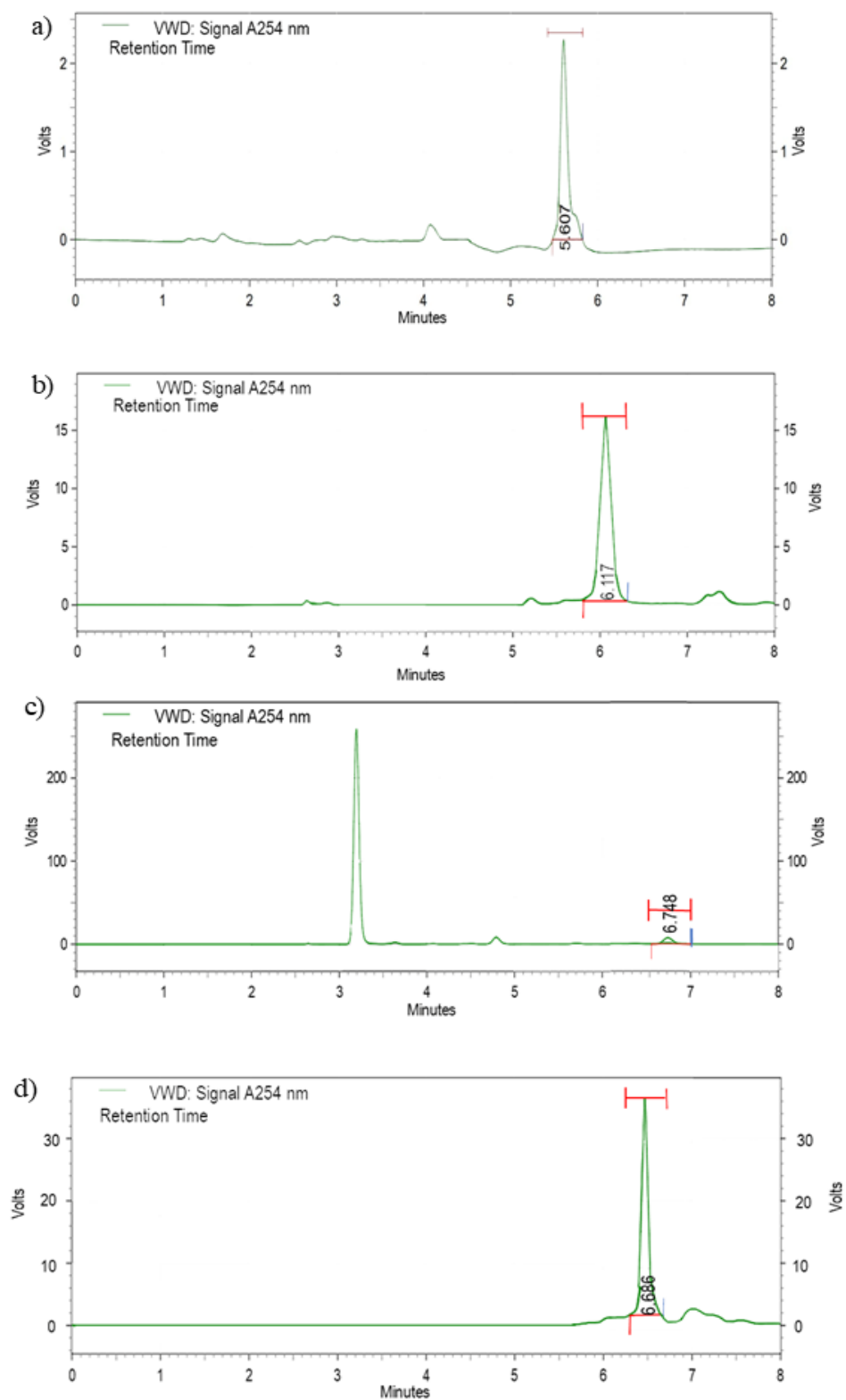


Fig. 4.23. Representative HPLC chromatogram illustrating the degradation of 1-nitropyrene by *Bacillus cereus* BG034 in 1-nitropyrene-spiked PBYS medium at different time intervals: (a) 0 hours, (b) 24 hours, (c) 48 hours, and (d) 72 hours.

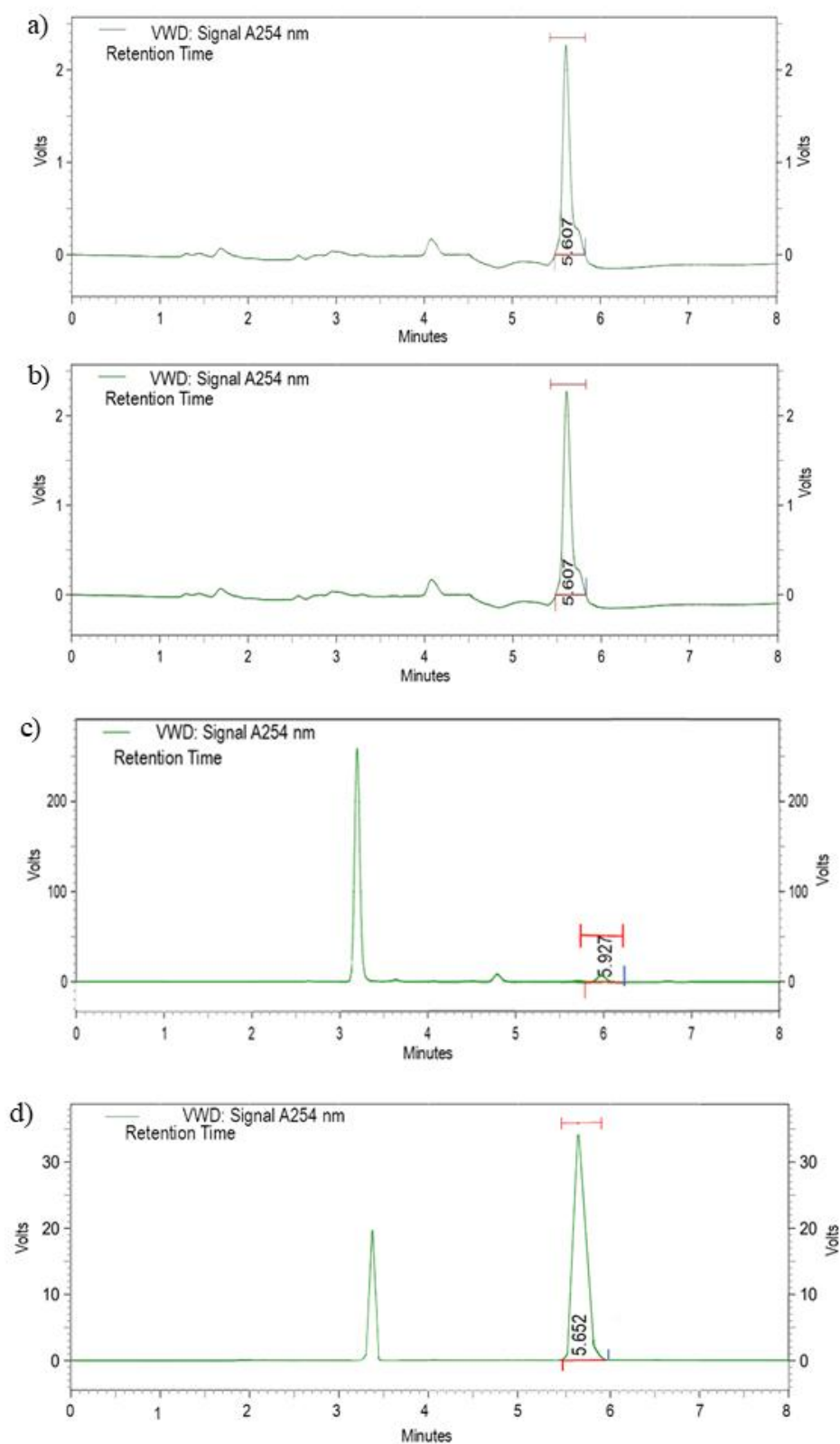


Fig. 4.24. Representative HPLC chromatogram illustrating the degradation of 1-nitropyrene by *Bacillus altitudinis* BG05 in 1-nitropyrene-spiked PBYS medium at different time intervals: (a) 0 hours, (b) 24 hours, (c) 48 hours, and (d) 72 hours.

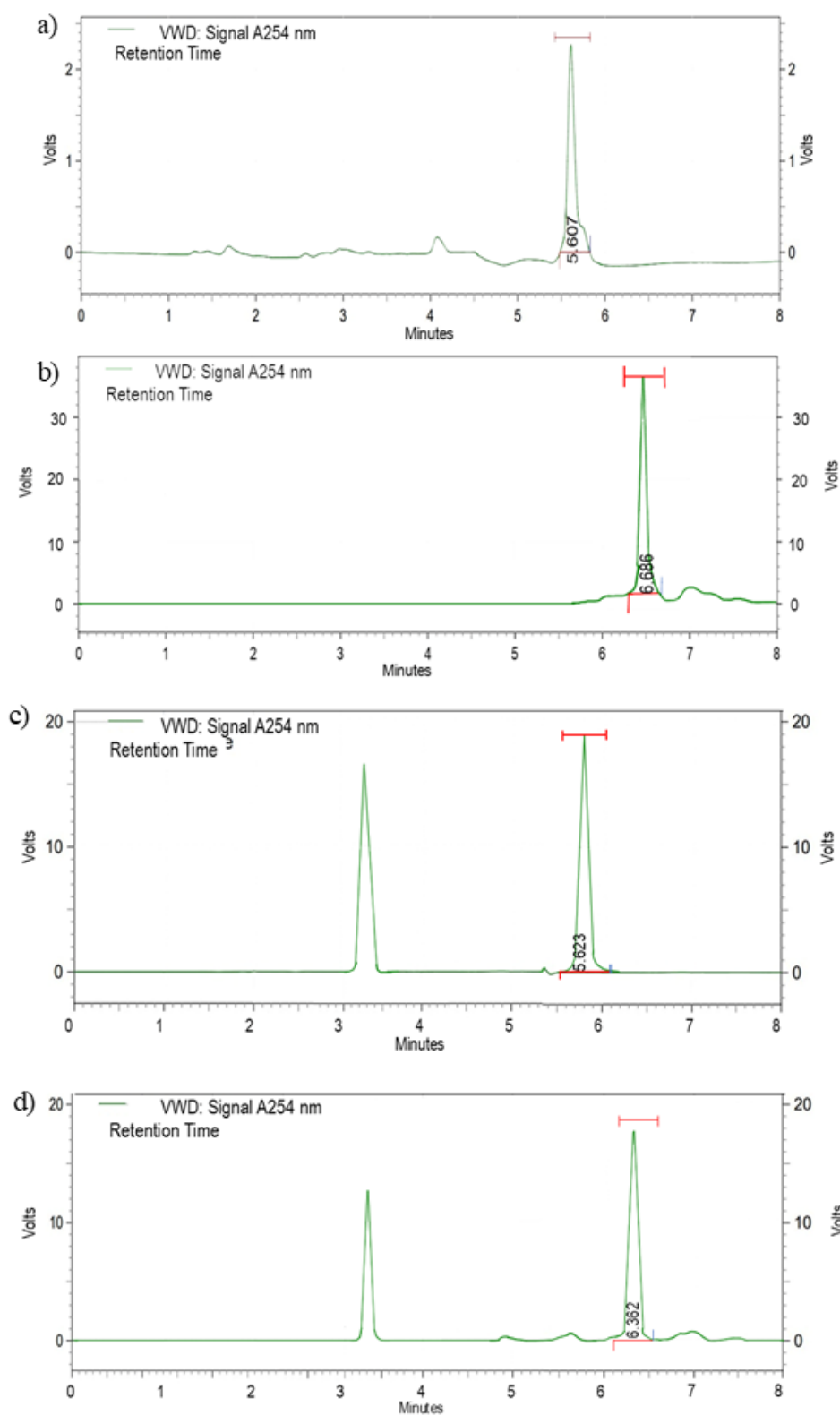


Fig. 4.25. Representative HPLC chromatogram illustrating the degradation of 1-nitropyrene by Co-inoculum BGC01 in 1-nitropyrene-spiked PBYS medium at different time intervals: (a) 0 hours, (b) 24 hours, (c) 48 hours, and (d) 72 hours.

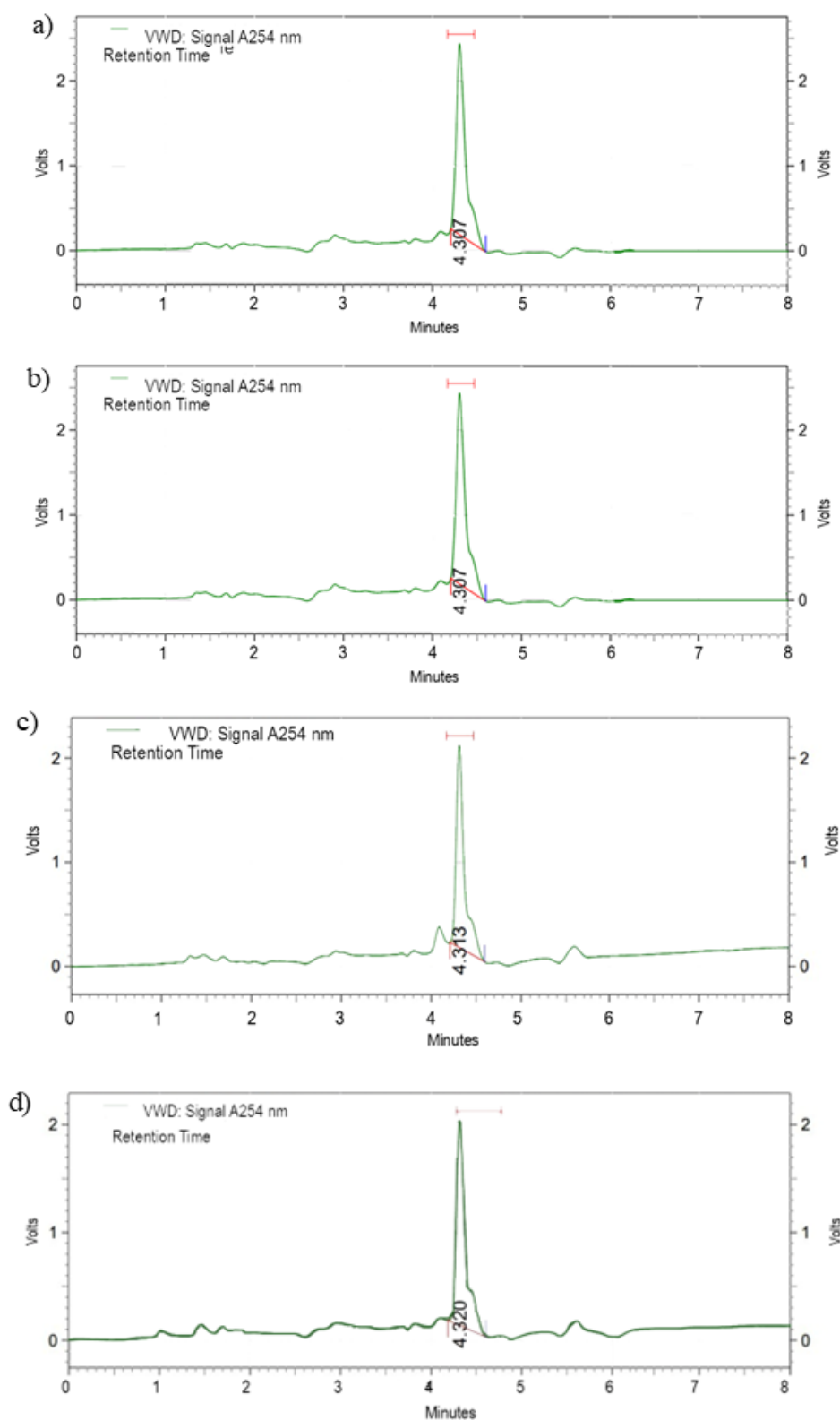


Fig. 4.26. Representative HPLC chromatogram illustrating the abiotic degradation of 2-nitrofluorene in 2-nitrofluorene-spiked PBYS medium at different time intervals: (a) 0 hours, (b) 24 hours, (c) 48 hours, and (d) 72 hours.

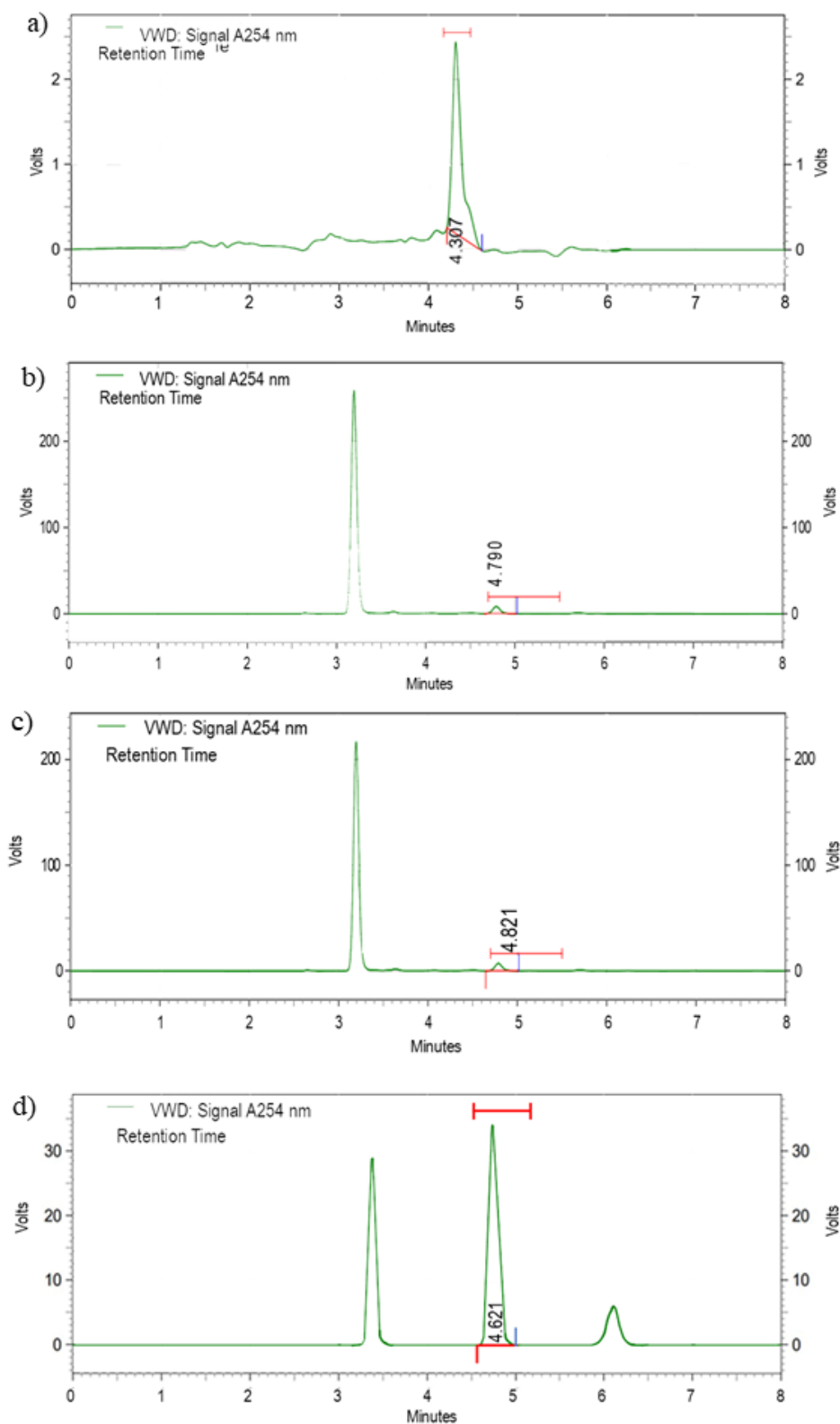


Fig. 4.27. Representative HPLC chromatogram illustrating the degradation of 2-nitrofluorene by *Bacillus cereus* BG034 in 2-nitrofluorene-spiked PBYS medium at different time intervals: (a) 0 hours, (b) 24 hours, (c) 48 hours, and (d) 72 hours.

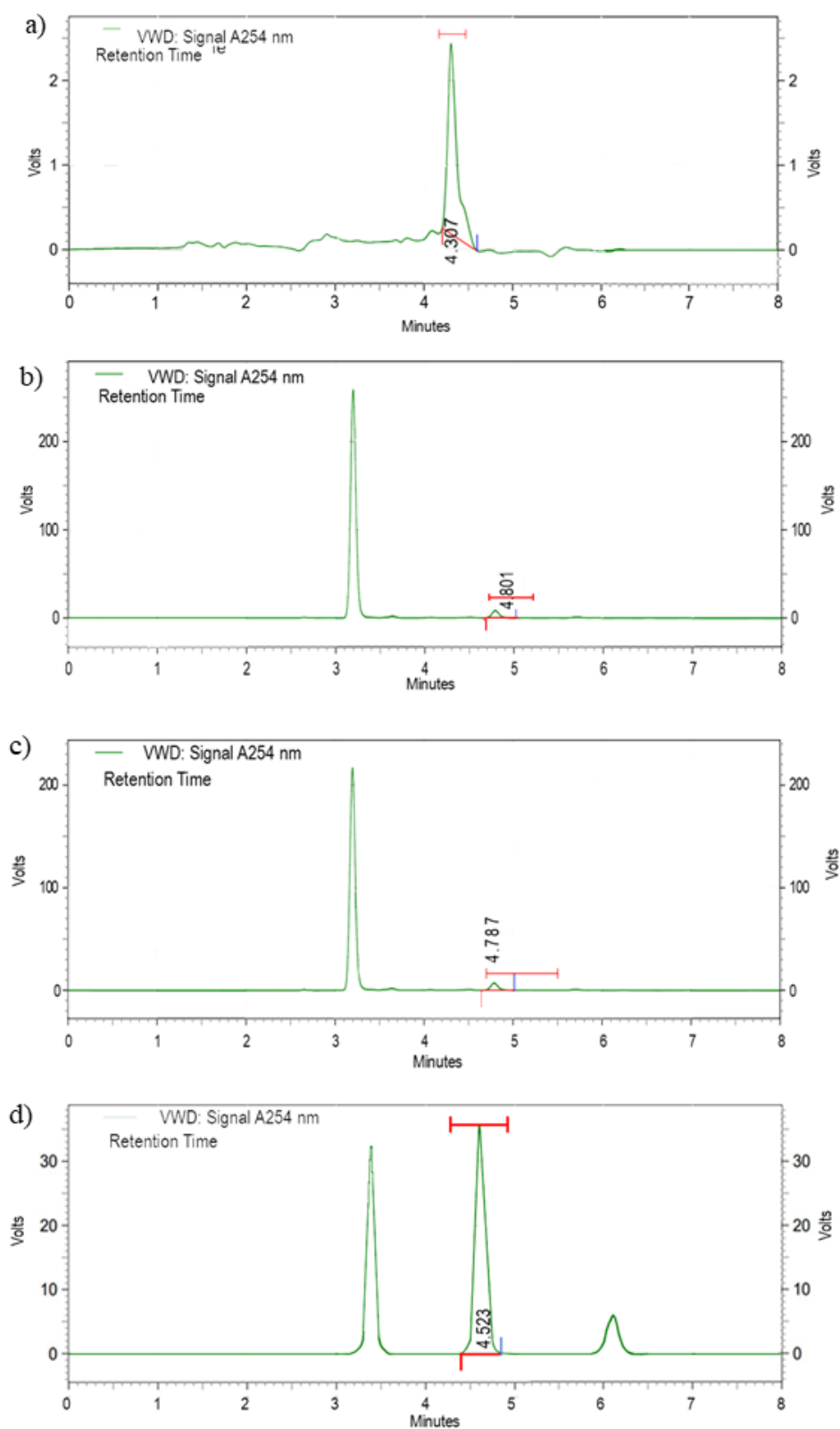


Fig. 4.28. Representative HPLC chromatogram illustrating the degradation of 2-nitrofluorene by *Bacillus altitudinis* BG05 in 2-nitrofluorene-spiked PBYS medium at different time intervals: (a) 0 hours, (b) 24 hours, (c) 48 hours, and (d) 72 hours.

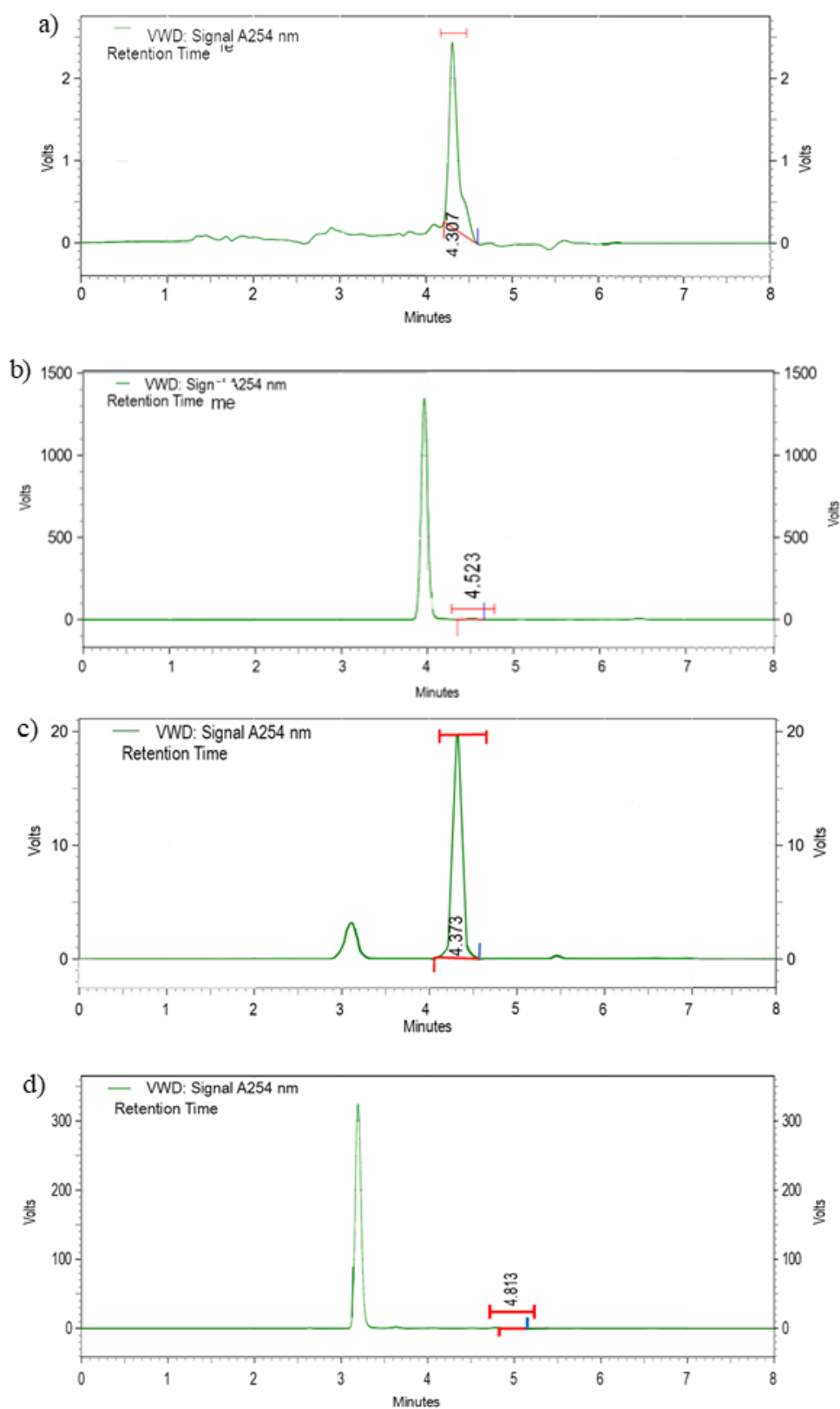


Fig. 4.29. Representative HPLC chromatogram illustrating the degradation of 2-nitrofluorene by Co-inoculum BGC01 in 2-nitrofluorene-spiked PBYS medium at different time intervals: (a) 0 hours, (b) 24 hours, (c) 48 hours, and (d) 72 hours.

A control group comprising nitro-PAHs (25 mg/L) in PBYS medium, devoid of bacterial inoculation, was also subjected to incubation to assess baseline degradation in abiotic conditions. These control samples were incubated under the same conditions (37 °C at 150 rpm) as the treatment groups to duplicate the experimental setting. This setting ensured that degradation observed in the treated groups could be distinctly attributed to bacterial activity instead of abiotic influences. After 72 hours of incubation, the control group showed only 6% degradation of 1-nitropyrene and 2-nitrofluorene. This minimal drop highlights the durability of degrading activity related only to bacterial strains, rather than any abiotic impacts. The findings suggest that the degradation observed in the inoculated samples can be conclusively ascribed to bacterial enzymatic processes, thereby reinforcing the appropriateness of these strains for specialized bioremediation of nitro-PAHs. These findings substantiate that the bacterial co-inoculum possesses higher capabilities in the degradation of nitro-PAHs, emphasizing their potential as efficacious bioremediation agents.

Table 4.5. Percentage degradation of 1-nitropyrene and 2-nitrofluorene by bacterial strains and co-inoculum over an incubation period of 0 to 72 hours.

Time (hours)	1-nitropyrene				2-nitrofluorene			
	Abiotic Control	Strain BG034	Strain BG05	BGC01	Abiotic Control	Strain BG034	Strain BG05	BGC01
0	0	0	0	0	0	0	0	0
24	0	19±2.40	26.40±4.44	46±3.24	0	31.16±3.12	26.16±2.96	54.08±3.12
48	4±0.2	40±4.0	36±4.34	66±3.46	4±0.4	43.16±2.60	42.16±3.2	75.88±6.40
72	5.92±1.06	47.84±3.20	49.04±2.80	76±4.04	5.72±1.44	59.96±3.04	59.88±3.60	87.20±2.34

Data are expressed as means ± S.D (n=3).

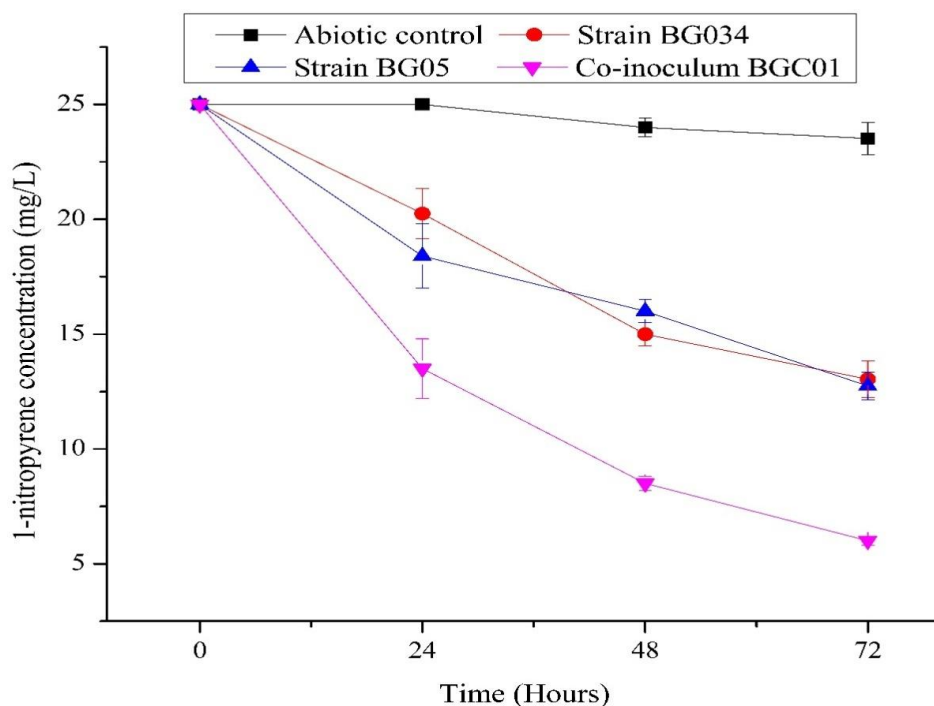


Fig. 4.30. (a). Degradation of 1-nitropyrene by the formulated bacterial co-inoculum and individual strains in a shaker flask over a 72-hour incubation period. Data are expressed as means \pm S.D (n=3)

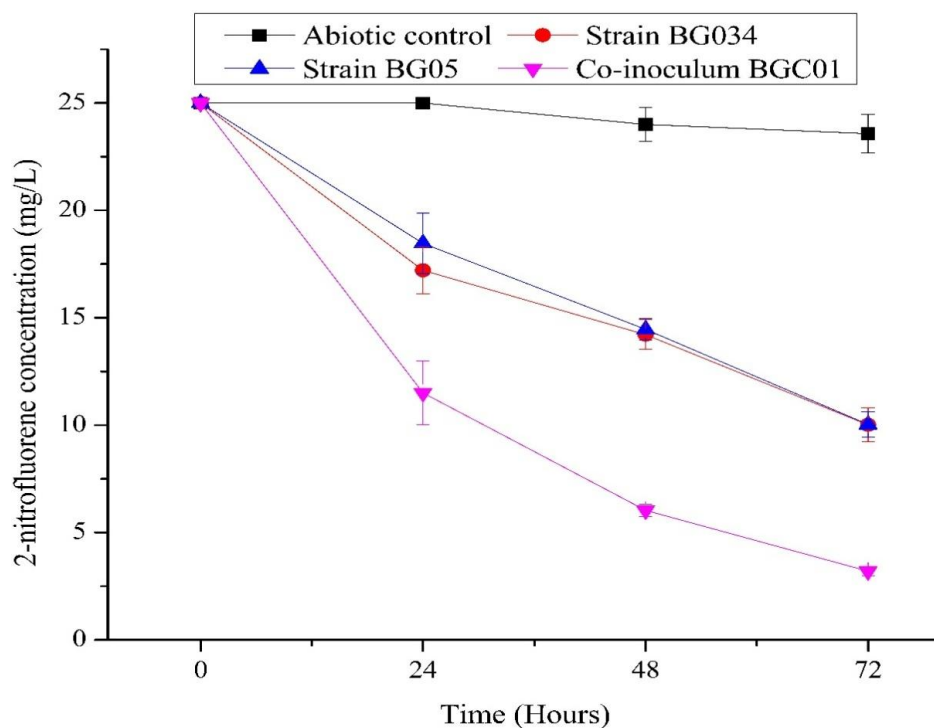


Fig. 4.30. (b). Degradation of 2-nitrofluorene by the formulated bacterial co-inoculum and individual strains in a shaker flask over a 72-hour incubation period. Data are expressed as means \pm S.D. (n = 3).

A comprehensive overview of the degradation rate of two hazardous nitro-PAH compounds, 1-nitropyrene and 2-nitrofluorene, by the bacterial strains BG034, BG05, and BGC01, in comparison to an abiotic control, was documented across different incubation periods (Table 4.6). The degradation rates ($\text{mg L}^{-1} \text{h}^{-1}$) were assessed at specific intervals of 0–24, 24–48, and 48–72 hours, along with cumulative time frames (0–48, 24–72, and 0–72 hours) to evaluate the overall degradation efficiency of each treatment.

Among all bacterial treatments, BGC01 had the highest degradation rates for both nitro-PAH compounds within the initial 24-hour incubation period. Specifically, for 1-nitropyrene, BGC01 attained a degradation rate of $1.91 \text{ mg L}^{-1} \text{h}^{-1}$, closely followed by BG05 at $1.1 \text{ mg L}^{-1} \text{h}^{-1}$ and BG034 at $0.79 \text{ mg L}^{-1} \text{h}^{-1}$. Similarly, for 2-nitrofluorene, BGC01 led with a degradation rate of $2.25 \text{ mg L}^{-1} \text{h}^{-1}$, marginally surpassing BG05 ($1.09 \text{ mg L}^{-1} \text{h}^{-1}$) and BG034 ($1.29 \text{ mg L}^{-1} \text{h}^{-1}$). This rapid degradation rate demonstrates that all bacterial strains successfully degraded the nitro-PAHs during the first 0-24 hours, with BGC01 exhibiting slightly superior efficacy. The abiotic control demonstrated zero degradation rates, indicating that the observed decreases in nitro-PAH concentrations were due to bacterial activity. In the succeeding 24-hour interval (24-48 hours), degradation rates decreased across all bacterial strains, indicating a reduction in activity compared to the first timeframe. For 1-nitropyrene, BGC01 had a degradation rate of $0.83 \text{ mg L}^{-1} \text{h}^{-1}$, whereas BG034 and BG05 had rates of 0.87 and $0.40 \text{ mg L}^{-1} \text{h}^{-1}$, respectively. In 2-nitrofluorene degradation, BGC01 outperformed BG034 ($0.50 \text{ mg L}^{-1} \text{h}^{-1}$) and BG05 ($0.66 \text{ mg L}^{-1} \text{h}^{-1}$) at a rate of $0.91 \text{ mg L}^{-1} \text{h}^{-1}$. The abiotic control showed a modest increase in degradation rates for both chemicals; nonetheless, these values remained low, reaffirming the biotic nature of the degradation process. During the final (48-72 hour) interval, the degradation rates for 2-nitrofluorene significantly increased for BGC01 attaining a rate of $0.47 \text{ mg L}^{-1} \text{h}^{-1}$, BG034 and BG05 at $0.70 \text{ mg L}^{-1} \text{h}^{-1}$ and $0.73 \text{ mg L}^{-1} \text{h}^{-1}$, respectively. On the other hand, for 1-nitropyrene, in comparison to 2-nitrofluorene, the rates exhibited a persistently low trend across all bacterial treatments. This finding might indicate that 1-nitropyrene persists longer due presence of a higher benzene ring or bacterial metabolic activity shifts more towards 2-nitrofluorene over prolonged exposure. The abiotic control group showed limited degradation, demonstrating the bacterial strains' ability to actively metabolize both substances.

Table 4.6. Degradation rate ($\text{mg L}^{-1} \text{h}^{-1}$) of 1-nitropyrene and 2-nitrofluorene by bacterial strains and co-inoculum over a 0-72 hour incubation period.

Time (hours)	1-nitropyrene				2-nitrofluorene			
	Abiotic	Strain	Strain	BGC01	Abiotic	Strain	Strain	BGC01
	Control	BG034	BG05		Control	BG034	BG05	
0-24	0	0.79±0.06	1.1±0.08	1.91±0.05	0	1.29±0.13	1.09±0.12	2.25±0.13
24-48	0.16±0.03	0.87±0.02	0.40±0.03	0.83±0.03	0.16±0.1	0.50±0.02	0.66±0.01	0.91±0.14
48-72	0.08±0.01	0.32±0.04	0.54±0.02	0.41±0.02	0.07±0.02	0.70±0.01	0.73±0.02	0.47±0.07
0-48	0.08±0.02	0.83±0.09	0.75±0.03	1.37±0.08	0.08±0.05	0.89±0.05	0.87±0.06	1.58±0.13
24-72	0.12±0.03	0.60±0.05	0.47±0.01	0.62±0.02	0.11±0.05	0.60±0.07	0.70±0.01	0.69±0.02
0-72	0.08±0.03	0.66±0.04	0.68±0.06	1.05±0.07	0.07 ±0.03	0.83±0.04	0.83±0.05	1.21±0.03

The data are expressed as mean ± S.D.(n=3).

The results of this study demonstrate the synergistic potential of co-inoculating isolated PGPR strains for the degradation of nitro-PAHs. The co-inoculum effectively degraded over 76% of 1-nitropyrene and 87.20% of 2-nitrofluorene within 72 hours, outperforming the individual strains. This finding supports previous research indicating that microbial consortia have improved degradation efficiency compared to single strains. For instance, Zhong et al. (2011) provided compelling evidence that a specific microbial consortium, consisting of *Mycobacterium* sp. APYR and *Sphingomonas* sp. PheB4 achieved an impressive 50% degradation of 10 mg/L pyrene within seven days. This performance was significantly higher than that of the individual strains (Zhong et al., 2011). Similarly, Shen et al. (2015) reported that a consortium consisting of *Bacillus* sp. PH2, *Pseudomonas* sp. PH1, *Pseudomonas* sp. PH4, and *Ochrobactrum* sp. PH3 was capable of degrading 38% of 100 mg/L pyrene after six days of experiment periods (Shen et al., 2015). These key findings supported our hypothesis which highlights the critical role of bacterial co-inoculum in the successful breakdown and remediation of a variety of environmental contaminants. These consortia's superior performance can be attributed in large part to the concept of metabolic synergy, in which one microorganism produces essential intermediates or cofactors that are then utilized by another

microorganism, significantly speeding up the degradation of complex pollutants such as PAHs and their nitro-derivatives. Wanapaisan et al. (2018) corroborated this by reporting that microbial consortia break down pyrene faster than individual strains, which was due to the division of metabolic labor and enhanced substrate utilization (Wanapaisan et al., 2018). The previous report also highlighted that substrate availability substantially impacts the bacterial breakdown of organic contaminants such as nitro-PAHs (Sarma et al., 2024). The study underlines that the bioavailability of nitro-PAHs in the PBYS medium is critical for degradation, with bacterial breakdown efficiency proportional to substrate concentration.

The degradation kinetics of 1-nitropyrene and 2-nitrofluorene demonstrated distinct patterns in our study underscoring the variations in their kinetics pathways. A second-order kinetic decay model better suited for 1-nitropyrene degradation, with R^2 values: 0.986 for BG034, 0.986 for BG05, and 0.994 for the co-inoculum BGC01 (Fig. 4.31). 2-nitrofluorene degradation followed a first-order kinetic decay model, with R^2 values of 0.986 for BG034, 0.994 for BG05, and 0.996 for BGC01, showing different microbial degradation dynamics between the two chemicals (Fig. 4.32). In the degradation kinetic of 1-nitropyrene, the co-inoculum BGC01 had the highest rate constant ($k = 0.0018 \text{ L mol}^{-1}\text{h}^{-1}$) and the shortest half-life ($T_{1/2} = 22.22$ hours) compared to the individual strains BG034 and BG05, which both presented lower rate constants ($k = 0.0005 \text{ L mol}^{-1}\text{h}^{-1}$) and longer half-lives ($T_{1/2} = 80$ hours). Similarly, in the case of 2-nitrofluorene, the co-inoculum BGC01 also had a higher degradation efficiency with a rate

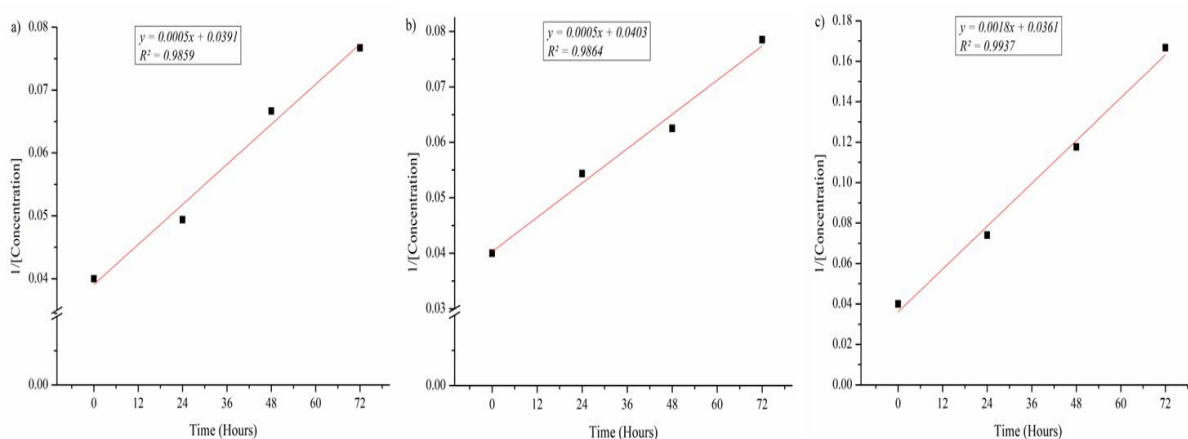


Fig. 4.31. The kinetic regression equation for 1-nitropyrene (Strain BG034 (a), BG05 (b), and BGC01(c))

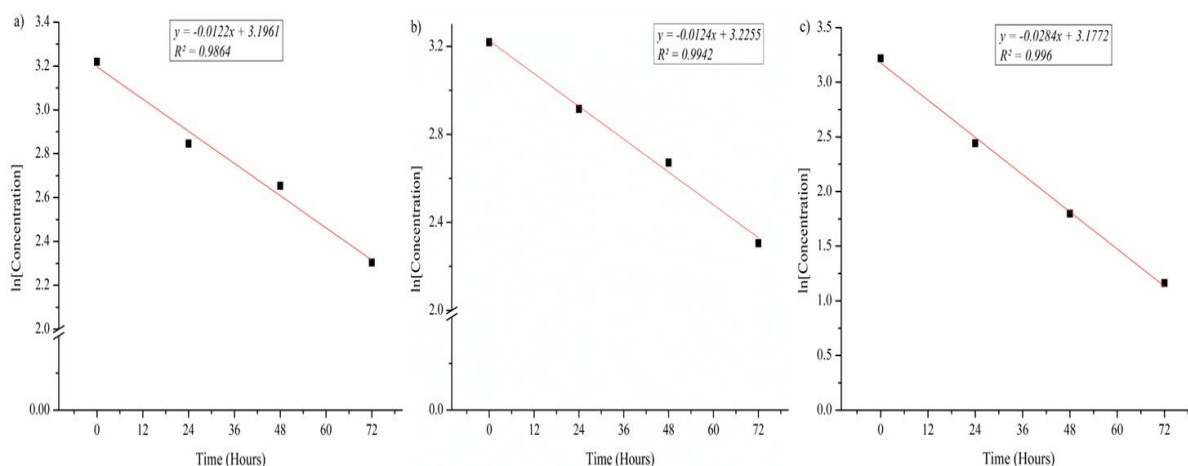


Fig. 4.32. The kinetic regression equation for 2-nitrofluorene (Strain BG034 (a), BG05 (b), and BGC01 (c)).

constant of $0.0284 \text{ L mol}^{-1}\text{h}^{-1}$ and a half-life of 24.40 hours. In contrast, individual strains BG034 and BG05 had lower rate constants ($0.0122 \text{ L mol}^{-1}\text{h}^{-1}$ and $0.0124 \text{ L mol}^{-1}\text{h}^{-1}$ respectively) and longer half-lives (56.80 and 55.89 hours). However, these results differ from previous studies. Li et al. (2020) reported that the degradation of 1-nitropyrene follows a first-order kinetic decay model (Li et al., 2020). Similarly, degradation of 2-nitrofluorene might follow zero-order or second-order kinetic models (Stewart et al., 2010). These variations highlight the influence of experimental factors, microbial consortia, and ambient circumstances on degradation kinetics. Table 4.7 summarizes the regression equation, rate constants (k), half-lives ($T_{1/2}$), and the kinetic question of 1-nitropyrene and 2-nitrofluorene in the presence of isolated bacterial strains and their co-inoculum.

Table 4.7. Kinetic parameters and regression equations for the degradation of 1-nitropyrene and 2-nitrofluorene by isolated bacterial strains and their co-inoculum over a 0–72 hour incubation period.

Parameter	1-nitropyrene			2-nitrofluorene		
	BG034	BG05	BGC01	BG034	BG05	BGC01
Regression equation	$y = 0.0005x + 0.0391$	$y = 0.0005x + 0.0403$	$y = 0.0018x + 0.0361$	$y = -0.0122x + 3.1961$	$y = -0.0124x + 3.2255$	$y = -0.0284x + 3.1772$
Coefficients of determination (R^2)	0.986	0.986	0.994	0.986	0.994	0.996
Rate constant (k) ($\text{L mol}^{-1}\text{h}^{-1}$)	0.0005	0.0005	0.0018	0.0122	0.0124	0.0284
Half-life ($T_{1/2}$) (Hours)	80	80	22.22	56.80	55.89	24.40
Kinetic question	$\frac{1}{[A]} = kt + \frac{1}{[A]_0}$			$\ln[A] = -kt + \ln[A]_0$		

4.6. Characterization of Plant growth-promoting (PGP) activities

4.6.1. *In Vitro* Assessment of Plant Growth-Promoting Traits

4.6.1.1. Phosphate Solubilization

The results reveal that both bacterial strains *Bacillus cereus* BG034 and *Bacillus altitudinis* BG05 exhibited positive results for phosphate solubilization. When the isolated bacteria were grown on Pikovskaya's agar media, each strain produced distinct clear halos around its colonies, demonstrating its ability to solubilize inorganic phosphate (Fig. 4.33 (a)). The Phosphate Solubilization Index (PSI) was calculated for each isolated strain, with *Bacillus cereus* BG034 having a PSI of 2.30 and *Bacillus altitudinis* BG05 having a slightly higher PSI of 2.58. The development of these halo zones indicates that both strains are capable of producing organic acids or other metabolites that promote the transformation of insoluble phosphate into bioavailable forms, thereby improving phosphorus accessibility in the surrounding environment. After 96 hours of incubation, the soluble phosphate content in the culture supernatant ranged from 122.67 µg/mL for *Bacillus cereus* BG034 to 119 µg/mL for *Bacillus altitudinis* BG05. The quantification of phosphate was performed using a standard calibration curve as a reference (Fig. 4.34 (a)), ensuring accurate measurement of phosphate solubilization by both bacterial strains. The statistical analysis revealed that there was no significant difference in phosphate solubilization activity between the two strains. Phosphorus is an essential macronutrient for plants, contributing to cellular division, energy transmission, and photosynthesis (Khan et al., 2023; Solovchenko et al., 2024). Despite its abundance in soils, phosphorus is typically found in insoluble forms that plants cannot readily absorb. This challenge is intensified in polluted or degraded soils, where the fixation and precipitation of phosphates further diminish their bioavailability which is critical for plant nutrition and growth, particularly in nutrient-deficient or polluted soils. *Bacillus* represents one of the most notable genera demonstrating phosphate-solubilizing capabilities (Saeid et al., 2018; Souza et al., 2023). Previous studies have consistently emphasized its importance in increasing soil phosphate concentrations and promoting plant growth by producing organic acids such as gluconic acid, citric acid, or lactic acid, which either directly dissolve rock phosphate or chelate metal ions such as calcium, iron, or aluminum, releasing phosphates into the soil (Amarasinghe et al., 2022; Bakki et al., 2024). Saeid et al. (2018) isolated several *Bacillus* strains that can solubilize phosphates *in vitro*, demonstrating their potential as plant growth promoters (Saeid et al., 2018). Furthermore, Souza et al. (2023) also reported the phosphate solubilization

activity of *Bacillus* spp., emphasizing their resilience in nutrient-deficient environments (Souza et al., 2023). One of the most important species of *Bacillus* is *Bacillus cereus*. Soares et al. (2023) revealed the significant phosphate-solubilizing ability of *Bacillus cereus* which was isolated from Cerrado soils. This strain was found to perform a critical role in increasing soil fertility, particularly in phosphorus-deficient locations (Soares et al., 2023). Moreover, Chakraborty et al. (2011) also reported *Bacillus cereus*'s phosphate-solubilizing capacity using *in vitro* growth evaluations, with plants treated with this strain exhibiting higher leaf and shoot phosphate content while decreasing total soil phosphate, confirming its bioavailability. Zhao et al. (2022) isolated another phosphate-solubilizing *Bacillus* species *Bacillus altitudinis* GQYP101 from the *Lycium barbarum* L. rhizosphere and showed its potential as a plant growth-promoting bacterium. This strain significantly increased stem diameter, leaf area, and fresh weight of maize in pot experiments via phosphorus solubilization (Zhao et al., 2022). A similar report from Laczieski et al. (2020) experiment noted that *Bacillus altitudinis*, isolated from the rhizosphere of *Ilex paraguariensis* exhibited robust phosphate-solubilizing activity, emphasizing its ecological function in nutrient cycling (Laczieski et al., 2020). Kaushal and Pati (2024) also elucidated that *Bacillus altitudinis* possesses dual functionalities as both a plant growth promoter and a bioremediation agent, further demonstrating its adaptability in agro-environmental contexts (Kaushal & Pati, 2024). These findings corroborated our finding that *Bacillus cereus* and *Bacillus altitudinis* solubilized phosphorus.

4.6.1.2. Siderophore Production

Both bacterial strains *Bacillus cereus* BG034 and *Bacillus altitudinis* BG05, demonstrated positive results in the siderophore production assay, indicating their ability to secrete the iron-chelating compounds. The presence of an orange halo around the bacterial colonies on chrome azurol S (CAS) confirmed their formation of siderophores (Fig. 4.33 (b)). The presence of this halo indicates that BG034 and BG05 are actively producing siderophores, which bind to iron and improve its absorption in iron-deficient conditions. The quantitative assessment of siderophore production was carried out using the following equation.

$$\text{Percentage of siderophore units} = \frac{\text{Absorbance of reference} - \text{Absorbance of sample}}{\text{Absorbance of reference}} \times 100$$

Bacillus cereus BG034 exhibited slightly higher siderophore production, with 50% siderophore units, while *Bacillus altitudinis* BG05 produced 47.27%. This proficiency is especially useful in nutrient-limited soils, where iron is usually unavailable in readily accessible usable forms.

The synthesis of siderophores by *Bacillus cereus* BG034 and *Bacillus altitudinis* BG05 highlights their potential role in enhancing plant growth, as these compounds help plants acquire essential iron while inhibiting the proliferation of pathogenic microorganisms by reducing iron availability in the rhizosphere. The findings suggest that *Bacillus cereus* BG034 and *Bacillus altitudinis* BG05 could be beneficial as plant growth-promoting rhizobacteria. This study's results align with previous research emphasizing the ability of *Bacillus* species, particularly *Bacillus cereus*, to produce siderophores, which is considered an important functional trait. For example, Kumar et al. (2017) assessed siderophore synthesis across a variety of *Bacillus* species, revealing their significant contribution to iron uptake and plant nutrient availability (Kumar et al., 2017). Furthermore, Manasa et al. (2021) documented *Bacillus cereus*' synthesis of siderophores, highlighting its potential as a plant growth-promoting rhizobacterium capable of alleviating iron shortage stress (Manasa et al., 2021). The contribution of *Bacillus altitudinis* in the realm of siderophore production is equally significant.

4.6.1.3. Ammonia Production

The results demonstrated that bacterial strains *Bacillus cereus* BG034 and *Bacillus altitudinis* BG05 exhibited positive ammonia production. When cultured in peptone water and incubated, both strains displayed a color change upon the addition of Nessler's reagent, shifting from brown to yellow (Fig. 4.33 (c)). This reaction highlighted their capacity for producing ammonia essential for plant growth and development. Quantitative analysis using a standard calibration curve as a reference (Fig. 4.34 (b)), revealed that *Bacillus altitudinis* BG05 produced 6.27 $\mu\text{mol/ml}$ of ammonia, slightly more than *Bacillus cereus* BG034 (5.5 $\mu\text{mol/ml}$). Nevertheless, no significant difference was observed between the two species, suggesting that both strains exhibit similar ammonia-producing potential. Ammonia generation by these bacterial strains revealed that they can increase soil nitrogen levels, which are essential for a variety of plant metabolic activities such as amino acid synthesis and chlorophyll production (Čepl et al., 2014; Watanabe et al., 2023). Positive ammonia test by *Bacillus cereus* BG034 and *Bacillus altitudinis* BG05 suggests their potential as PGPR since they can boost nitrogen availability in the rhizosphere, supporting healthier and more vigorous plant growth and development under nutrient-limited conditions. The affirmative ammonia test observed in this investigation also correlates positively with prior studies that emphasize the ammonium-producing capabilities of *Bacillus cereus* and *Bacillus altitudinis*. For instance, Cao et al. (2024) demonstrated that *Bacillus cereus* J1, isolated from a sewage treatment plant, produced significant amounts of

ammonia through dissimilatory nitrate reduction to ammonium (Cao et al., 2024). This finding highlights the species' flexibility in nitrogen cycling. Similarly, Parvin et al. (2023) isolated *Bacillus cereus* from rice rhizospheres and discovered that it also produced substantial amounts of ammonia, making it a suitable bio-inoculant for enhancing soil conditions and promoting plant growth (Parvin et al., 2023). Additionally, *Bacillus altitudinis* plays an important role in ammonium synthesis. Bhutani (2022) found that *Bacillus altitudinis* strains efficiently convert organic nitrogen sources into ammonium, which is particularly beneficial for plants in nitrogen-deficient soils (Bhutani et al., 2018). The findings of this study, along with previous research, clearly indicate that these strains have significant potential for ammonium production.

4.6.1.4. Indole Acetic Acid Production

PGPR play a crucial role in plant growth and development, especially under stress conditions, by producing IAA. IAA is an important bacterial signaling molecule involved in plant-microbe interactions. It significantly influences various physiological processes in plants, including root elongation, the production of lateral roots and root hairs, cell division, and cell expansion, all of which contribute to increased growth rates. The enhanced root structure resulting from IAA production greatly improves the efficiency of water and nutrient absorption, which is particularly beneficial during stressful conditions such as drought, salinity, or heavy metal exposure. In this study, two isolated rhizosphere strains demonstrated a remarkable ability to produce IAA when cultured on a tryptophan-enriched medium, as indicated by a significant color change upon the addition of Salkowski's reagent. The transition from pale pink to pinkish-red (Fig. 4.33 (d)) validated the IAA synthesis, supporting previous findings regarding the IAA-producing capabilities of *Bacillus* species. The quantitative analysis using a standard calibration curve as a reference (Fig. 4.34 (c)) further revealed that *Bacillus cereus* BG034 produced 40.6 µg/mL of IAA, while *Bacillus altitudinis* BG05 produced 43.46 µg/mL after 96 hours of incubation, indicating similar IAA synthesis capabilities among the strains. Our results are consistent with previous research has highlighted *Bacillus cereus* and *Bacillus altitudinis*' ability to produce IAA. For example, Bhutani et al. (2018) reported that *Bacillus cereus* MJHN10, isolated from *Vigna radiata*, generated a significant amount of IAA, confirming its role as a powerful PGPR (Bhutani et al., 2018). Similarly, Ozdal et al. (2016) revealed that *Bacillus cereus* synthesizes IAA efficiently, encouraging plant development (Özdalet al., 2016). Recent studies on *Bacillus cereus* have expanded to include a variety of environmental situations. For example, Ghosh et al. (2024) isolated an arsenic-resistant strain, *Bacillus cereus*

PMM6, from rice fields, with high IAA production capability. This demonstrates *Bacillus cereus*' flexibility and efficacy in promoting plant development even under severe metal stress (Ghosh et al., 2024). Chauhan et al. (2024) also reported that *Bacillus cereus* produces IAA, lending credence to its position as a strong PGPR (Chauhan et al., 2024). Similarly, *Bacillus altitudinis* has demonstrated a high affinity for IAA synthesis. Sun et al. (2017) reported that *Bacillus altitudinis* WR10 produced IAA, which contributed to improved root systems in plants (Sun et al., 2017). Furthermore, Sunar et al. (2015) demonstrated that *Bacillus altitudinis* produced IAA, underlining its potential for agricultural use (Sunar et al., 2015). The results of these experiments correspond with the findings of the current research, where both *Bacillus cereus* and *Bacillus altitudinis* exhibited significant IAA production in tryptophan-supplemented media.

4.6.1.5. HCN Production

HCN production is another prominent feature of PGPR, and it is frequently associated with improved plant health via biocontrol mechanisms. HCN, a volatile secondary metabolite, is formed by the oxidative decarboxylation of amino acid precursors (such as glycine, methionine, or glutamate) inside the microbial cell (Blumer & Haas, 2000; da Cruz Nizer et al., 2023). This chemical disrupts the respiratory processes of soilborne pathogens, which is critical for biological control (Lahlali et al., 2022). At low concentrations, cyanide efficiently inhibits aerobic organisms, whereas producer strains have a natural tolerance to its harmful effects. In this study, *Bacillus cereus* BG034 and *Bacillus altitudinis* BG05 were tested for their HCN production capabilities. Both strains were grown on a medium rich in glycine, and after incubation, a notable reddish-brown color shift on filter paper (treated with picrate solution) was noted (Fig. 4.33 (e)). This visible color shift demonstrated that both the strains *Bacillus cereus* BG034 and *Bacillus altitudinis* BG05 release HCN, indicating their potential as biocontrol agents. Quantitative investigation using a standard calibration curve as a reference (Fig. 4.34 (d)) revealed that *Bacillus cereus* BG034 produced slightly higher HCN production (185.67 μM) compared to *Bacillus altitudinis* BG05 (169.23 μM). These results indicate that both strains possess strong cyanogenic activity. *Bacillus* species' ability to produce HCN has been extensively documented in previous studies, supporting the findings of this study. For example, Narayanan et al. (2022) demonstrated that *Bacillus cereus* NDRMN001, isolated from *Cajanus cajan* grown in metal-contaminated soils, successfully produced HCN, assisting in pathogen control and plant resistance (Narayanan et al., 2022). Similarly, Sivakumar et al.

(2012) found that *Bacillus cereus* TS1, isolated from a location designated for chicken feather waste, produced a significant amount of HCN, highlighting its potential for biocontrol applications (Sivakumar et al., 2012). Furthermore, Kumar et al. (2020) isolated an HCN-producing variant, *Bacillus cereus* LPR2, from the rhizosphere of spinach and illustrated its inhibitory action against *Macrophomina phaseolina*, the causative organism responsible for maize charcoal rot (Kumar et al., 2020). Furthermore, Sunar et al. (2015) found HCN generation in *Bacillus altitudinis* isolated from the rhizosphere of *Sechium edule*, emphasizing the prevalence of this trait in a variety of ecological situations (Sunar et al., 2015). These observations further substantiate the multifunctional capabilities of HCN-producing *Bacillus* strains in alleviating plant stressors, particularly in contaminated environments. Their ability to prevent phytopathogenic organisms while growing under stressed environments suggests that these strains offer great promise for sustainable agriculture.

4.6.1.6. The Triple Sugar Iron (TSI) Test

TSI test was positive for both bacterial strains *Bacillus cereus* BG034 and *Bacillus altitudinis* BG05, suggesting metabolic flexibility and the ability to ferment sugars in both aerobic and anaerobic conditions. After incubating on TSI agar slants, *Bacillus cereus* BG034 and *Bacillus altitudinis* BG05 generated color changes in the medium, with both strains displaying yellow coloring, indicating their capacity to ferment sucrose (Fig. 4.33 (f)). This study's findings, together with prior research, clearly suggest that these strains have significant potential for fermented sucrose (Staicu et al., 2020).

Overall, the results of the phosphorus solubilization, HCN production, IAA production assay, ammonium production assay, TSI assay, and siderophore production assay support the various roles that these bacterial strains play in improving soil fertility, nutrient accessibility, and plant growth. The *in vitro* PGP characteristics of the isolated bacteria strains were summarized in Table 4.8. The findings of our study provide compelling evidence of isolated *Bacillus cereus* BG034 and *Bacillus altitudinis* BG05's ability to promote plant development, as demonstrated by a series of *in vitro* plant growth-promoting assessments.

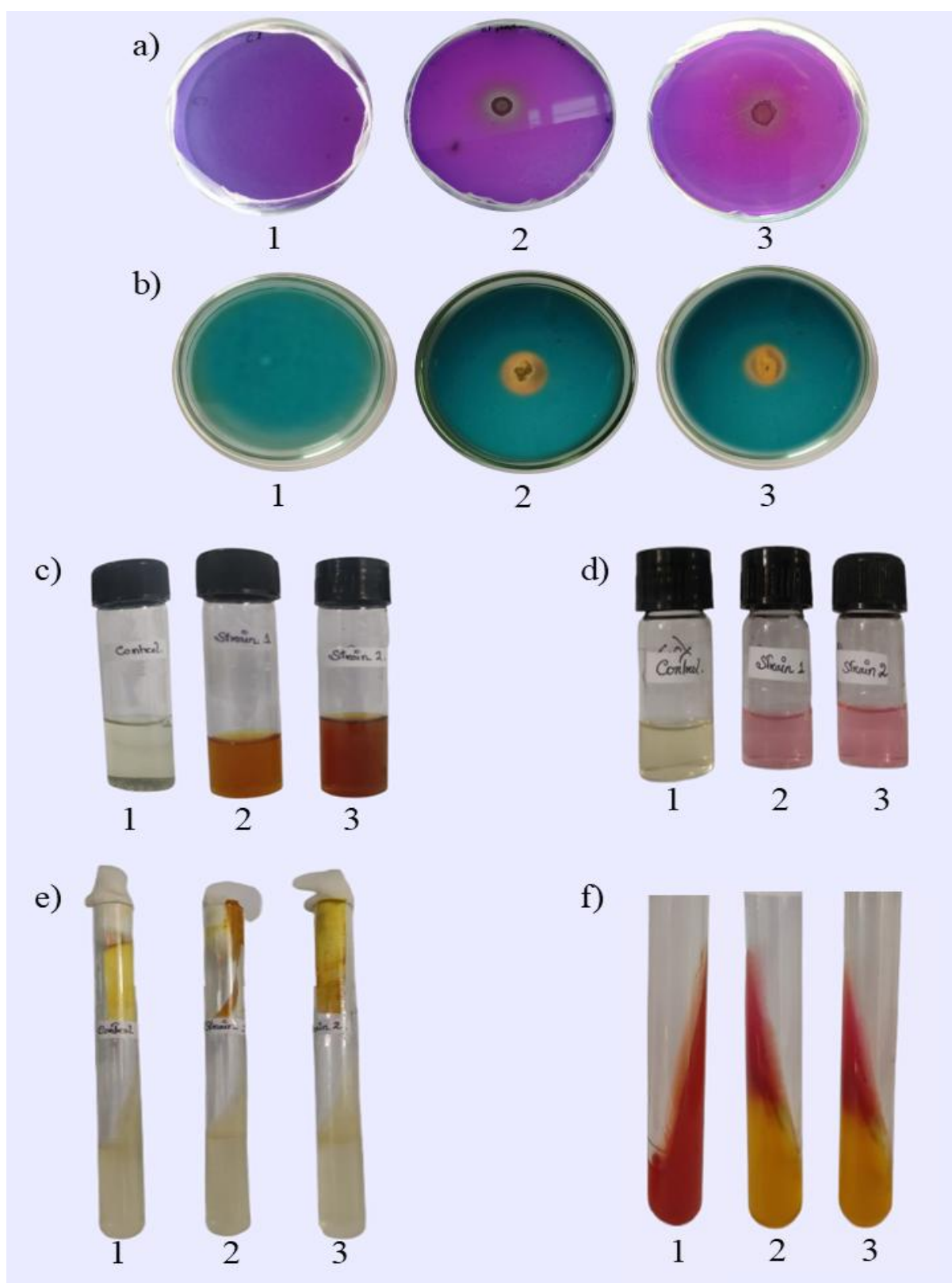


Fig. 4.33. The *in vitro* PGP test of the isolated bacterial strains. Phosphate solubilization test (a), Siderophore production test (b), Ammonia Production test (c), IAA test (d), HCN production test (e), Triple Sugar Iron (TSI) test (f). In each test, (1) represents the control, (2) represents strain BG034, and (3) represents strain BG05.

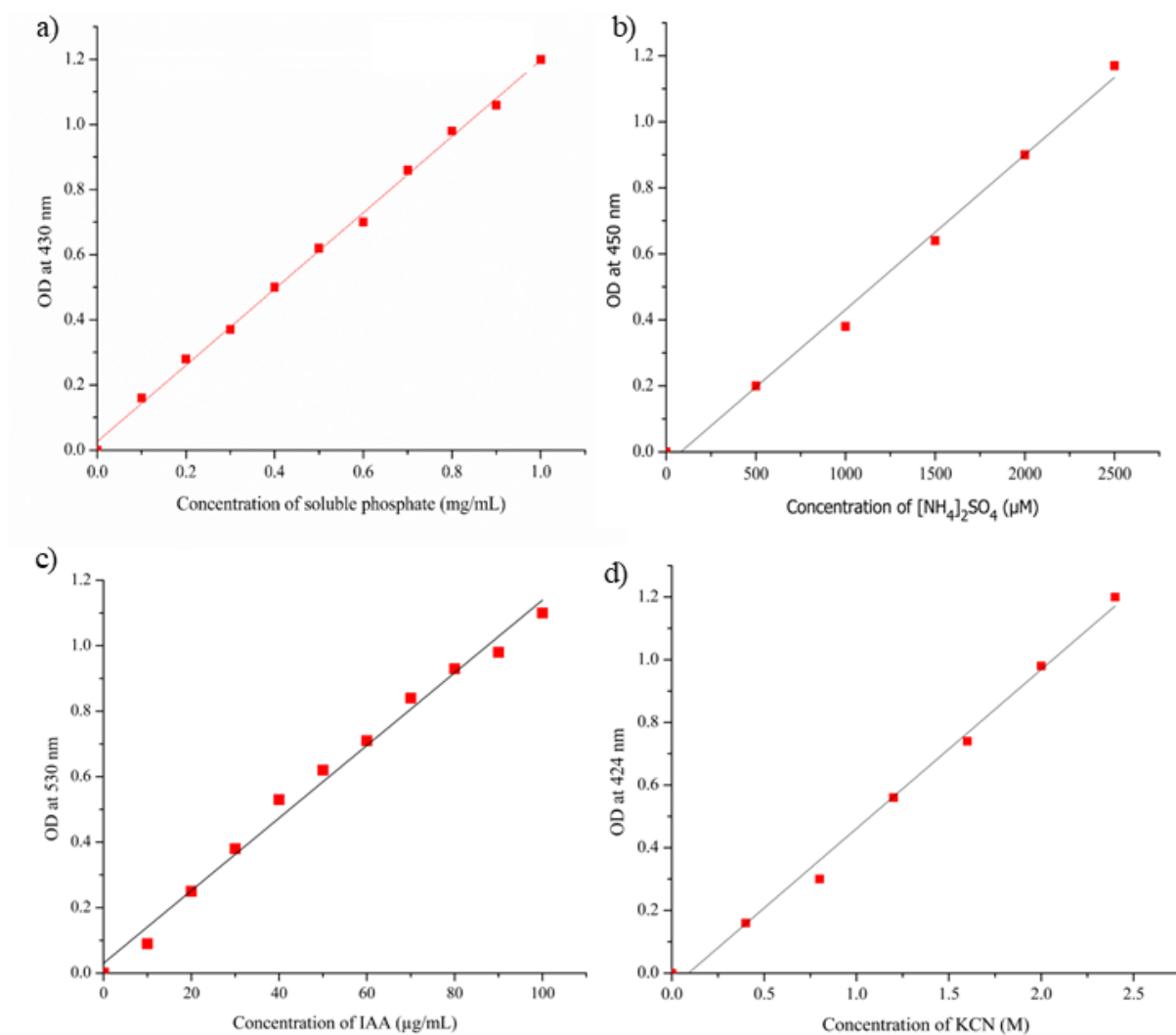


Fig. 4.34. Standard calibration curve of soluble phosphate (a), ammonium (b), IAA (c), and HCN (d).

Table 4.8. PGP traits of isolated bacteria

PGP test	<i>Bacillus cereus</i> BG034 (Strain 1)	<i>Bacillus altitudinis</i> BG05 (Strain 2)
Phosphate solubilization	+ ve	+ ve
HCN production	+ ve	+ ve
Indole Acetic Acid production	+ ve	+ ve
Ammonia production	+ ve	+ ve
Triple Sugar Iron (TSI) test	+ ve	+ ve
Siderophore production	+ ve	+ ve

4.6.2. Rhizobacterial Inoculation and Growth Assessment in Plants

The isolated bacterial strains *Bacillus cereus* BG034 and *Bacillus altitudinis* BG05, along with their combined co-inoculum (BGC01), were investigated using *in vitro* and greenhouse trials to determine their ability to improve plant growth and development, with a focus on critical growth parameters such as root and shoot lengths on four selected plant species: *C. rotundus*, *C. esculentus*, *A. compressus*, and *I. cylindrica* (Fig. 4.35). The greenhouse studies predominantly corroborated the outcomes obtained from the *in vitro* screening, demonstrating that the usage of these bacterial strains successfully promotes plant growth and development. The impact of these bacterial treatments on root length was noticeable across all plant species tested, with BGC01 showcasing consistently superior efficacy (Fig. 4.36). During the 21-day treatment intervals, a significant statistical difference was observed between the co-inoculum and the individual strains treatments (from 7 days to 21 Days) as detailed in Table 4.9. Nonetheless, no significant difference was found between the strains' (BG034 and BG05) treatments. For example, *C. rotundus*, treated with BGC01 attained a root length of 3.3 cm after 21 days, which was significantly greater than that of the control group (2.36 cm) and also exceeded the results of the individual strain treatments, where BG034 and BG05 yielded root lengths of 3.0 cm and 3.13 cm, respectively. A similar result was reported in *C. esculentus*, where the root length in the BGC01 treatment reached 3.47 cm after 21 days of the experiment period, exceeding both the individual strains (3.13 cm for BG034 and 3.03 cm for BG05). Also, in *A. compressus*, a consistent increase in root length was reported across all bacterial treatments, with BGC01 reaching the maximum root length of 3.23 cm by the end of the investigation period, compared to 2.17 cm in the control. The case of *I. cylindrica* shows significantly similar results at 3.97 cm with BGC01 treatment compared to individual strains (BG034 is 3.63 cm, and BG05 is 3.73 cm) at the 21 days of treatment periods.

Data on shoot length also supported the growth-promoting impact of BGC01. Throughout the treatment periods (7 days to 21 days), there was a significant statistical difference between the co-inoculum (BGC01) and the treatments involving individual strains (BG034 and BG05) (Table 4.10). However, no significant difference was found between the performances of the individual strains. Treated with co-inoculum in *C. rotundus* showed an increase in shoot length, reaching 36.17 cm after 21 days, compared to control plants that measured only 15.23 cm. Individual strain treatments also improved shoot development, albeit to a lesser extent, with BG034 and BG05 treatments resulting in shoot lengths of 20.37 cm and 20.8 cm, respectively.

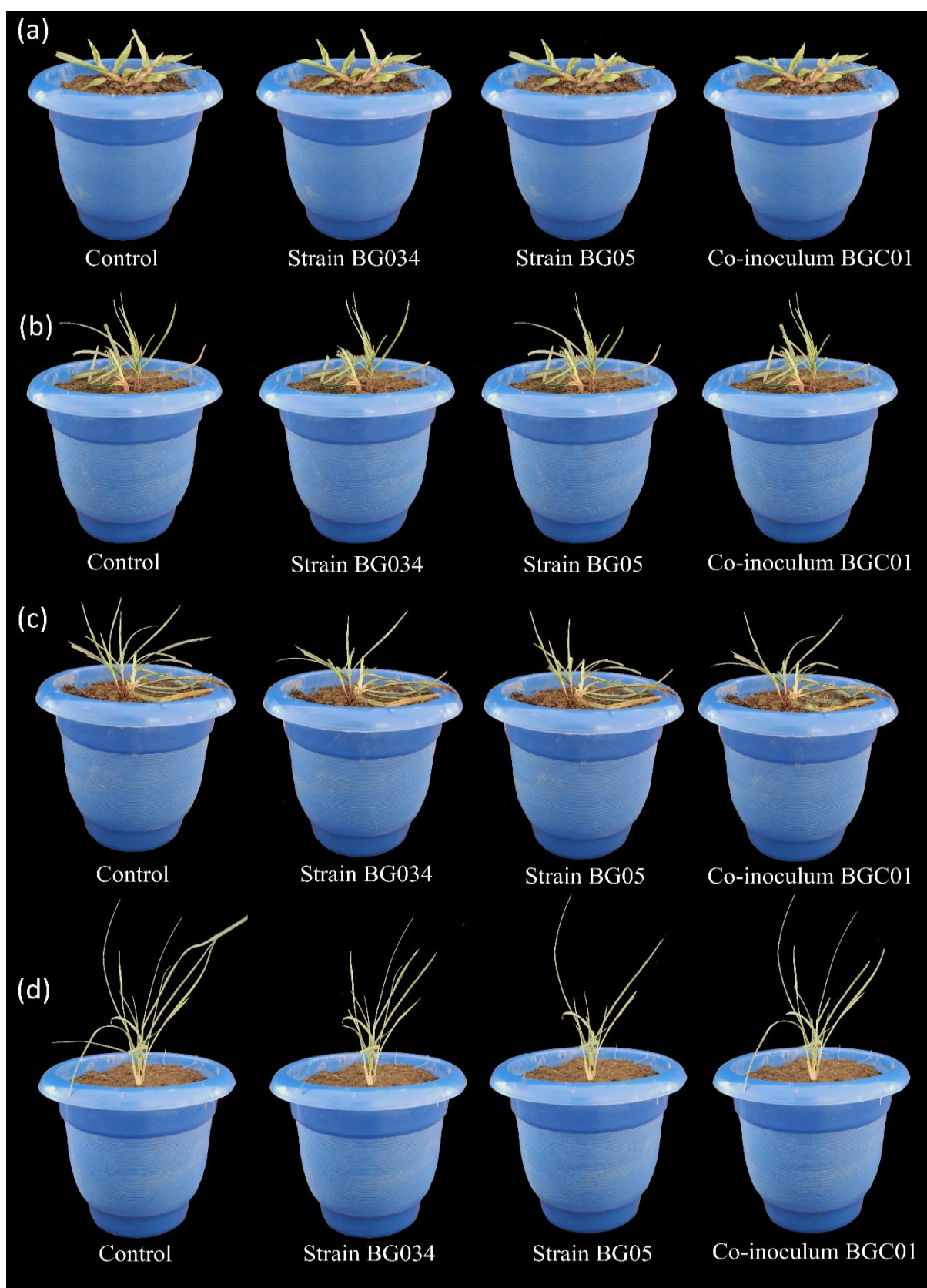


Fig. 4.35. *In vivo* experiment setup for plant growth-promoting by isolated bacterial strains and formulated co-inoculum. *Cyperus rotundus* (a), *Cyperus esculentus* (b), *Imperata cylindrica* (c), and *Axonopus compressus* (d).

Table 4.9. Statistical results on root length among the species upon application of bacterial strains and their co-inoculum (from 7 days to 21 days experiment periods).

Plant species	df	Test-statistics	<i>p</i>	Statistical Test
<i>Cyperus rotundus</i>	3, 32	F = 3.08	0.041*	one-way ANOVA
<i>Cyperus esculentus</i>	4	H = 8.72	0.033*	Kruskal-Wallis
<i>Axonopus compressus</i>	3, 32	F= 5.68	0.003**	one-way ANOVA
<i>Imperata cylindrica</i>	3, 32	F= 5.24	0.004**	
H= Chi square, F= F-statistic, *= Significant, **= Moderately significant				

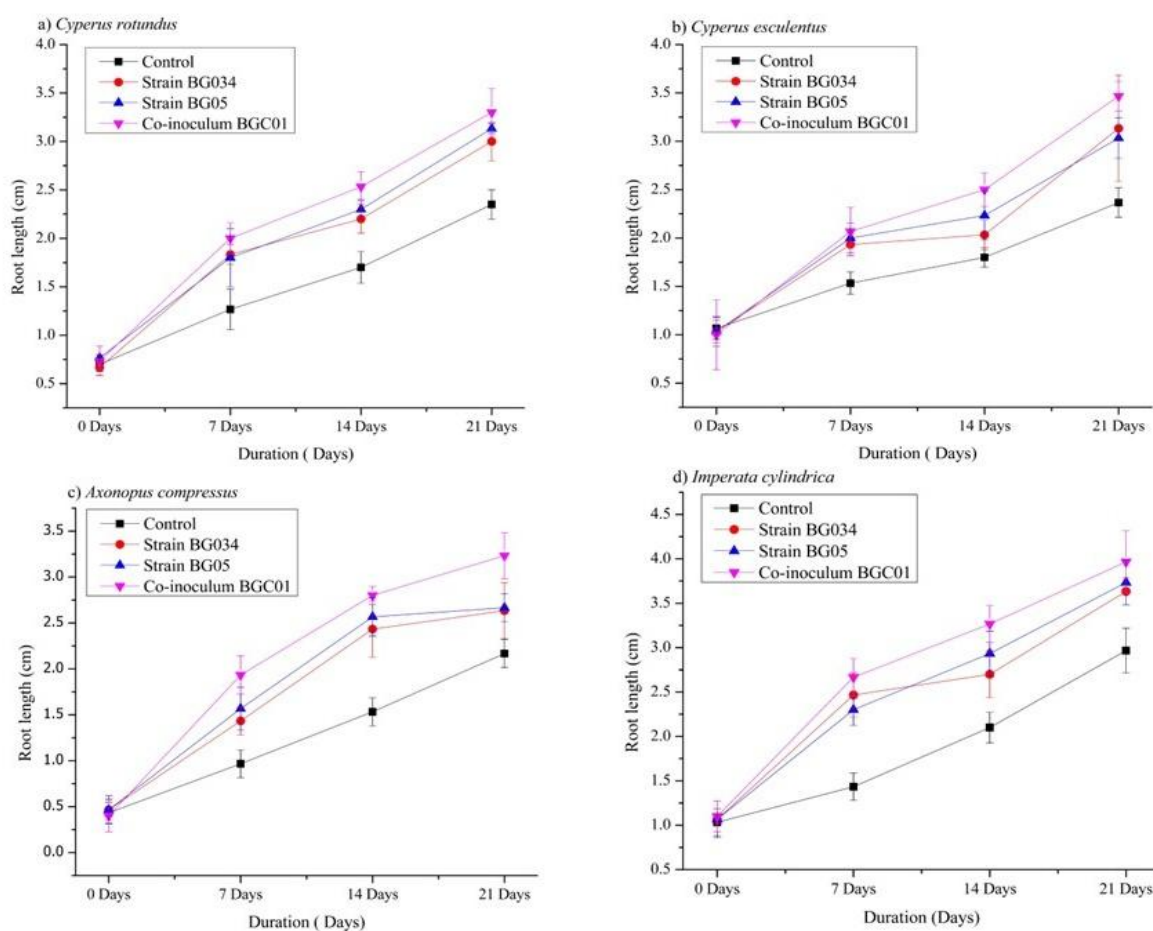


Fig. 4.36. Effects of bacterial inoculation on the root length (a-d) of *Cyperus rotundus* (a) *Cyperus esculentus* (b), *Imperata cylindrica* (c), and *Axonopus compressus* (d)— throughout 21 days. The study assessed the PGP properties of isolated bacterial strains and their co-inoculum. Data are expressed as means \pm S.D. (n = 3).

A similar result was observed in *C. esculentus*, where plants treated with BGC01 reached a shoot length of 33.67 cm by the end of the experiment, which was higher than the control group (10.63 cm) and the individual strains (18.8 cm for BG034 and 19.5 cm for BG05).

In response to BGC01, *A. compressus*, and *I. cylindrica* also demonstrated to significantly enhanced the shoot length for *A. compressus* 4.83 cm by day 21, compared to the control group's 2.53 cm, and *I. cylindrica* 47.3 cm and control 24.27 cm. In both cases, individual strains significantly increased in shoot length concerning the control but were less efficient than the co-inoculum. The enhanced growth effects associated with BGC01 are plausibly attributable to the synergistic interactions between BG034 and BG05 (Fig. 4.37). These strains showcase complementing metabolic activities, including nutrient solubilization, phytohormone synthesis, and pathogen control by hydrogen cyanide formation all of which contribute to a more conducive rhizosphere environment for plant growth. This study demonstrated that co-inoculums of plant growth-promoting rhizobacteria can more efficiently promote plant development than individual strains because they combine a wide range of microbial capabilities. In the case of BGC01, the combined proficiencies of BG034 and BG05 may improve nutrient availability, root and shoot growth, and plant resistance to environmental challenges.

The findings of this study clearly support previous research highlighting the PGP properties of *Bacillus altitudinis* and *Bacillus cereus*. Yue et al. (2022) demonstrated that *Bacillus altitudinis* significantly increased both root and shoot lengths in wheat plants, showcasing its ability to positively influence important growth metrics (Yue et al., 2022). Similarly, Kaushal and Pati (2024) reported significant increases in the root and shoot lengths of rice seedlings after they were inoculated with *Bacillus altitudinis*, further confirming its PGP effects (Kaushal & Pati 2024)

Table 4.10. Statistical results on shoot length among the species upon application of bacterial strains and their co-inoculum (from 7 days to 21 days experiment periods).

Plant species	df	Test-statistics	<i>p</i>	Statistical Test
<i>Cyperus rotundus</i>	4	H= 9.35	0.025*	Kruskal-Wallis
<i>Cyperus esculentus</i>	4	H= 8	0.046*	
<i>Axonopus compressus</i>	4	H= 15.68	0.0012**	
<i>Imperata cylindrica</i>	3, 32	F = 4.14	0.014*	one-way ANOVA
H= Chi square, F= F-statistic, *= Significant, **= Moderately significant				

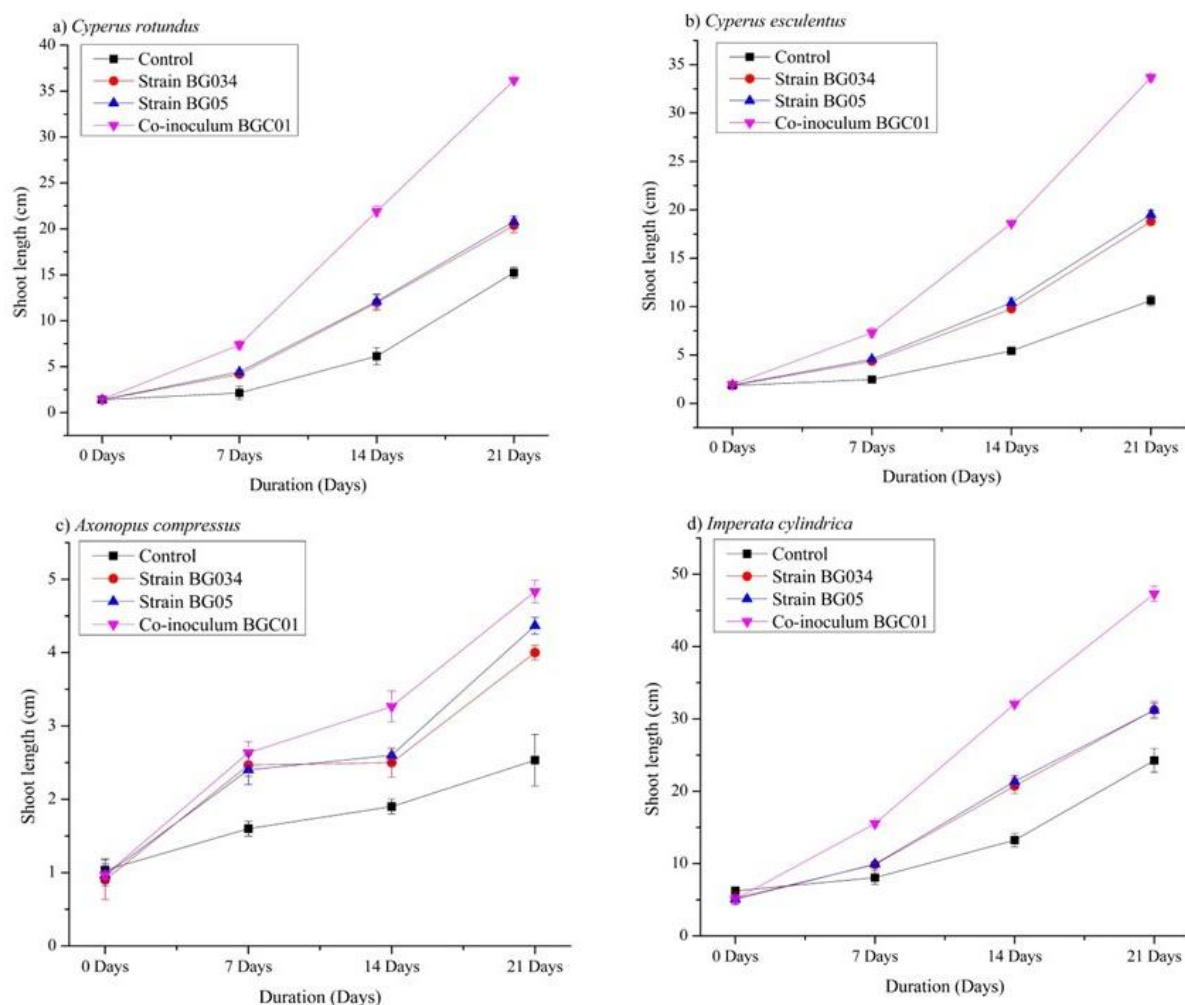


Fig. 4.37. Effects of bacterial inoculation on the shoot length (a-d) of *Cyperus rotundus* (a) *Cyperus esculentus* (b), *Imperata cylindrica* (c), and *Axonopus compressus* (d)— throughout 21 days. The study assessed the PGP properties of isolated bacterial strains and their co-inoculum. Data are expressed as means \pm S.D. (n = 3).

across a variety of crops. The PGP attributes of *Bacillus cereus* have also been extensively documented in previous studies (Naseem et al., 2024; Sahile et al., 2021). Notably, Zhao et al. (2024) revealed the effectiveness of *Bacillus cereus* isolated from cyanobacterial crusts by significantly enhancing parameters in maize seedlings, notably shoot and root lengths (Zhao et al., 2024). The findings of the current study, when considered alongside these earlier observations, affirm the two isolated strains' potential as efficient PGPR. These strains were also compatible when employed as a co-inoculum, as proven by previous assessments done within this study paradigm. Their synergistic combination enhanced the effectiveness of the treatments, resulting in better plant growth results than individual applications. The *in vivo*

results of this study highlight the efficiency of co-inoculum BGC01, which demonstrated robust biostimulant properties, positioning it as a promising candidate for enhancing plant growth under unfavorable conditions.

4.7. Preparation of Biostimulant from Agricultural Byproducts

4.7.1. Amino Acid Analysis Using an Amino Acid Analyzer

The amino acid analysis of mustard cake treated with 1% papain shows a significant increase in the levels of various amino acids compared to untreated mustard cake. This indicates that the enzymatic treatment effectively enhances the nutritional value of the biostimulant produced (Table 4.11). Mustard cake, a nutrient-rich byproduct from mustard seed oil extraction, is well-known for its high concentration of vital nutrients, particularly amino acids, which promote plant growth and development (Vichare & Morya, 2024). Nonetheless, in its raw state, the amino acids present in the mustard cake are complexly formed (protein) making them difficult for plants to access and utilize easily. Plants absorb nutrients in simpler forms, such as free amino acids or short peptides, which may be directly taken by their root systems and incorporated into metabolic processes. Because of the intricate nature of amino acids in untreated mustard cake, plants typically fail to break them easily, limiting the direct nutritional benefits that mustard cake may otherwise provide. Papain, a proteolytic enzyme derived from papaya latex, was exploited to deconstruct the complex protein structures in mustard cake into simpler peptides and free amino acids, thus enhancing the accessibility of these nutrients for plant absorption (Choudhary et al., 2024). This breakdown process is crucial for plant growth and development. The findings demonstrate that increases in key amino acids such as isoleucine, leucine, lysine, and methionine, are required for several metabolic processes in plants, including protein synthesis, cellular development, and better resistance to environmental stresses. For example, the content of isoleucine in treated mustard cake increased from 5.17 mg/L to 7.57 mg/L in the biostimulant, whereas methionine levels rose from 2.12 mg/L to 4.52 mg/L. These elevated levels of essential amino acids in the biostimulant help plants to meet nutritional requirements. Other amino acids that have substantial increases include valine, histidine, and alanine, which are also essential for cellular function and stress response in plants. It reported that valine concentrations increased from 0.8 mg/L to 3.2 mg/L, while histidine concentrations increased from 0.03 mg/L to 2.43 mg/L, respectively. Furthermore, increases in amino acids such as aspartate, glycine, serine, and tyrosine enhance the biostimulant's nutritional profile highlighting papain's efficacy in

breaking down complex proteins and releasing these essential amino acids. The amino acids are essential for photosynthesis, nitrogen metabolism, and general plant health, which may make the biostimulant particularly effective for promoting optimum development (Khan et al., 2019; Yang et al., 2020). The enhanced profile of amino acids indicates that the biostimulant has the potential to significantly contribute to plant development and growth. They do this by improving nutrient absorption and utilization, as well as providing plants with a more bioavailable form of amino acids.

Table 4.11. The composition of amino acids (mg/L) in mustard cake and prepared biostimulant.

Amino Acids	Mustard Cake	Biostimulant
Isoleucine	5.17 ± 1.20	7.57 ± 1.06
Leucine	0.44 ± 0.14	2.84 ± 1.05
Lysine	4.15 ± 1.32	6.55 ± 2.30
Methionine	2.12 ± 0.5	4.52 ± 1.05
Tryptophan	1.56 ± 0.5	3.96 ± 1.12
Threonine	18.79 ± 4.62	21.19 ± 3.52
Valine	0.8 ± 0.2	3.2 ± 1.01
Histidine	0.03 ± 0.0	2.43 ± 0.43
Alanine	3.16 ± 0.82	5.56 ± 1.32
Arginine	2.33 ± 0.61	4.73 ± 1.20
Aspartate	4.09 ± 0.52	6.49 ± 1.35
Glycine	2.14 ± 0.20	4.54 ± 1.42
Serine	2.55 ± 0.52	4.95 ± 0.74
Tyrosine	0.7 ± 0.2	3.19 ± 1.24

The data are expressed as mean ± S.D.(n=3).

4.7.2. Greenhouse Experiment for Biostimulant Effectiveness

The findings from the greenhouse study illustrate the effects of different biostimulant concentrations (25%, 50%, 75%, and 100%) on shoot and root lengths in four plant species *C. rotundus*, *C. esculentus*, *A. compressus*, and *I. cylindrica*—measured at intervals of 0, 7, 14, and 21 days (Fig. 4.38). As the trial proceeded, higher concentrations of biostimulant led to significant increases in the shoot lengths (Fig. 4.39). At 7 days of experiment period, *C. rotundus* plants treated with 75% and 100% biostimulant had shoot lengths of 10.26 cm and 10.4 cm, respectively, in contrast to 3.03 cm for the control group. The pattern continued, with plants receiving 75% and 100% treatments reaching 34.7 cm and 34.76 cm, respectively, on day 21, compared to 14.23 cm in the control. No significant difference observed between the 75% and 100% treatments indicates a saturation effect beyond the 75% concentration. *C. esculentus* showed a similar growth pattern with shoot lengths of 11.4 cm and 11.7 cm at day 7 under the 75% and 100% treatments, respectively, whereas the control was 2.43 cm. By day 21, the shoot lengths of the 75% and 100% treatments were 35.1 cm and 35.33 cm, respectively, whereas the control reached 11.36 cm. Similarly, *A. compressus* also demonstrated a positive response, with shoot lengths of 4.26 cm and 4.36 cm by day 21 under the 75% and 100% treatments, compared to 2.93 cm in the control. *I. cylindrica* had the most positive response to biostimulant, with shoot lengths of 55.83 cm and 56 cm in the 75% and 100% treatments by day 21, compared to 25.43 cm for the control, emphasizing its potential for enhanced growth through nutrient and hormone supplementation. The comprehensive statistical results are summarized in Table 4.12.

Table 4.12. Statistical results on shoot length among the species upon biostimulant treatment (from 7 days to 21 days experiment periods).

Plant species	df	Test-statistics	<i>p</i>	Statistical Test
<i>Cyperus rotundus</i>	4	H= 11.26	0.023*	Kruskal-Wallis
<i>Cyperus esculentus</i>	4	H= 14.79	0.005**	
<i>Axonopus compressus</i>	4, 40	F= 5.16	0.001**	one-way ANOVA
<i>Imperata cylindrica</i>	4	H= 12.95	0.011*	Kruskal-Wallis
H= Chi square, F= F-statistic, *= Significant, **= Moderately significant				

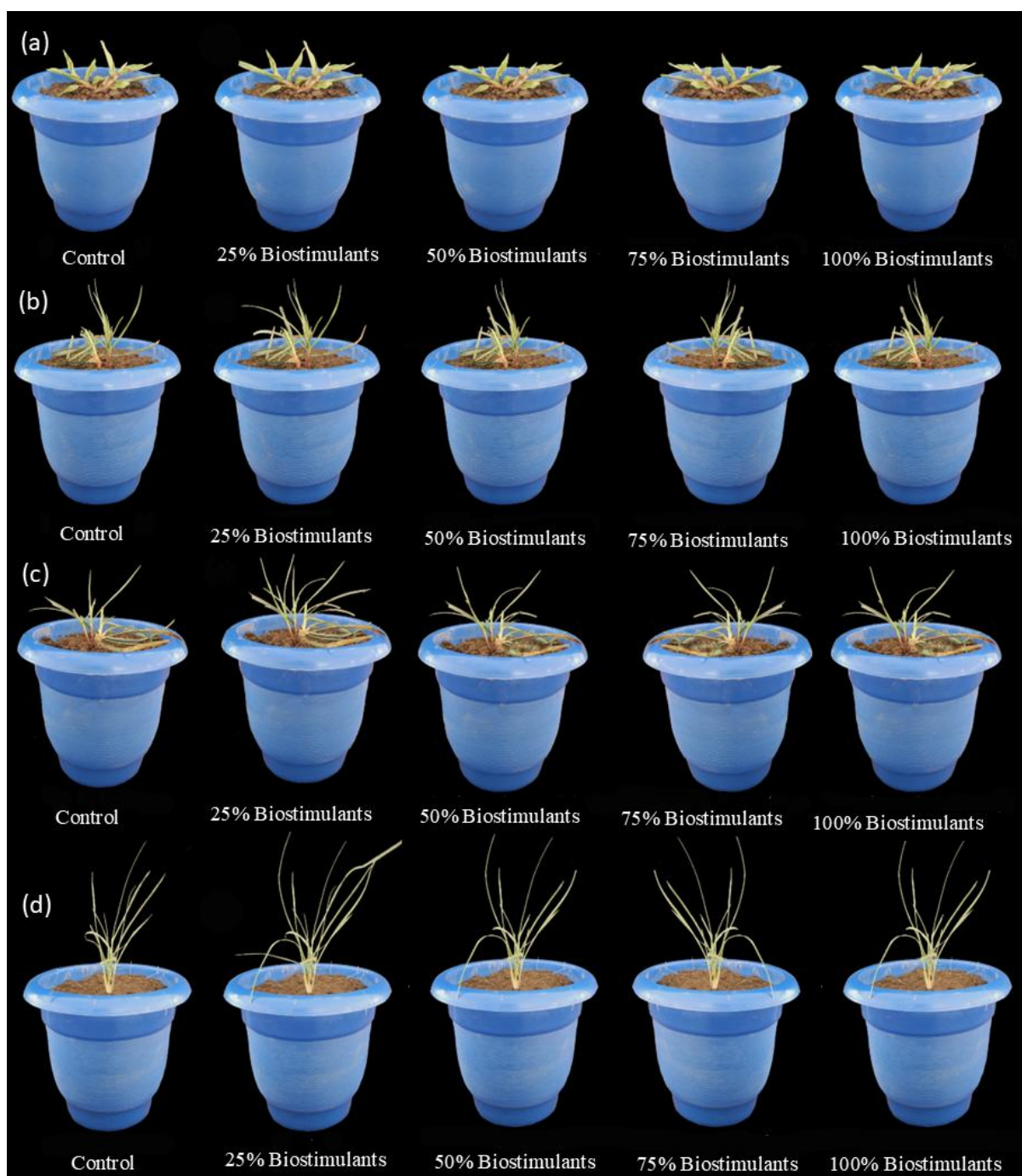


Fig. 4.38. *In vivo* experimental setup for plant growth-promoting test by formulated biostimulant. *Cyperus rotundus* (a), *Cyperus esculentus* (b), *Imperata cylindrica* (c), and *Axonopus compressus* (d).

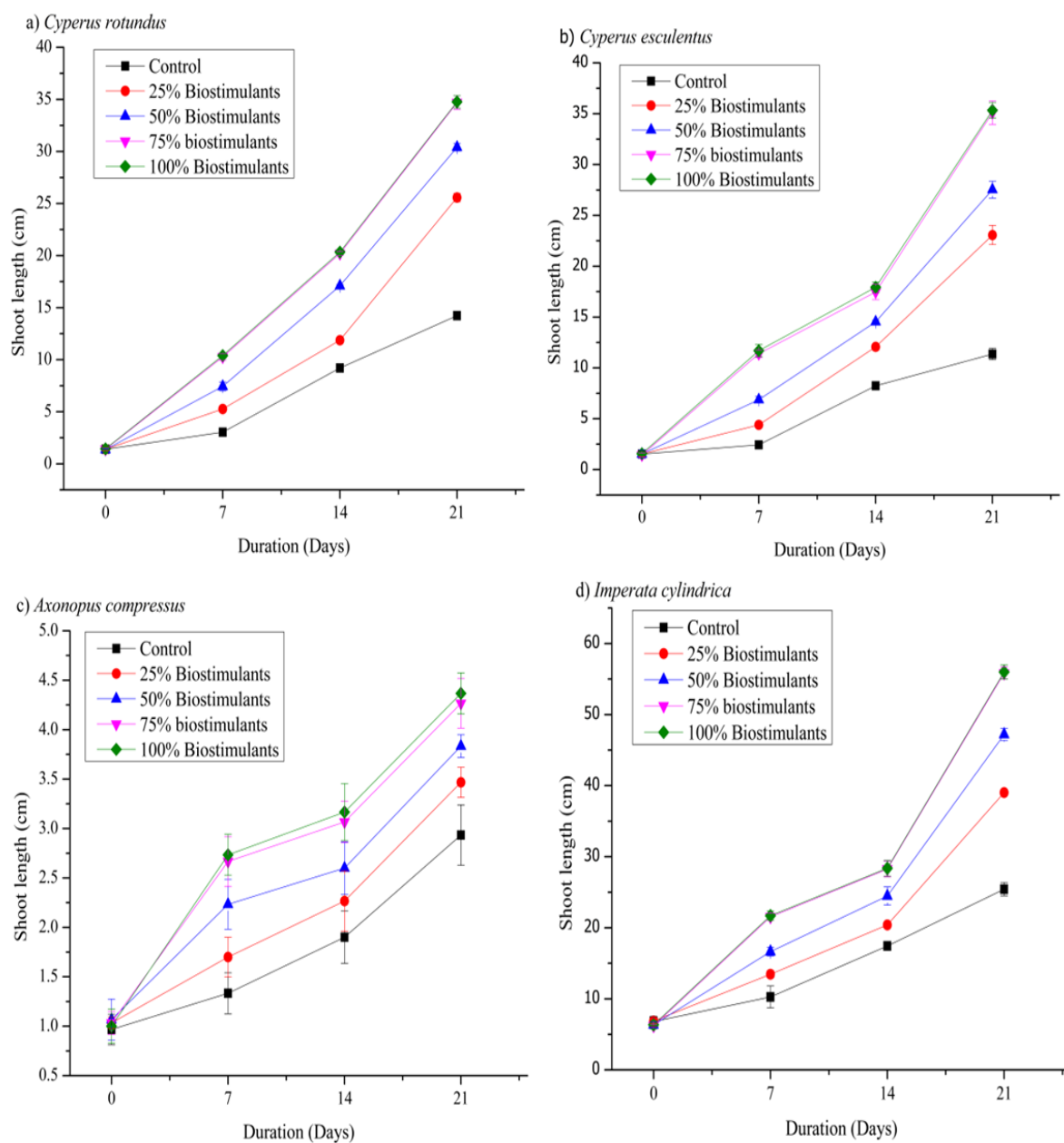


Fig. 4.39. Effects of biostimulant on the shoot length (a-d) of *Cyperus rotundus* (a), *Cyperus esculentus* (b), *Imperata cylindrica* (c), and *Axonopus compressus* (d)— throughout 21 days. Data are expressed as means \pm S.D (n = 3).

The results on root length showed a similar pattern across all studied plant species (Fig. 4.40). At $p < 0.05$ a significant difference was observed (Table 4.13). In *C. rotundus*, the 100% treatment resulted in a root length of 3.33 cm by day 21, whereas the control group only attained 2.01 cm, with the 75% treatment measuring 3.26 cm, demonstrating a saturation effect at higher concentration. Similarly, in *C. esculentus*, the 75% and 100% treatments yielded root lengths of 3.9 cm and 3.93 cm, respectively, compared to the control, which measured 2.33 cm. The other species showed significant increases in root length with higher concentrations of the biostimulant. These findings suggest that elevated concentrations of biostimulant significantly promote growth in both shoot and root lengths compared to the control, with growth peaking at 75% biostimulant concentration. Beyond this point, further increasing concentration to 100% yielded negligible growth, suggesting a saturation point. Collectively, these results imply that the formulated biostimulant exerts a beneficial effect on plant growth by improving nutrient absorption and hormone synthesis, likely promoting cell division and expansion in both shoots and roots.

Table 4.13. Statistical results on root length among the species upon treatment of biostimulant (from 7 days to 21 days experiment periods).

Plant species	df	Test-statistics	<i>p</i>	Statistical Test
<i>Cyperus rotundus</i>	4, 40	F= 3.97	0.008**	one-way ANOVA
<i>Cyperus esculentus</i>	4	H= 13.23	0.009**	Kruskal-Wallis
<i>Axonopus compressus</i>	4, 40	F= 9.086	2.56E-05***	one-way ANOVA
<i>Imperata cylindrica</i>	4, 40	F= 6.36	0.00046***	
H= Chi square, F= F-statistic, **= Moderately significant, ***= Highly significant				

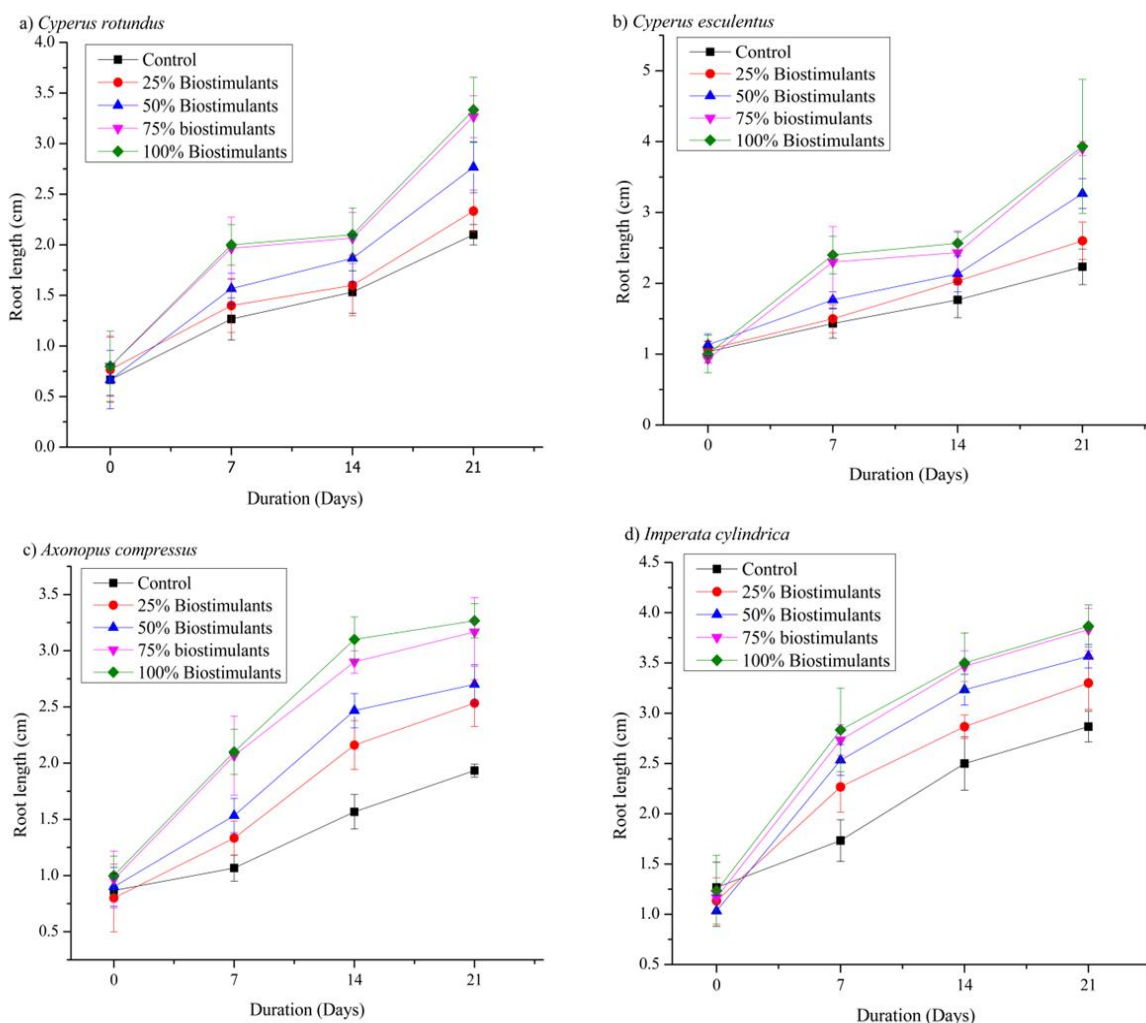


Fig. 4.40. Effects of biostimulant on the root length (a-d) of *Cyperus rotundus* (a), *Cyperus esculentus* (b), *Imperata cylindrica* (c), and *Axonopus compressus* (d) throughout 21 days. Data are expressed as means \pm S.D. (n = 3).

4.8. Nitro-PAH Degradation by Plant-Bacterial Co-Inoculum and Biostimulant in Microcosmic Soil

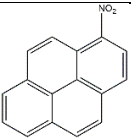
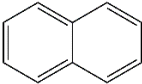
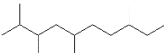
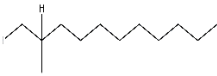
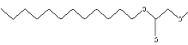
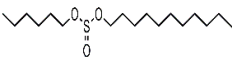
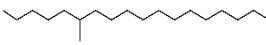
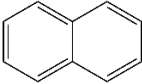
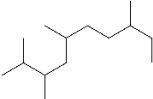
Over 60 days, the experiment used two distinct microcosms (M2 for 1-nitropyrene and M3 for 2-nitrofluorene) and tracked variations in nitro-PAHs degradation intermediates and ultimate breakdown products at intervals of 0, 30, and 60 days, respectively. GC-MS analysis provided useful insights into nitro-PAHs transformation routes and assisted in the identification of intermediate metabolites (Table 4.14 and Table 4.15), validating that plant-bacterial co-inoculum (BGCP01) can significantly improve the conversion of nitro-PAHs to simpler hydrocarbons.

4.8.1. 1-nitropyrene Degradation Dynamics

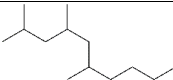
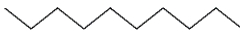
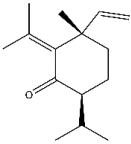
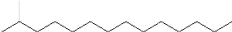
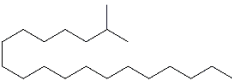
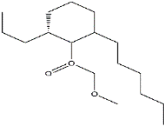
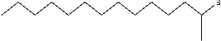
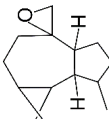
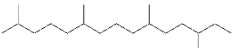
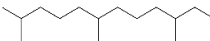

In the microcosm spiked with 1-nitropyrene, the GC-MS analysis revealed that 1-nitropyrene remained unchanged during the initial sampling period (0 days), indicating minimal plant-bacterial or biochemical interaction with the substance at the start of the experiment. By the 30-day sampling period, considerable breakdown products of 1-nitropyrene had emerged, highlighting the early phases of degradation. Among these products was naphthalene, a two-ring PAH, indicating that the intricate nitro-PAH structure was initially broken down. Additional compounds found at the time were 2,3,5,8-tetramethylene and 1-iodo-2-methylundecane, indicating additional conversions and possibly bacterial acclimatization to the chemical. Furthermore, other compounds such as methoxyacetic acid, 2-tridecyl ester, sulfurous acid hexyl pentadecyl ester, and 6-methyloctadecane were also identified, showing different metabolic pathways including methylation, esterification, and oxidative or reductive reactions that are most likely intermediate steps in the breakdown of 1-nitropyrene.

The 60-day period reported a broader array of transformation products within the 1-nitropyrene spiked microcosm, indicating progressive and further advanced degradation processes. Naphthalene persisted as detectable, illustrating the continuous transformation of 1-nitropyrene through bacterial and phytogenic activities. Additional breakdown products, including aliphatic hydrocarbons like decane and 2,4,6-trimethyldecane, point to a shift toward smaller molecular structures and, eventually, mineralization. A variety of molecules formed, including isoshyobunone, 2-methyltridecane, and aromadendrene oxide-(1), demonstrating complex interactions between microbial enzymes and nitro-PAHs intermediates. Additionally, compounds like 2-bromotetradecane, 2,6,10,15-tetramethylheptadecane, and 2,6,10-trimethyldodecane were reported due to subsequent demethylation and halogenation processes. The presence of various methylated and decane derivatives at 60 days highlights the substantial breakdown into smaller aliphatic compounds, which could suggest a widespread breakdown of the 1-nitropyrene which may represent the penultimate phase preceding complete mineralization. This range of products suggests a clear reduction in molecular complexity and supports the effectiveness of plant-bacterial interaction in the bioremediation of 1-nitropyrene in terrestrial environments. Fig. 4.41 presents the Total Ion Chromatogram (TIC) at baseline conditions (0 days). After 30 days of treatment with the plant bacterial co-inoculum, the chromatogram in Fig. 4.42 reveals notable shifts in metabolite composition, indicating active biotransformation. These metabolic alterations continue to progress, as shown in Fig. 4.43,

Table 4.14. Identified metabolites of 1-nitropyrene in spiked microcosms at baseline (0 days) and after 30 and 60 days of treatment with plant-bacterial co-inoculum and biostimulant.

Incubation Periods	Retention time (min)	Area count*min	Peak area (in %)	Compounds	Molecular formulas	Molecular weight(g/mol)	Chemical formula
0 days	44.712	849768344	95.65	1-nitropyrene	C ₁₆ H ₉ NO ₂	247.25	
	5.47	132363.4	63.6	Naphthalene	C ₁₀ H ₈	128.17	
	6.034	17918.56	8.61	2,3,5,8-tetramethyldecane	C ₁₄ H ₃₀	198.388	
30 days	8.946	19525.92	9.38	1-Iodo-2-methylundecane -	C ₁₂ H ₂₅ I	296.23	
	9.959	10230.08	4.92	Methoxyacetic acid, 2-tridecyl ester	C ₁₆ H ₃₂ O ₃	272.42	
	15.942	17688.79	8.5	Sulfurous acid, hexyl pentadecyl ester	C ₂₁ H ₄₄ O ₃ S	376.6	
	22.387	10398.13	5	6methyloctadecane-	C ₁₉ H ₄₀	268.5209	
60 days	5.463	145339.5	33.36	Naphthalene	C ₁₀ H ₈	128.17	
	6.031	50428.05	11.57	2,3,5,8-tetramethyldecane,	C ₁₄ H ₃₀	198.388	

Contd.

Incubation Periods	Retention time (min)	Area count*min	Peak area (in %)	Compounds	Molecular formulas	Molecular weight(g/mol)	Chemical formula
60 days	6.456	32339.27	7.42	2,4,6-trimethyldecane	C ₁₃ H ₂₈	184.3614	
	7.303	8564.466	1.97	Decane	C ₁₀ H ₂₂	142.2817	
	8.602	7313.159	1.68	Isoshyobunone	C ₁₅ H ₂₄ O	220.3505	
	8.949	46906.35	10.77	2-methyltridecane	C ₁₄ H ₃₀	198.388	
	9.963	36181.36	8.3	2-methylnonadecane	C ₂₀ H ₄₂	282.5475	
	15.942	32105.07	7.37	Methoxyacetic acid, 4-tetradecyl ester	C ₁₇ H ₃₄ O ₃	286.4	
	17.486	21407.33	4.91	2-Bromotetradecane	C ₁₄ H ₂₉ Br	277.28	
	22.268	7112.942	1.63	Aromadendrene oxide-(1)	C ₁₅ H ₂₄ O	220.3505	
	22.387	17585.69	4.04	2,6,10,15-tetramethylheptadecane	C ₂₁ H ₄₄	296.5741	
	23.417	16102.53	3.7	2,6,10-trimethyldodecane,	C ₁₅ H ₃₂	212.4146	
	27.125	14295.63	2.12	6-methyloctadecane,	C ₁₉ H ₄₀	268.5	

where GC-MS analysis at 60 days demonstrates the further breakdown of 1-nitropyrene, leading to the formation of intermediate degradation products and ultimately yielding linear aliphatic hydrocarbons. The corresponding mass spectra of these metabolites are provided in Fig. S1, further confirming the structural transformations occurring throughout the degradation process.

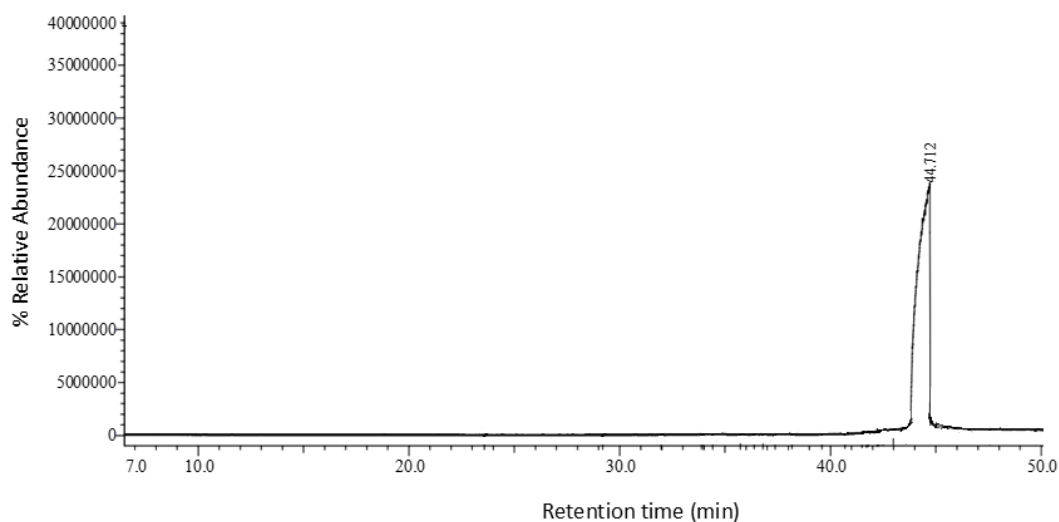


Fig. 4.41. TIC of 1-nitropyrene metabolites via GC-MS under the plant-bacterial co-inoculum and biostimulant treatment at baseline condition (0 days).

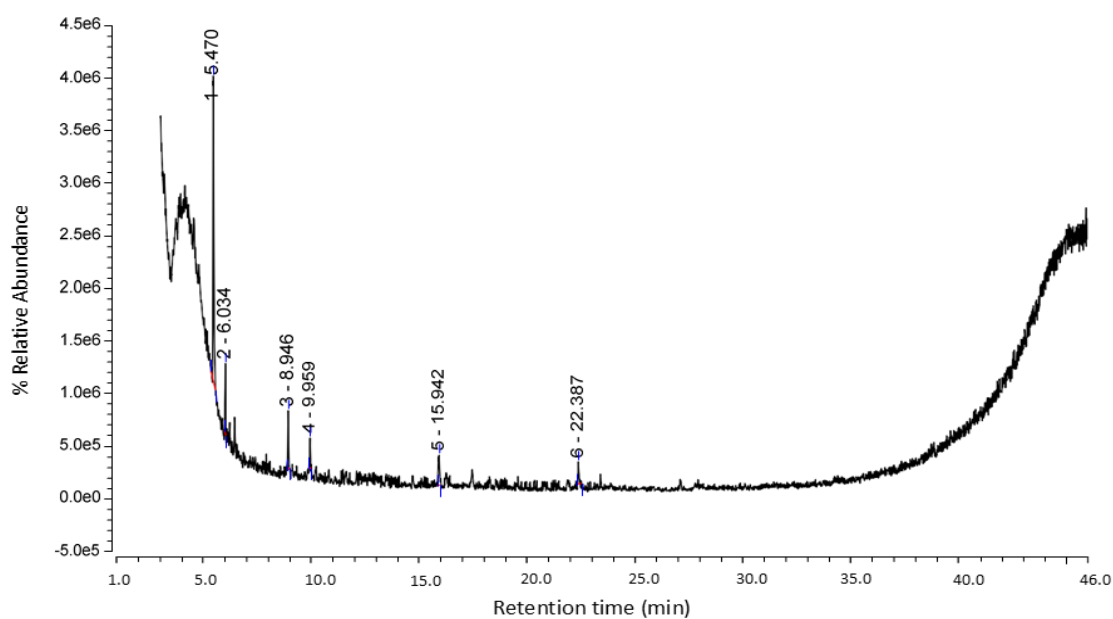


Fig. 4.42. TIC of 1-nitropyrene metabolites via GC-MS throughout the plant-bacterial co-inoculum and biostimulant treatment following 30 days of incubation.

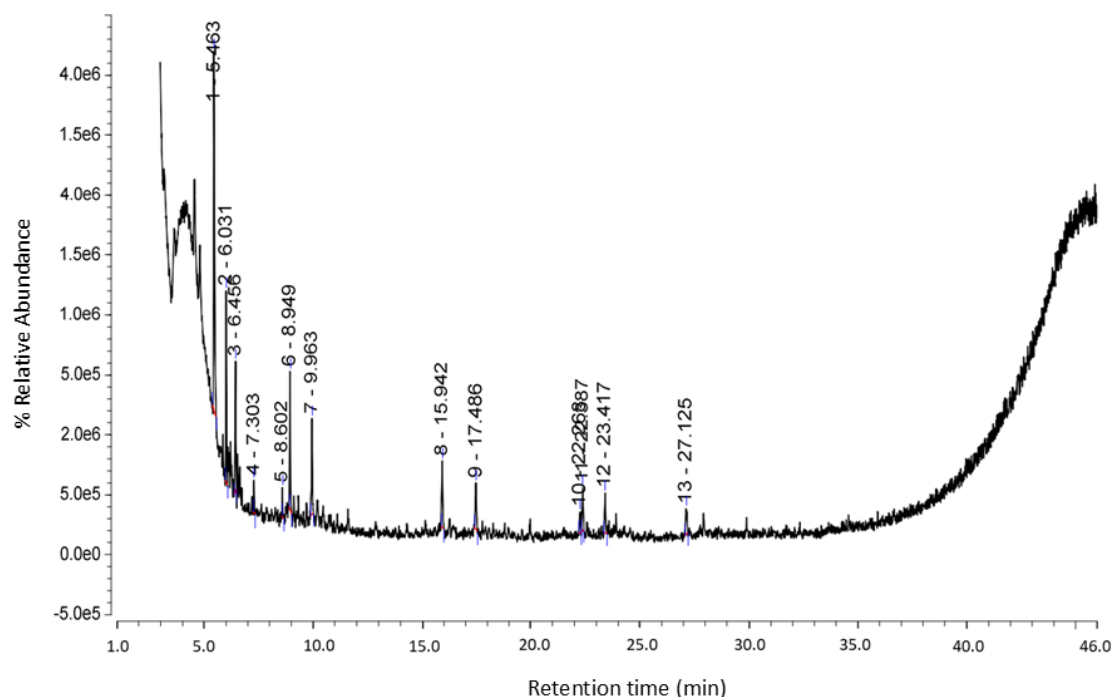


Fig. 4.43. TIC of 1-nitropyrene metabolites via GC-MS throughout the plant-bacterial co-inoculum and biostimulant treatment following 60 days of incubation. The chromatograms demonstrate the progressive alterations in metabolite profiles throughout the degradation process.

4.8.2. 2-nitrofluorene Degradation Dynamics

A similar degradation and change pattern were observed in the plant-bacterial co-inoculum and biostimulant treated 2-nitrofluorene-spiked microcosm. At the initial time point of 0 days, only the parent compound, 2-nitrofluorene, was confirmed to be present in the microcosm. Naphthalene was detected after 30 days of sampling periods, consistent with the degradation trend observed in the 1-nitropyrene-treated microcosm and showing that the first transformation of nitro-PAHs in these contexts may follow comparable routes. The appearance of naphthalene implies that microbial activity has begun the structural change of 2-nitrofluorene, either by ring cleavage or reductive de-nitration pathways, which are widely used by bacteria to break down nitro-aromatic compounds. After 60 days, the spectrum of transformation products significantly increased, indicating substantial degradation and biotransformation of 2-nitrofluorene. GC-MS analysis revealed a wide range of molecules, including 1H-Indene, 1-methylene-, and 5,8-diethyldodecane, indicating further de-aromatization and conversion into compounds with higher alkyl chains. Other molecules, such

as 2,3,5,8-tetramethyldecane, 1-iodo-2-methylnonane, and 2,9-dimethyldecane, show additional methylation and iodination, suggesting that several microbial metabolic pathways may be involved. The presence of 2,3,5,8-tetramethyldecane, 1-iodo-2-methylnonane, and 2,6,10,15-tetramethylheptadecane shows that the breakdown mechanisms are comparable to those observed in the 1-nitropyrene microcosm. These alterations demonstrate that plant-microbial systems may enhance both reductive and oxidative processes within nitro-PAHs breakdown pathways. The presence of methoxyacetic acid, 4-tetradecyl ester, in both microcosms indicates that plant-microbe systems may facilitate ester-linked intermediates during the bioremediation of nitro-PAHs, potentially as a byproduct of microbial enzymatic processes.

The study demonstrates that plants, bacteria, and biostimulant interactions efficiently aid in the breakdown of nitro-PAHs by employing these compounds as exclusive sources of carbon and energy. Fig. 4.44 presents the TIC at baseline conditions (0 days), providing an initial profile of 2-nitrofluorene metabolites before microbial treatment. Following 30 days of plant-bacterial co-inoculum and biostimulant treatment, the chromatogram in Fig. 4.45 shows significant alterations in metabolite composition, indicating ongoing biotransformation. Further metabolic changes are evident in Fig. 4.46, which depicts the TIC after 60 days of incubation, highlighting the progressive breakdown of 2-nitrofluorene and the formation of intermediate degradation products eventually yielding linear aliphatic hydrocarbons (Fig. S2 shows their respective mass spectra).

Fig. 4.47 illustrates the proposed degradation pathways of nitro-PAHs by plant-bacterial co-inoculum (BGCP01) in a microcosm system. The schematic representation highlights the sequential breakdown of 1-nitropyrene and 2-nitrofluorene through bacterial enzymatic activity and plant-assisted remediation. These bacterial enzymes help to break down complex hydrocarbons, making them more accessible for subsequent degradation into simpler compounds. Previous studies have highlighted that the bacterial breakdown of 1-nitropyrene and 2-nitrofluorene adheres to well-documented enzymatic pathways that encompass nitro group reduction, ring cleavage, mineralization, and assimilation (Grifoll et al., 1992; Rafil et al., 1991). A variety of bacterial enzymes, both extracellular and intracellular, are integral to these mechanisms, including nitroreductases, dioxygenases, and cytochrome P450 monooxygenases (Li et al., 2023). Nitroreductases are a key enzyme that reported to conversion of nitro groups to amino groups, facilitating the structural modifications necessary for subsequent degradation (Claus, 2014; Penning et al., 2022). Dioxygenases, including RHO

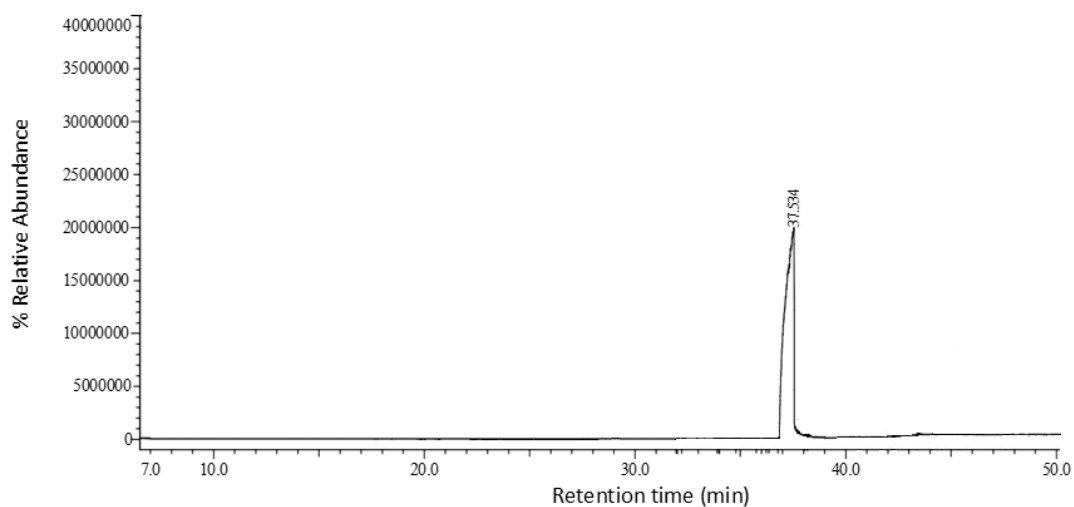


Fig. 4.44. TIC of 2-nitrofluorene metabolites via GC-MS under the plant-bacterial co-inoculum and biostimulant treatment at baseline conditions (0 days).

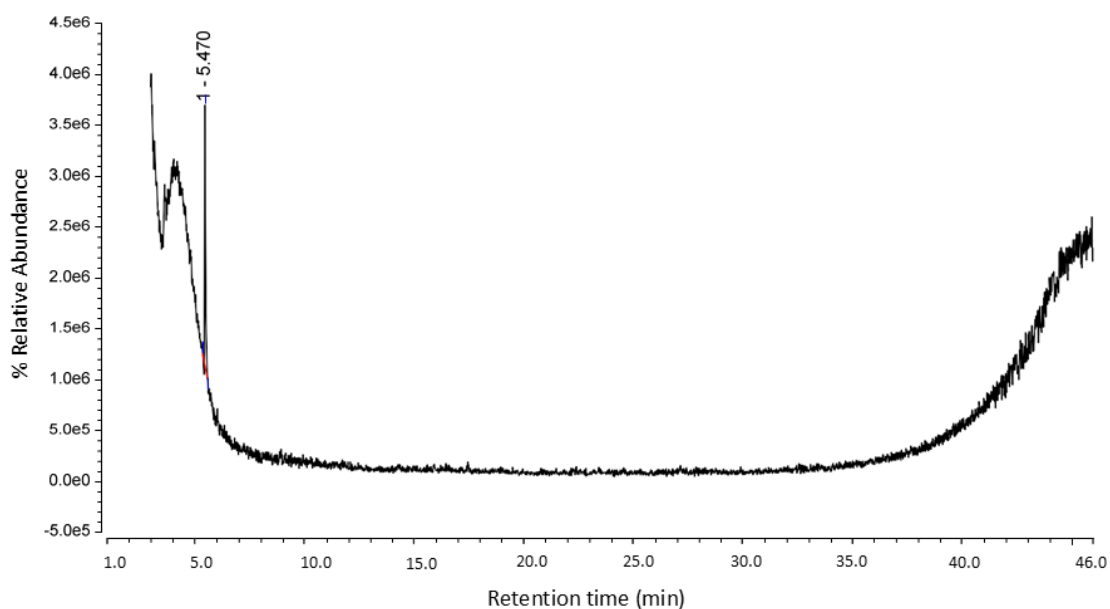


Fig. 4.45. TIC of 2-nitrofluorene metabolites via GC-MS throughout the plant-bacterial co-inoculum and biostimulant treatment following 30 days of incubation.

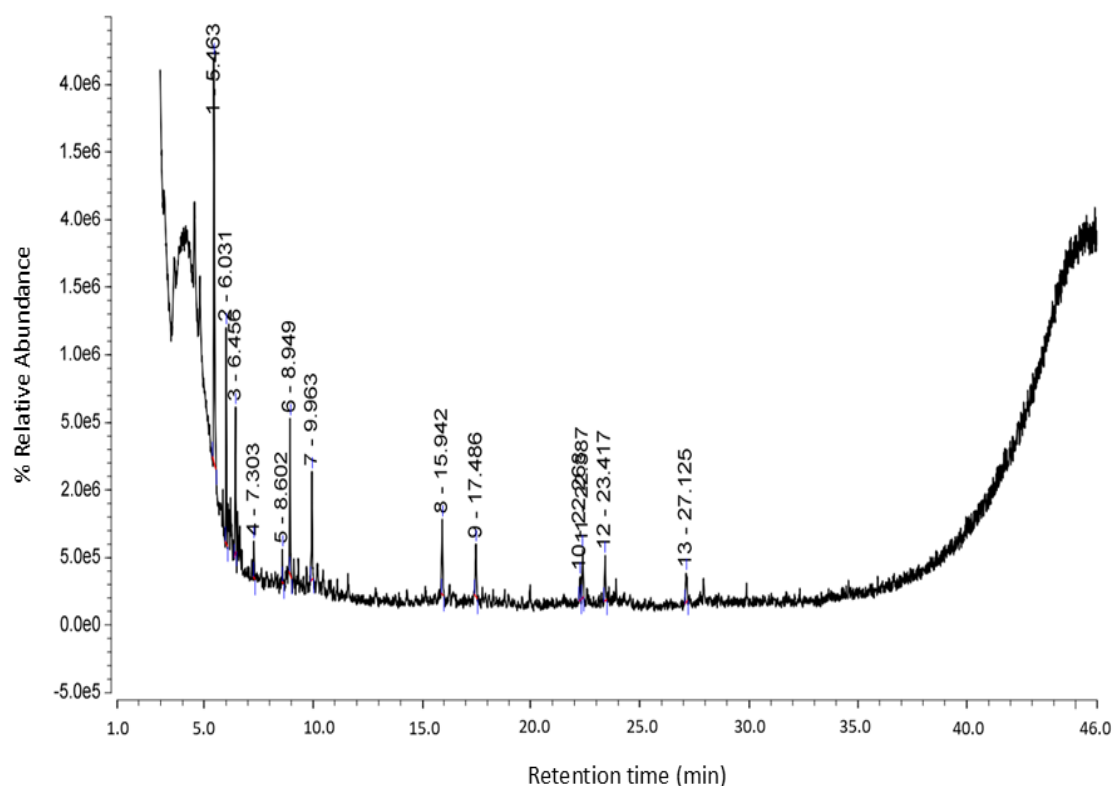


Fig. 4.46. TIC of 2-nitrofluorene metabolites via GC-MS throughout the plant-bacterial co-inoculum and biostimulant treatment following 60 days of incubation. The chromatograms demonstrate the progressive alterations in metabolite profiles throughout the degradation process.

and CYP450s, improve the solubility of nitro-PAHs through the hydroxylation of aromatic rings (Sun et al., 2023). Subsequently, intradiol and extradiol dioxygenases cleave the aromatic structures and formation of intermediates like catechol, which were subsequently metabolized into fatty acids. These metabolic derivatives further entered into the TCA cycle, culminating in the complete mineralization of the studied pollutants (Das et al., 2023; Lipscomb, 2008). Another crucial element that markedly improved the efficacy of this bioremediation approach was the utilization of biostimulant. They act as catalysts for both plant and bacterial processes, facilitating the breakdown of nitro-PAHs. Our findings underline the importance of

biostimulant in this degrading pathway. Our previous experiment revealed that the biostimulant used for this study have a high concentration of amino acids, which are essential for plant growth and development. These amino acids not only provided nourishment to the plants under the stress caused by nitro-PAH pollution but also increased their physiological resilience. By improving root development and metabolic activity of the plants which enhanced the interaction with rhizosphere bacteria, contributing to the overall efficacy of this remediation process. Furthermore, the biostimulants also had a direct and significant effect on rhizosphere bacteria. Following their application, these chemicals aided the bacterial community's multiplication and metabolic activities by providing necessary nutrients. These nutrients supply extra energy for the bacteria, allowing them to adapt to this nitro-PAH-contaminated environment and facilitate the breakdown of nitro-PAHs. Through this process, the bacterial metabolic activity was boosted, which was for remediated nitro-PAHs. Biostimulants' dual functionality—facilitating plant development while also enhancing microbial activity—was especially important in bioremediation. Plants provide an extra carbon source for bacteria through root exudates, while bacteria convert nitro-PAHs into less harmful intermediates that are easier for further phytoaccumulation. Where plants easily accumulate and detoxify through the help of phytostabilization, phytovolatilization, and photodegradation mechanisms. The biostimulants also provide a favorable habitat for indigenous bacteria and plants, fostering a synergistic ecosystem in which both biotic elements thrive, thereby speeding up nitro-PAH breakdown. Furthermore, the data from our experiment support the notion that enzymatic mechanisms are critical in the transformation of nitro-PAHs but were not accessed in this study. The fluctuations in concentrations of the introduced nitro-PAHs within microcosms, as well as their gradual decline, were also noted in this study. A gradual decrease of 1-nitropyrene and 2-nitrofluorene was detected, leading to a significant result. HPLC analysis revealed that after 30 days of incubation, no visible residues of the parent nitro-PAHs remained within the microcosms. This observation is consistent with the results of the prior qualitative GC-MS investigation which showed that by the end of the 30-day experimental period, both microcosms had shown the absolute breakdown of the parent chemicals, with no detectable residues remaining. The consistent agreement between the HPLC and GC-MS results accentuates the reliability of the experimental findings.

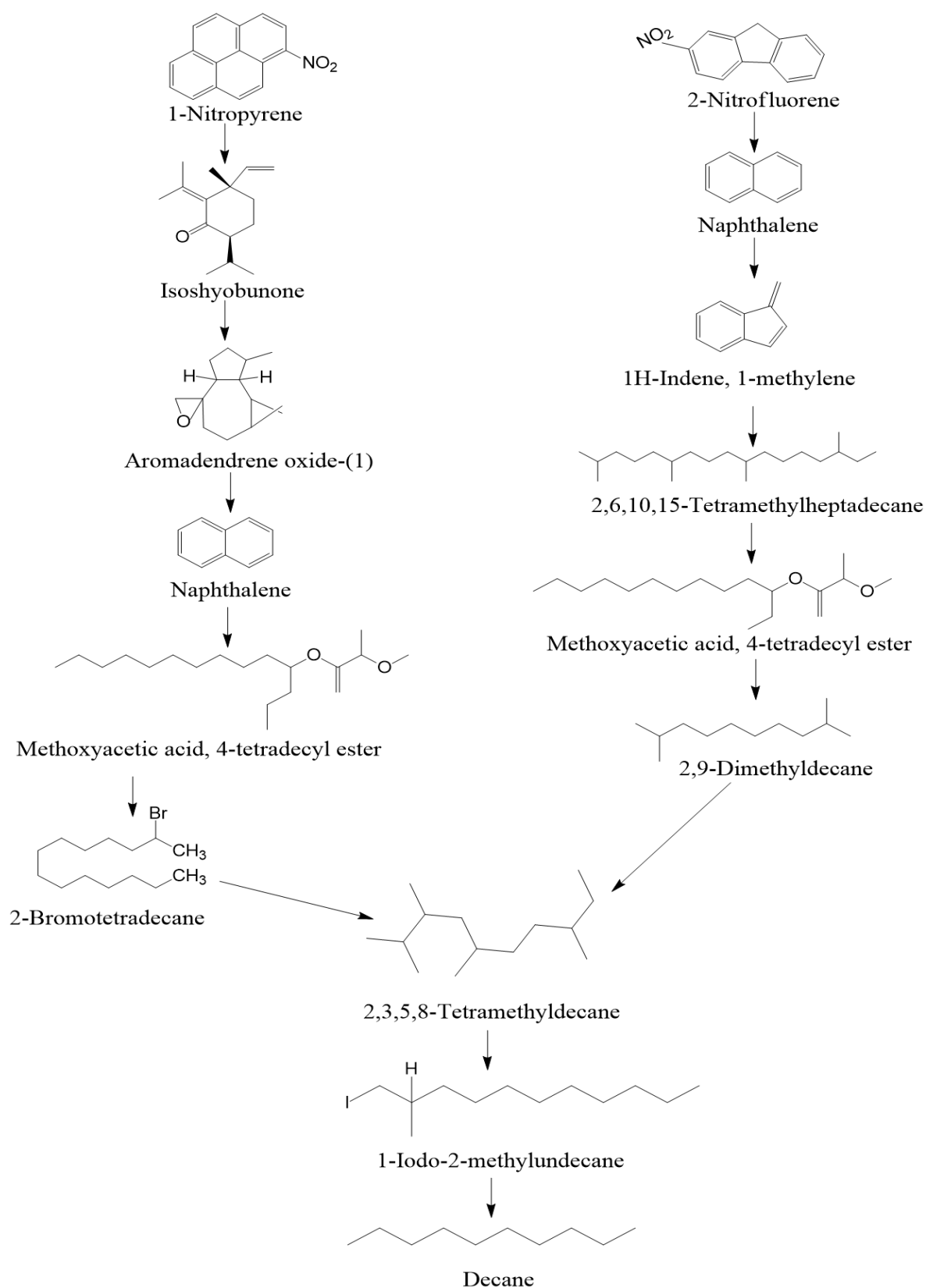
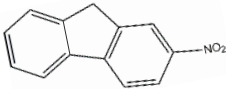
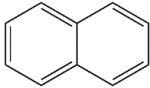
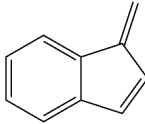
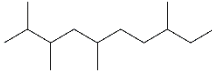
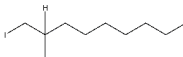
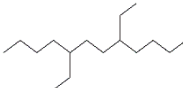
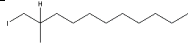
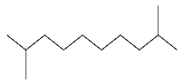

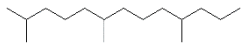

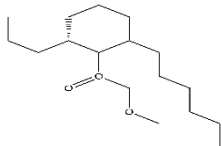


Fig. 4.47. Proposed nitro-PAH degradation pathways by plant-bacterial co-inoculum in microcosms. It elucidates the stepwise degradation of 1-nitropyrene and 2-nitrofluorene via bacterial enzymatic processes complemented by plant-mediated remediation.

Table 4.15. Identified metabolites of 2-nitrofluorene in spiked microcosms at baseline (0 days) and after 30 and 60 days of treatment with plant-bacterial co-inoculum and biostimulant.

Incubation Periods	Retention time (min)	Area count*min	Peak area (in %)	Compounds	Molecular formulas	Molecular weight(g/mol)	Chemical structures
0 days	37.534	565333742	98.94	2-nitrofluorene	C ₁₃ H ₉ NO ₂	211.21	
30 Days	5.47	118891.3	100	Naphthalene	C ₁₀ H ₈	128.17	
	5.47	70381.56	24.03	1H-Indene, 1-methylene-	C ₁₀ H ₈	128.1705	
60 Days	6.034	37457.11	12.79	2,3,5,8-tetramethyldecane	C ₁₄ H ₃₀	198.388	
	6.459	20819.88	7.11	1-Iodo-2-methylnonane	C ₁₀ H ₂₁ I	268.1782	
	6.565	15367.61	5.25	5,8-diethyldodecane	C ₁₆ H ₃₄	226.4412	

Contd.

Incubation Periods	Retention time (min)	Area count*min	Peak area (in %)	Compounds	Molecular formulas	Molecular weight(g/mol)	Chemical structures
60 days	8.946	41003.83	14	1-Iodo-2-methylundecane	C ₁₂ H ₂₅ I	296.23	
	9.959	31653.07	10.81	2,9-dimethyldecane	C ₁₂ H ₂₆	170.334	
	15.945	33243.5	11.35	2,6,10,15-tetramethylheptadecane	C ₂₁ H ₄₄	296.5741	
	17.476	16239.51	5.54	2,6,10-trimethyltetradecane	C ₁₇ H ₃₆	240.4677	
	22.383	13430.83	4.59	2-methyleicosane	C ₂₁ H ₄₄	296.5741	
	23.428	13284.26	4.54	Methoxyacetic acid, 4-tetradecyl ester	C ₁₇ H ₃₄ O ₃	286.4	

4.9. Effect of Plant-Bacterial Co-Inoculum and Biostimulant on Soil Properties in nitro-PAH Microcosms

Soil physicochemical parameters are important markers of fertility, microbial diversity, and overall soil health, especially in bioremediation studies. In this study, we analyzed the alteration of soil parameters over 60 days under microcosm circumstances, with a particular emphasis on the impacts of plant-bacterial co-inoculum (BGCP01) and biostimulant on nitro-PAHs breakdown (1-nitropyrene and 2-nitrofluorene). The study sought to assess changes in pH, electrical conductivity, accessible nitrogen, phosphorus, potassium, and organic carbon throughout three time periods: 0, 30, and 60 days, and the results are presented in Table 4.16. Additionally, the statistical analysis of these parameters is summarized in Table 4.17, offering a comparative assessment of significance across different time points.

At the start of the investigation (0 days), all microcosms had baseline metrics for organic carbon, accessible potassium, phosphate, nitrogen, electrical conductivity, and pH. These values indicate the soil's original state before the application of microbial and plant-biostimulant treatments. For example, the organic carbon content in all design microcosms ranged between 0.50% and 0.61%, while the available potassium and phosphorus concentrations were measured at 122.13-123 kg/ha and 21.73-22.4 kg/ha, respectively. Available nitrogen levels were ranging from 286-287 kg/ha. Electrical conductivity and pH were 0.10-0.12 dS/m and 5.06-5.3, respectively. These basic measures define the foundational conditions for each microcosm, allowing for comparison examination after 30 and 60 days of treatment.

Following the application of the designed plant-bacterial co-inoculum (BGCP01) and biostimulant resulted in significant changes in soil physicochemical parameters, notably nitrogen, phosphorus, potassium, and organic carbon levels. In the microcosm spiked with 1-nitropyrene, treatment with plant-bacterial co-inoculum (BGCP01) and biostimulant resulted in an organic carbon content increase from 0.57% to 0.70% at 30 days, eventually reaching 0.93% at the end of the experiment period (60 days). This increase was attributed to the microbial breakdown of organic contaminants and the integration of plant-derived organic matter, which assists in soil carbon sequestration. Similarly, there was a pronounced enhancement in the levels of available potassium and phosphorus, which reached 159 kg/ha and 26.13 kg/ha at 30 days, respectively, and further escalated to 215.33 kg/ha and 33.13 kg/ha at 60 days, compared to their initial levels of 122.13 kg/ha and 21.73 kg/ha. The available nitrogen also demonstrated to rise from 286 kg/ha to 343.67 kg/ha at 30 days, culminating in

a final concentration of 421.67 kg/ha at 60 days. A similar trend was observed in the 2-nitrofluorene-spiked microcosms. In the plant-microbes and biostimulant treated microcosm organic carbon content increased dramatically from 0.61% to 0.71% after 30 days and then to 0.91% after 60 days. This rise correlates to plants- bacterial decomposition of organic pollutants, which improves soil fertility. Similarly, available potassium levels increased from 123 kg/ha to 163 kg/ha at 30 days, eventually reaching 226.33 kg/ha at 60 days. Phosphorus and nitrogen levels also increased significantly, with phosphorus escalating from an initial value of 21.9 kg/ha to 26.83 kg/ha at 30 days and 36 kg/ha at 60 days. Nitrogen content showed an even greater increase, from 286.3 kg/ha at 0 days to 349.67 kg/ha at 30 days, and ultimately to 427.83 kg/ha at 60 days. Moreover, the stability of pH levels and reduction in electrical conductivity suggest that including plant-bacterial inoculation increases soil purification and creates a more conducive environment for both plant and microbial development. Initially, the soil exhibited a slightly acidic pH, which increased to 5.4 by day 30 and 5.53 by day 60 in the 1-nitropyrene-spiked microcosm. Similarly, in the 2-nitrofluorene-spiked microcosm, pH increased from 5.3 on day 0 to 5.3 on day 30, and then to 5.56 on day 60. In comparison, the control microcosm showed just a slight increase in pH from 5.01 to 5.1 throughout the 60 days reinforcing the necessity of bacterial amendments in altering soil physicochemical properties. Similarly, at the commencement of the study, electrical conductivity values across all contaminated spiked microcosms were noted at 0.12 dS/m. Electrical conductivity decreased consistently throughout the treatment period, reaching 0.11 dS/m at day 30 and 0.09 dS/m at day 60 in the 1-nitropyrene-spiked microcosm. A similar pattern was seen in the 2-nitrofluorene-spiked microcosm, where electrical conductivity decreased from 0.12 dS/m on day 0 to 0.11 dS/m on day 30, and finally to 0.10 dS/m at the end of 60 days. A sterile soil microcosm (contaminated and plant-bacterial co-inoculum and biostimulant free) was set up as a baseline control to acquire a better understanding of the soil's inherent properties without the impact of nitro-PAH spiking or microbial and plant interaction. This microcosm's properties remained relatively stable over the 60 days, with only marginal increases in organic carbon (from 0.5% to 0.59%) and available potassium (from 122.13 kg/ha to 124.33 kg/ha), indicating negligible biological activity and nutrient cycling due to the absence of active microbial communities and plants. Available phosphorus and nitrogen levels similarly showed little fluctuation, with nitrogen increasing slightly from 287 kg/ha to 293.67 kg/ha and phosphorus from 22.4 kg/ha to 23.33 kg/ha. Electrical conductivity remained constant at 0.10 dS/m, but pH levels increased slightly from 5.06 to 5.1, indicating that limited soil activities

were taking place in the absence of plant-bacterial co-inoculum (BGCP01) inoculation and biostimulant administration. This substantial improvement in soil physicochemical parameters suggests that the synergistic action of plants, bacteria, and biostimulant enabled the breakdown and conversion of nitro-PAHs into bioavailable carbon substrates, which were then incorporated into the soil matrix. The applied bacterial species, *Bacillus cereus*, and *Bacillus altitudinis*, efficiently used nitro-PAHs as carbon and energy substrates, resulting in a significant reduction in contaminant concentrations in the soil and an increase in the organic matter reservoir, promoting long-term soil carbon sequestration. Similarly, biostimulant contributed significantly to organic carbon buildup by stimulating plant growth and biomass output. Applied biostimulant, which are rich in amino acids increased plant vitality, root exudation, and microbial activity, creating an ideal environment for pollutant decomposition and nutrient assimilation. The increased root biomass also contributed to increased carbon input into the soil, which aided carbon sequestration and organic matter enrichment. Yang et al. (2014) reported that including *Bacillus cereus* in microbial consortia significantly enhanced soil physicochemical properties under field circumstances (Yang et al., 2014). Furthermore, the extraordinary improvement in soil health can be linked to numerous plant-microbe interactions, such as biological nitrogen fixation, phosphate solubilization, and potassium mobilization. The capacity of *Bacillus cereus* and *Bacillus altitudinis* to solubilize phosphate was validated through *in vitro* phosphate solubilization assays, wherein both strains produced distinct clear halos on Pikovskaya's agar, signifying the secretion of organic acids or chelating metabolites that transformed insoluble phosphorus into forms accessible to plants. These findings were supported by Zhao et al. (2022), who reported that the application of *Bacillus altitudinis* in the rhizosphere of *Zea mays* resulted in a 73.2% increase in available phosphorus content, underscoring the essential role of plant-associated microbes in nutrient solubilization and soil fertility enhancement (Zhao et al., 2022). Furthermore, Zhang et al. (2023) reported that a consortium of *Bacillus altitudinis* and *Pseudomonas chlororaphis* considerably enhanced soil physicochemical parameters (Zhang et al., 2023). Overall, observed increases in the availability of organic carbon, nitrogen, phosphorus, and potassium, combined with decreased electrical conductivity and stabilized pH levels in our microcosms, highlight the synergistic interactions between plants, bacteria, and biostimulant, which collectively foster a more favorable soil environment for nutrient cycling and microbial activity.

Table 4.16. Soil Physicochemical properties of microcosm at 0, 30, and 60 days of treatment.

Microcosms	0 days						30 days						60 days					
	pH	EC (dS/m)	N (kg/ha)	P (kg/ha)	K (kg/ha)	OC%	pH	EC (dS/m)	N (kg/ha)	P (kg/ha)	K (kg/ha)	OC%	pH	EC (dS/m)	N (kg/ha)	P (kg/ha)	K (kg/ha)	OC%
1 nitropyrene	5.3± 0.21	0.12±0. 01	286±2. 94	21.73±1. 18	122.13±1. 34	0.57± 0.06	5.4± 0.14	0.11±0. 02	343.67 ±2.94	26.13±0. 62	159±1.41	0.70± 0.02	5.53 ±0.1	0.09±0. 01	421.67 ±3.40	33.13± 1.47	215.33±4. 50	0.93± 0.02
2- nitrofluorene Spiked	5.3± 0.26	0.12±0. 01	286.3± 1.63	21.9±2.0 7	123±0.57	0.61± 0.03	5.3± 0.08	0.11±0. 01	349.67 ±2.05	26.83±1. 68	163±3.26	0.71± 0.03	5.56 ±0.1	0.10±0. 01	427.83 ±2.40	36±0.8 2	226.33±5. 79	0.91± 0.02
Control	5.06 ±0.0 9	0.10±0. 01	287±0. 08	22.4±1.7 7	122.13±1. 23	0.50 ±0.03	5.1± 0.08	0.10±0. 01	288.67 ±2.49	22.67±1. 62	124.33±1. 18	0.55± 0.02	5.1± 0.08	0.09±0. 01	293.67 ±1.25	23.33± 1.25	124.33±2. 28	0.59± 0.02
EC= Electrical conductivity, N= Available nitrogen, P=Available phosphorus, K= Available potassium, OC= Organic carbon. The data are expressed as mean ± S.D.(n=3).																		

Table 4.17. Statistical test of soil physicochemical properties in the microcosms at the treatment periods.

Soil Parameters	Microcosms	df	Test-statistics	<i>p</i>	Statistical Test
Organic Carbon	Control	2, 6	F=14.08	0.005**	one-way ANOVA
	1-nitropyrene treated	2,6	F= 44.93	0.0002***	
	2 -nitrofluorene treated	2, 6	F=68.17	7.49E-05***	
Potassium	Control	2	H=1.69	0.42	Kruskal-Wallis
	1-nitropyrene treated	2	H=7.2	0.027*	
	2 -nitrofluorene treated	2, 6	F=356.6	25.39E-07***	one-way ANOVA
Phosphorus	Control	2, 6	F= 0.19	0.19	one-way ANOVA
	1-nitropyrene treated	2, 6	F=50.25	0.0001***	
	2 -nitrofluorene treated	2, 6	F=39.47	0.0003***	
Nitrogen	Control	2, 6	F=9.28	0.014*	one-way ANOVA
	1-nitropyrene treated	2, 6	F=2393	1.96E-09***	
	2 -nitrofluorene treated	2, 6	F=1052	2.30E-08***	
pH	Control	2	H=0.27	0.86	Kruskal-Wallis
	1-nitropyrene treated	2	H=1.4	0.48	
	2 -nitrofluorene treated	2, 6	F= 1.78	0.25	one-way ANOVA
EC	Control	2	H= 1.69	0.30	Kruskal-Wallis
	1-nitropyrene treated	2	H=4.62	0.09	
	2 -nitrofluorene treated	2	H=4.1	0.12	

H= Chi square, F= F-statistic, *= Significant, **= Moderately significant, ***= Highly significant

4.10. Effect of Plant-Bacterial Co-inoculum and Biostimulant Interactions on the Plant's Stress Response in nitro-PAH-Contaminated Microcosms

Plants have ingeniously developed special mechanisms to adapt and survive amid environmental stresses such as pollution, which typically result in the formation of ROS (Dumanović et al., 2021; Huang et al., 2019). These ROS are produced as byproducts of oxygen metabolism and include substances such as superoxide radicals, hydrogen peroxide, and hydroxyl radicals (Mandal et al., 2022). While elevated levels of ROS can wreak havoc on cellular structures—targeting lipids, proteins, and nucleic acids—they also serve as vital signaling molecules during periods of stress and developmental transitions. This dual-role hinge relies on a delicate balance maintained by the plant's antioxidative defense systems. When pollution or other environmental stressors induce an overabundance of ROS, this equilibrium is disrupted, resulting in oxidative stress, which can impair normal development and physiological processes (Sahu et al., 2022). To combat the effects of oxidative stress, plants initiate a formidable antioxidative defense arsenal. This armament includes enzymatic antioxidants including SOD, POD, CAT, and APX, alongside other non-enzymatic antioxidants. These enzymes operate harmoniously to neutralize ROS and protect cells from injury (Saddique et al., 2018). The intricate defense mechanism eliminated the ROS, reinstating cellular balance and empowering the plant to withstand environmental adversities.

In the context of this study, the enzymatic activity of vital antioxidative enzymes—POD, APX, SOD, and CAT—was examined in four selected plant species subjected to the influences of contaminants (1-nitropyrene and 2-nitrofluorene), bacterial co-inoculum and biostimulants within microcosms. The studied species—*C. rotundus*, *C. esculentus*, *A. compressus*, and *I. cylindrica*—showed considerably increased enzymatic activities throughout the experimental period, especially at 30 and 60 days. The reported antioxidant enzyme activities at 0, 30, and 60 days are presented in Table 4.18, with the corresponding statistical analyses in Table 4.19. This enzyme upregulation shows that plants were subjected to oxidative stress as a result of the presence of 1-nitropyrene and 2-nitrofluorene, which triggered their defense systems to fight the pollutants' toxicity. At the initial time point (0 days), the leaf enzymes showcased minor differences among the plant species across the three microcosms (control, 1-nitropyrene treated, and 2-nitrofluorene treated). *I. cylindrica* had the highest POD activity, calculating 9.32 U/g F.W. in the control, 9.2 U/g F.W. in the 1-nitropyrene treatment, and 9.5 U/g F.W. in the 2-nitrofluorene treatment. APX activity was also high in *I. cylindrica*, ranging between 3 and

Table 4.18. Antioxidant enzyme activities of the plant species in the experimental microcosm at 0, 30, and 60 days of treatment by plant-bacterial co-inoculum and biostimulant.

Microcosms	Plants species	0 days				30 days				60 days			
		POD (U/g F.W.)	APX (U/min/mg F.W.)	SOD (U/min/mg F.W.)	CAT (U/min/mg F.W.)	POD (U/g F.W.)	APX (U/min/mg F.W.)	SOD (U/min/mg F.W.)	CAT (U/min/mg F.W.)	POD (U/g F.W.)	APX (U/min/mg F.W.)	SOD (U/min/mg F.W.)	CAT (U/min/mg F.W.)
Control microcosm	<i>Cyperus rotundus</i>	2.95±0.36	1.3±0.22	6.28±0.28	3.3±0.29	3±0.16	1.77±0.20	7.1±0.25	3.57±0.33	3.3±0.16	2.1±0.29	7.5±0.41	4.1±0.08
	<i>Cyperus esculentus</i>	1.8±0.36	1.5±0.16	5.4±0.43	4.3±0.57	2.2±0.22	1.83±0.49	7.2±0.24	4.6±0.33	3±0.16	2.43±0.29	8.34±0.39	5.5±0.37
	<i>Axonopus compressus</i>	1.54±0.26	2.03±0.49	2.97±0.25	1.54±0.20	2±0.22	3.4±0.24	3.32±0.31	2±0.22	2.83±0.12	5.2±0.16	4.17±0.17	2.7±0.54
	<i>Imperata cylindrica</i>	9.32±0.52	3.2±0.37	1.97±0.05	8.3±0.59	10.5±0.45	3.5±0.49	3±0.33	10.03±0.37	13.3±0.50	5.4±0.59	5.77 ±0.26	12.7±0.62
1-nitropyrene spiked microcosm	<i>Cyperus rotundus</i>	2.5±0.16	1.5±0.24	6.4±0.29	3.3±0.59	4.33±0.29	3.17±0.17	10.47±0.41	8.23±0.21	6.63±0.26	7.2±0.22	19.5±0.41	14.69±0.41
	<i>Cyperus esculentus</i>	1.93±0.49	1.6±0.29	5.1±0.73	4.6±0.33	3.5±0.16	3.73±0.21	11.3±0.24	10.4±0.33	6.3±0.37	8±0.37	20.87±0.62	17.4±0.99
	<i>Axonopus compressus</i>	1.5±0.29	2±0.57	3±0.37	1.5±0.37	3.87±0.12	5.23±0.26	9.14±0.20	3.3±0.36	8.45±0.50	12±1.42	17.1±0.82	7.1±0.59
	<i>Imperata cylindrica</i>	9.2±0.36	3±0.6	1.5±0.22	8.5±0.50	15.77±0.56	7.2±0.43	5.63±0.39	15.47±0.41	25.6±0.43	12.75±0.32	13.56±0.34	23.5±0.45

Contd.

		0 days				30 days				60 days			
Microcosms	Plants species	POD (U/g F.W.)	APX (U/min/mg F.W.)	SOD (U/min/mg F.W.)	CAT (U/min/mg F.W.)	POD (U/g F.W.)	APX (U/min/mg F.W.)	SOD (U/min/mg F.W.)	CAT (U/min/mg F.W.)	POD (U/g F.W.)	APX (U/min/mg F.W.)	SOD (U/min/mg F.W.)	CAT (U/min/mg F.W.)
2-nitrofluorene spiked microcosm	<i>Cyperus rotundus</i>	2.9±0.33	1.3±0.22	6.4±0.37	3.5±0.41	3.3±0.22	3.97±0.12	9.8±0.59	8.97±0.29	7.77±0.26	8.2±0.22	17.9±0.54	15.7±0.43
	<i>Cyperus esculentus</i>	2±0.33	1.8±0.22	5.1±0.29	4.1±0.29	3.9±0.37	3.97±0.12	11.47±0.46	9.25±0.25	7.53±0.25	8.50±0.37	19.8±1.31	18.17±0.85
	<i>Axonopus compressus</i>	1.53±0.29	2.3±0.36	3±0.16	1.5±0.37	3.4±0.28	4.5±0.41	8.87±0.63	2.83±0.17	8±0.33	11.27±1.08	16.33±0.83	7±0.24
	<i>Imperata cylindrica</i>	9.5±0.37	3.2±0.28	2±0.24	8.5±0.37	13.43±0.42	6.33±0.24	6.93±0.74	13.13±0.84	21±0.50	14.3±0.29	15.7±0.65	22.67±1.45
The data are expressed as mean ± S.D.(n=3).													

Table 4.19. Statistical results of antioxidant enzymes of the plant species in the experimental microcosm at 0, 30, and 60 days of treatment by plant-bacterial co-inoculum and biostimulant.

Microcosms	Plant species	Enzymes	df	Test-statistics	<i>p</i>	Statistical Test
Control	<i>Cyperus rotundus</i>	POD	2, 6	F = 1.066	0.40	
		APX	2, 6	F= 5.519	0.044*	
		SOD	2, 6	F=7.428	0.024*	
		CAT	2, 6	F=4.92	0.54	
	<i>Cyperus esculantus</i>	POD	2, 6	F=11.2	0.009**	
		APX	2, 6	F=3.68	0.09	
		SOD	2, 6	F=33.06	0.0006***	one-way ANOVA
		CAT	2, 6	F=4.08	0.076	
	<i>Axonopus compressus</i>	POD	2, 6	F=19.89	0.002*	
		APX	2, 6	F=46.02	0.0002***	
		SOD	2, 6	F=12.18	0.008**	
		CAT	2, 6	F=5.429	0.045*	
	<i>Imperata cylindrica</i>	POD	2, 6	F=34.74	0.005**	
		APX	2, 6	F=11.75	0.008**	
		SOD	2	H=7.2	0.026*	Kruskal-Wallis
		CAT	2, 6	F=34.19	0.0005***	one-way ANOVA

Contd.

Microcosms	Plant species	Enzymes	df	Test-statistics	p	Statistical Test
1-nitropyrene treated	<i>Cyperus rotundus</i>	POD	2, 6	F= 144.8	8.369E-06***	one-way ANOVA
		APX	2, 6	F=380.2	4.799E-07***	
		SOD	2, 6	F=638.9	31.021E-07***	
		CAT	2, 6	F=349	6.169E-07***	
	<i>Cyperus esculantus</i>	POD	2, 6	F=71.81	6.449E-05***	
		APX	2, 6	F=270.5	1.32E-06***	
		SOD	2, 6	F=390.7	4.42E-07***	
		CAT	2, 6	F=205.4	2.98E-06***	
	<i>Axonopus compressus</i>	POD	2, 6	F=211.7	2.729E-06***	
		APX	2, 6	F=65.04	8.572E-05***	
		SOD	2, 6	F=345.3	6.39E-07***	
		CAT	2, 6	F=79.96	4.729E-05***	
	<i>Imperata cylindrica</i>	POD	2, 6	F=635.1	1.039E-07***	
		APX	2, 6	F=360.3	5.632E-07***	
		SOD	2, 6	F=733.6	6.757E-08***	
		CAT	2, 6	F=557.6	1.533E-07***	

Contd.

Microcosms	Plant species	Enzymes	df	Test-statistics	p	Statistical Test
2-nitrofluorene treated	<i>Cyperus rotundus</i>	POD	2, 6	F=224	2.31E-06***	one-way ANOVA
		APX	2, 6	F=667.1	8.972E-08***	
		SOD	2, 6	F=270.8	1.315E-06***	
		CAT	2, 6	F=524.4	1.949E-07***	
	<i>Cyperus esculantus</i>	POD	2, 6	F=153.5	7038E-06***	one-way ANOVA
		APX	2, 6	F=346.8	6.307E-07***	
		SOD	2, 6	F=160.7	6.153E-06***	
		CAT	2, 6	F=296	6.419E-06**	
	<i>Axonopus compressus</i>	POD	2	H=7.2	0.265	Kruskal-Wallis
		APX	2, 6	F=90.2	3.355E-05***	one-way ANOVA
		SOD	2, 6	F=396	4.25E-07***	
		CAT	2, 6	F=215.8	2.578E-06***	
	<i>Imperata cylindrica</i>	POD	2, 6	F=364.6	5.436E-07***	one-way ANOVA
		APX	2	H=7.2	0.0257*	
		SOD	2, 6	F=280.8	1.182E-06***	
		CAT	2, 6	F=104.7	2164E-05***	

H= Chi square, F= F-statistic, *= Significant, **= Moderately significant, ***= Highly significant

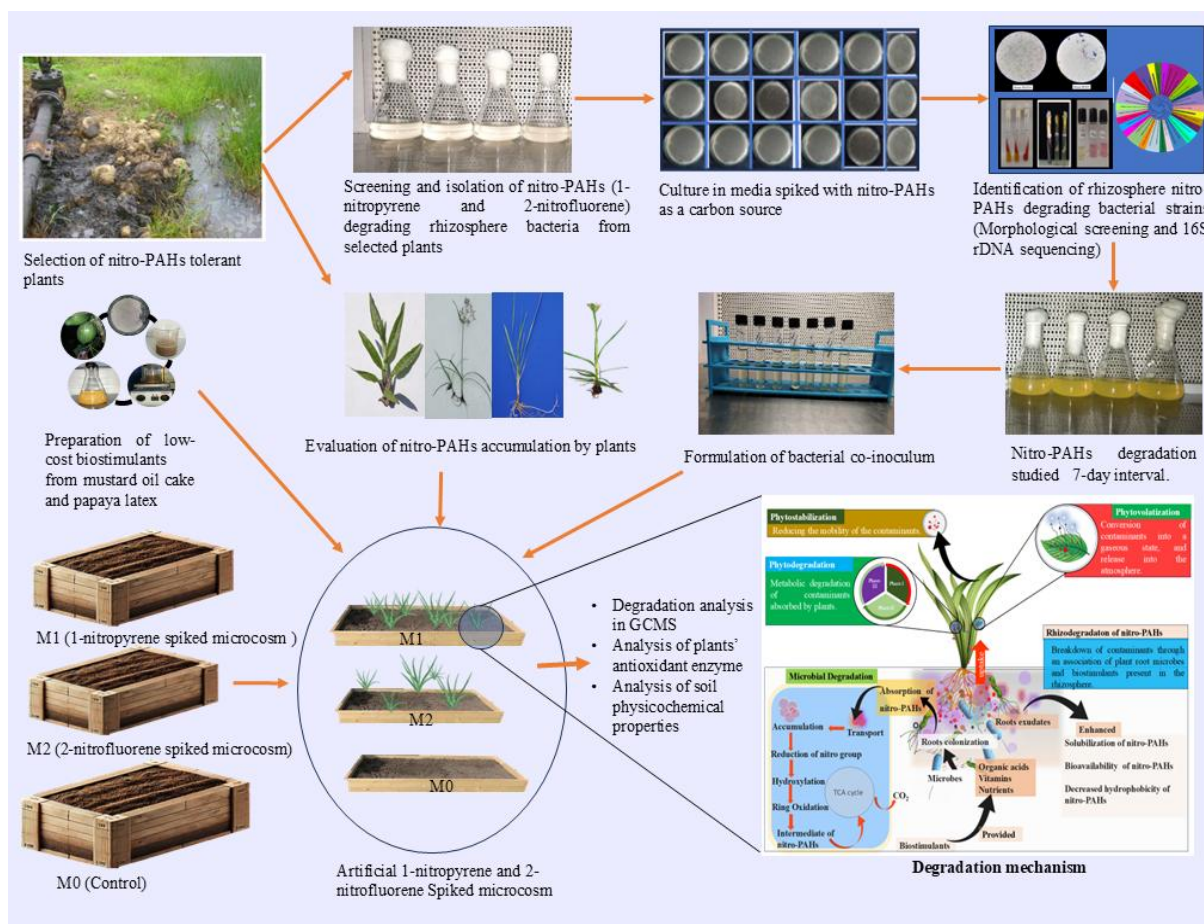


Fig. 4.48. Graphical representation of the study.

3.2 U/min/mg F.W. across all microcosm settings. On the other hand, the SOD activity is high in *C. rotundus* i.e. 6.28 U/min/mg F.W. in control and 6.4 U/min/mg F.W. in both pollutant-affected conditions. Simultaneously, catalase activity was high in *I. cylindrica* with 8.3 U/min/mg F.W. in the control and 8.5 U/min/mg F.W. in both 1-nitropyrene and 2-nitrofluorene exposure.

In the controlled microcosm, *I. cylindrica* showed a slight increase in POD activity and exhibited a relatively consistent, increasing from 9.32 U/g F.W. at day 0 to 10.5 U/g F.W. on day 30, and eventually reaching 13.3 U/g F.W. by day 60. When 1-nitropyrene was present in the microcosm, the POD activity increased significantly, initially at 9.2 U/g F.W. raised to 15.77 U/g F.W. by day 30, and peaked at 25.6 U/g F.W. on day 60. A similar trend was observed within the 2-nitrofluorene microcosm, where POD activity increased from 9.5 U/g F.W. on day 0 to 13.43 U/g F.W. on day 30, eventually reaching 21 U/g F.W. on day 60. These significant increases suggest that *I. cylindrica* has a strong mechanism for oxidative stress management, effectively leveraging its enzymatic defense system to reduce ROS created as a result of nitro-PAH exposure. A similar trend has been reported in *C. rotundus*, which showed considerable

increases in POD activity. POD activity in the 1-nitropyrene-spiked microcosm increased to 4.33 U/g F.W. at day 30 and 6.33 U/g F.W. at day 60. Similarly, in the 2-nitrofluorene-spiked microcosm, POD activity was 3.33 U/g F.W. at day 30 and 7.77 U/g F.W. at day 60. Furthermore, *C. esculentus* POD activity increased from 3.5 to 6.3 U/g F.W. in the 1-nitropyrene-spiked microcosm and from 3.9 to 7.53 U/g F.W. in the 2-nitrofluorene-spiked microcosm at the 30 and 60-day treatment intervals, respectively. Even *A. compressus*, which initially had lower enzymatic levels, showed a considerable increase in POD activity after exposure to nitro-PAHs. The POD activity in the 1-nitropyrene microcosm increased to 3.87 U/g F.W. at day 30 and 8.45 U/g F.W. at day 60, whereas in the 2-nitrofluorene microcosm, it increased to 3.4 U/g F.W. protein at day 30 and 8.0 U/g F.W. at day 60. The antioxidant enzyme APX also showed a significant rise across all treated plant species, with *I. cylindrica* having the highest enzymatic activity. By day 60, *I. cylindrica*'s APX activity reached 12.75 U/min/mg F.W. in the 1-nitropyrene-spiked microcosm and 14.3 U/min/mg F.W. in the 2-nitrofluorene-spiked microcosm, indicating a strong response to oxidative stress. *C. rotundus*, *C. esculentus*, and *A. compressus*, on the other hand, showed enhanced APX activity in response to both 1-nitropyrene and 2-nitrofluorene stress, albeit at relatively lower levels. Moreover, by 60 days, all plant species showed considerable overexpression of SOD. *C. esculentus* demonstrated the greatest SOD activity, increasing from 5.1 U/min/mg F.W. at day 0 to 20.87 U/min/mg F.W. in the 1-nitropyrene microcosm and peaked at 19.8 U/min/mg F.W. in the 2-nitrofluorene microcosm. At day 60, *I. cylindrica* exhibited the highest catalase activity, with 23.5 U/min/mg F.W. (1-nitropyrene spiked microcosm) and 22.67 U/min/mg F.W. (2-nitrofluorene spiked microcosm). Other plant species also showed significant increases in antioxidant enzyme activity, demonstrating a strong adaptive response to nitro-PAH-induced oxidative stress. Furthermore, the enzymatic activities recorded in the baseline cohort under controlled conditions showed a minor increase at the 30 and 60-day mark compared to the initial time point (0 days), even in the absence of any contaminant impact. This finding shows that plants undergo fundamental metabolic adaptations throughout time as part of their natural growth and development. This slightly increasing enzymatic activity might be attributed to the slow accumulation of ROS as a result of their normal metabolic processes, which causes a delicate activation of antioxidative defense systems. These modifications may also be caused by environmental factors such as light, temperature, or nutrition availability, which can all have an impact on the basic enzymatic activity levels in plants. The overall graphical representation of the study is shown in Fig. 4.48.